STARS

Electronic Theses and Dissertations, 2020-

2020

The Impacts of Wave Energy Conversion on Coastal Morphodynamics in a Changing Climate

Cigdem Ozkan
University of Central Florida

Showcase of Text, Archives, Research & Scholarship

THE IMPACTS OF WAVE ENERGY CONVERSION
ON COASTAL MORPHODYNAMICS
IN A CHANGING CLIMATE

by

CIGDEM OZKAN
B.S. Middle East Technical University, 2015
M.S. University of Central Florida, 2018

A dissertation submitted in partial fulfillment of the requirements
for the degree of Doctor of Philosophy
in the Department of Civil, Environmental, and Construction Engineering
in the College of Engineering and Computer Science
at the University of Central Florida
Orlando, Florida

Fall Term
2020

Major Professor: Talea L. Mayo

ABSTRACT

Fossil fuels, i.e., petroleum, natural gas, and coal, are the primary sources of global energy. Studies on the impacts of fossil fuels on climate change have shown the immediate need to reduce greenhouse gas emissions and adopt sustainable alternatives since these emissions result in warmer atmospheric temperatures, ocean acidification, glacier melting, sea level rise, and many other ramifications. In recent years, these alarming results have prompted governments worldwide to develop adaptation strategies for climate change, leading to increased investments in renewable energy resources.

Globally, solar energy, wind energy, and hydropower have been the leading sources of renewable energy. Ocean wave energy, however, has become increasingly recognized as another promising source of electricity, as waves contain as much as 2 TW of power and offer a highly predictable energy resource in comparison to more conventional sources.

Wave energy can be converted into electricity by Wave Energy Converters (WECs). WECs extract energy from the motion of surface waves or fluctuations in the water pressure below the ocean surface. Surface waves or pressure fluctuations drive a generator or a power take-off system, allowing the energy of the waves to be converted into electricity. WECs are commonly configured in arrays, i.e., wave farms, to increase the span across which waves can be captured and optimize the use of materials such as underwater cables used to transfer the generated electricity to the shore. There are various types of WECs based on various physical principles and their efficiencies of converting the total available wave power into electricity range from 20-40%. For any given location, the most suitable type should be determined for deployment based on the coastal region's

local needs and characteristics, such as the bathymetry, wave climate, coastline properties, and marine life.

Wave energy conversion technologies have recently attracted more attention as part of global efforts to replace fossil fuels with renewable energy resources. While ocean waves can provide renewable energy, they can also be destructive for the coastal areas that are usually densely populated and vulnerable to coastal erosion. There have been a variety of efforts to mitigate the impacts of wave- and storm-induced erosion; however, they are either temporary solutions or approaches that are not able to adapt to changing climate. It is only recently recognized that traditional coastal protection methods may not be adequate in adapting to climate change, and diverse defense methods employing nature-based solutions and non-invasive technology (e.g. wave farms and electric reefs) are needed. This dissertation explores a green and sustainable approach to mitigating coastal erosion from hurricanes through wave energy conversion in a changing climate, i.e., rising sea levels. The potential use of wave energy converter farms to mitigate erosion while generating renewable energy is explored through simulations using the numerical model, XBeach. It is shown that wave farms can impact coastal morphodynamics and have the potential to reduce dune and beach erosion. The capacity of wave farms to influence coastal morphodynamics varies with the storm intensity.

Dedicated to my family and friends for their unconditional love and support.

ACKNOWLEDGMENTS

I would like to offer my sincerest gratitude to my mentor and advisor, Dr. Talea Mayo. I am beyond grateful for her handpicking me to be her first graduate student. Throughout all the long meetings and chains of emails, she never failed to always be there for me. She has managed to achieve so much at an early point in her career and is one of the strongest women I know. I aspire to be half the woman and scientist she is today. Through the knowledge and guidance she has provided, I am confident that I will be able to thrive in my future career. Thank you, Dr. Mayo.

I want to thank my committee members Joseph Donoghue, Stephen Medeiros, Davina L. Passeri, Thomas Wahl, and Dingbao Wang, for their valuable contribution and support throughout my Ph.D. journey. Your feedback and guidance helped shape my dissertation tremendously.

I am forever grateful for my parents Hasan and Simsir Ozkan, my sister Didem Ozkan, and my sisters from other mothers, Pelin Tasanlar and Aysu Senyuz, for always being there for me and believing in me. I could not have done it without your tireless support.

TABLE OF CONTENTS

LIST OF FIGURES

LIST OF TABLES

CHAPTER 1:   INTRODUCTION

As the climate continues to change, the need for renewable energy resources is becoming increasingly evident. Fossil fuels being depleted, and the carbon dioxide emissions produced from burning those fossil fuels that remain are largely contributing to global warming. This has catalyzed interest in renewable energy. It is estimated that as much as 2 TW of wave power is available globally (Gunn and Stock-Williams, 2012). Unfortunately, there are many challenges surrounding the integration of wave energy into the electrical grid. One significant barrier has been the cost of installation, operation, and maintenance of devices that can efficiently capture, store, and then transport available wave energy. Thus, a critical first step in the implementation of these devices is assessing the wave power available to be converted in the first place. The wave power available has large spatial variability and thus must be assessed for each region of interest. When estimating the wave power potential, it is also important to consider the impacts of climate change and variability since wave energy converters are designed to last 25-30 years, and potential changes in available wave power may have substantial implications for wave farms.

It is well known that waves offer an immense amount of clean and renewable energy; however, the energy-harnessing process may have unforeseen environmental impacts. These must be carefully investigated prior to Wave Energy Converter (WEC) implementation. Like most manufactured devices, WECs cause greenhouse gas emissions during their production, deployment, maintenance, and removal processes. Several studies have assessed these impacts, and most of them have found that the carbon payback can be achieved in a short time relative to the lifetime of the devices (Dalton et al., 2014; Thomson et al., 2011; Uihlein, 2016). In addition to a short carbon payback time, WECs can also have positive effects on coastal ecosystems. The

dynamic underwater mechanisms of WECs can improve water circulation and promote the diversity of marine life by acting as artificial reefs (Langhamer, 2012).

More recently, a small number of researchers have also begun to investigate the impacts of WECs on coastal erosion. Coastal erosion is defined as the loss or displacement of coastal sediments due to the impacts of storms, strong waves, tides, flooding events, and/or human activities. It is a critical challenge that many urbanized coastal areas face, particularly as the climate changes and global wave power increases (Reguero et al., 2019). Wave attack is one of the main causes of coastal erosion, and a number of studies have begun to investigate how WECs impact wave-induced erosion, as discussed in the following chapters.

1.1   Coastal Erosion

Coastal erosion is a global problem. Domestically in the U.S., the average coastline recession rates are measured as 7.62 m per year for some barrier islands, and this rate increases to 15.2 m per year along the Great Lakes (U.S. Climate Resilience Toolkit, 2016). Coastal sediment can be transported offshore, onshore, and alongshore. When the water levels are high due to storm events, coastal sediment is taken away from the beach face and dune area and deposited *offshore,* creating a nearshore sand bar. Conversely, sediment can be transported *onshore* by high water levels*,* i.e., over the top of the beaches when a dune structure is not present. Sediment is taken away from the beachfront and deposited inland. Alternatively, waves can strike a beach with a large angle and generate currents where sediment is moved *alongshore*. While one end of the beach is eroded, the opposing end is accreted. Offshore, onshore, and alongshore erosion of the beaches are illustrated in Figure 1-1

Figure 1-1: Coastal erosion (a) Offshore (b) Onshore (c) Alongshore

Figure source: Unknown

1.1.1   Effects of Coastal Erosion

The effects of coastal erosion can be devastating. Coastal erosion endangers the protection of coastal communities and cities, causes loss of property and lives, disrupts the natural habitats of animal and plant species, and economically impacts coastal cities by reducing the area where navigation, recreation, and fishing activities take place (Scott et al., 2012). Additionally, coastal erosion causes the property values of beachfront real estate to decrease. For example, it is estimated that coastal erosion has resulted in a $5.4 billion loss in real estate value over a dozen years in Florida. This number is $4.5 billion for New Jersey and $1.3 billion for New York (Layne, 2019).

The effects of coastal erosion are made worse by climate change. Sea level rise (SLR), increased storminess and storm surges, and increased wave power are some of the major drivers of high

coastal erosion rates (Masselink and Russell, 2013). Therefore, coastal management strategies that can easily be adapted to the changing climate are preferable and ultimately necessary.

1.1.2 *Solutions to Coastal Erosion*

Coastal counties host 29% of the U.S. population (87 million people) (US Census Bureau, 2015). More than 41 million people live in Atlantic counties and 32 million people live in Pacific counties, and these numbers are expected to increase (US Census Bureau, 2015). These highly populated areas have been heavily managed in order to mitigate the destructive impacts of coastal erosion. Various coastal management strategies have been employed for coastal erosion mitigation, which can be categorized as structural measures and nature-based solutions, both of which come with a number of advantages and disadvantages. Structural measures include revetments, seawalls, breakwaters, groins, and jetties. While providing a temporary solution to the erosion problem locally, these structures are very expensive to build and are likely to introduce coastal erosion elsewhere by affecting the natural water currents and preventing the natural processes that allow sand to shift along coastlines and replenish beaches. These structures have high wave reflection coefficients, which means larger wave heights occur in front of the structures and often result in loss of sediment. Moreover, the inability of the coastal structures to adapt to SLR is unfavorable. There have been many cases of coastal structure failures for structures that could not adapt to the changing climate (Guarino, 2019; Summers et al., 2018).

On the other hand, nature-based solutions, including beach renourishment, dune stabilization with fences and vegetation, wetland protection, habitat restoration, living shorelines, and structure relocation and debris removal have also been commonly employed in the U.S. Despite having less

impact on the environment, nature-based solutions require extensive maintenance. They are relatively short-term solutions that need to be reimplemented frequently, depending on the local coastal erosion rates. In Miami Beach (Figure 1-2), for example, 30 beach renourishment projects were conducted between 1979 and 2017 (Division of Water Resource Management, 2018). From 1970 to 2015, beaches along the East Coast of Florida were renourished over 200 times, where 120 million cubic yards of sand were deposited along the beaches (Florida Shore and Beach Preservation Association, 2017). It can be concluded that nature-based solutions can mitigate the problem temporarily; however, they do not address the root cause of coastal erosion.
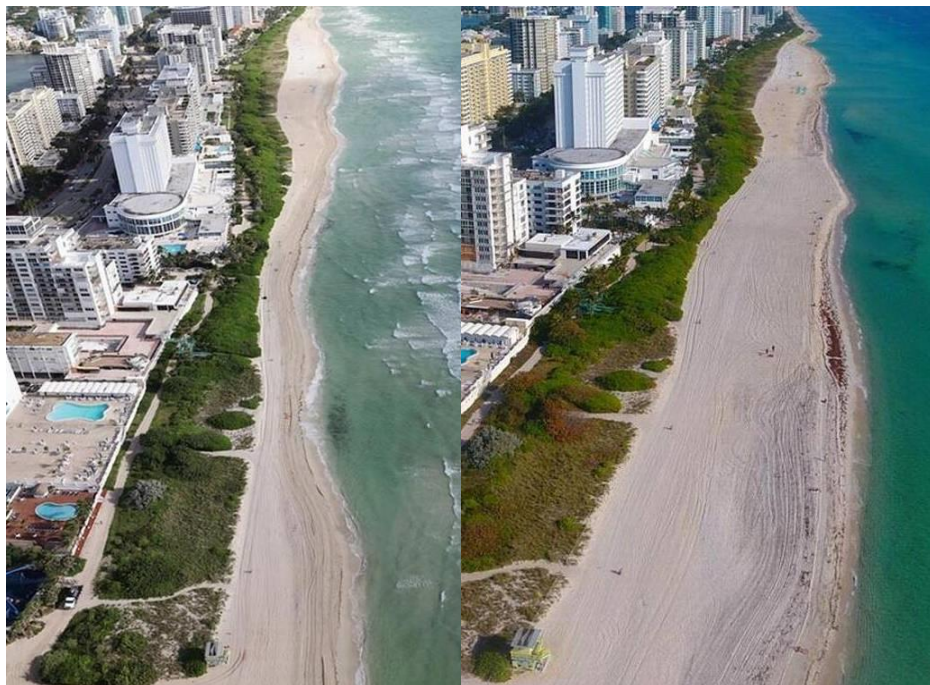
Figure 1-2: Miami Beach before and after beach renourishment
Adapted from (Dailymail, 2017)

1.1.3   Causes of Coastal Erosion

Beach erosion can occur naturally or due to anthropogenic alterations to the sediment budget or the physical processes that impact the coastal sediment. Some of the causes of beach erosion are given by Bird and Lewis (2015) as follows: "reduction in sediment supply from eroding cliffs, reduction of fluvial sediment supply to the coast, reduction of sediment supply from the seafloor, reduction of sand supply from inland dunes, submergence and increased wave attack, increased wave energy because of increased storminess, losses of beach sediment alongshore, a change in the angle of incidence of waves, interception of longshore drift by breakwaters, beach weathering, a rise in the beach water table, [and] removal of beach sediment by runoff."

Investigation of the main causes of coastal erosion is where the research question of this work emerges: If wave action is one of the main causes of coastal erosion, can harnessing wave energy help reduce coastal erosion rates? We explore this question in the following sections.

1.2   Wave Energy Conversion

Wave energy conversion is the process of converting the kinetic and potential energy of ocean waves into mechanical or electrical energy. Ocean wave energy is abundant, consistent, and highly predictable and is an emerging source of renewable energy (Ozkan and Mayo, 2019). The energy in the waves can be harnessed and converted into electricity through devices known as wave energy converters (WECs). WECs are commonly configured in arrays, i.e., wave farms, in order to increase the span across which the waves can be captured and to optimize the use of materials such as underwater cables that are used to transfer the generated electricity to the shore.

As described above, global wave energy potential is substantial and a promising form of renewable energy. Considering the stability of waves in the ocean, wave energy is a highly reliable resource, unlike solar and wind energy that are powerful seasonally but may not be sufficient when there is a lack of sunshine or wind in the area of installment.

The initial cost of wave farms can be high (G. J. Dalton, Alcorn, & Lewis, 2009; Rusu & Onea, 2018); however, coastal communities can doubly benefit from them as they both provide electricity and have the potential to reduce coastal erosion. Several studies have begun to explore the impacts of WECs on coastal morphodynamics and have shown that they can mitigate coastal erosion for gravel and sandy beaches. These studies are reviewed in detail in Chapter 2.

1.3   Research Objectives

Both coastal erosion and depleting conventional energy resources are major global challenges. The motivation of this research is to explore innovative and environmentally friendly solutions to mitigating coastal erosion while providing green and sustainable energy to highly populated coastal areas. The adaptability of the coastal mitigation strategies to the changing climate is also considered. For this purpose, this dissertation examines the impacts of wave energy conversion on coastal erosion. The goal of this work is to understand coastal erosion, the impacts of wave action on coastal erosion, the potential for wave energy extraction, and the role of such extraction on coastal morphodynamics and morphology.

CHAPTER 2:   LITERATURE REVIEW

2.1   Introduction

Fossil fuels, i.e., petroleum, natural gas, and coal, are primary sources of global energy. Although fossil fuels are currently inexpensive and easy to access relative to alternative sources, it is widely understood that they are being depleted at a faster rate than they can be produced. Shafiee and Topal (2009) estimated that oil and gas resources will be depleted by 2042, and coal reserves will become the only type of fossil fuel left on Earth until 2112, when all fossil fuels will cease to exist. Furthermore, studies on the impacts of fossil fuels on climate change (Boden et al., 2010; Gregory et al., 2007; Lehmann, 2007; Siegenthaler and Sarmiento, 1993) have shown the immediate need to reduce greenhouse-gas emissions and adopt sustainable alternatives since these emissions result in warmer atmospheric temperatures, ocean acidification, glacier melting, sea level rise, and many other ramifications.

In recent years, these alarming results have prompted governments all around the world to develop adaptation strategies for climate change. The Paris Agreement (UNFCCC, 2015) is one of the largest, cooperative efforts to address climate change, and was developed with the goal of decreasing global warming; it has prompted many countries to reduce greenhouse gas emissions by investing in renewable energy. The most recent Intergovernmental Panel on Climate Change (IPCC) and National Climate Assessment reports also identify decreasing greenhouse gas

emissions and utilizing renewable energy resources as crucial steps for climate change adaptation (IPCC, 2018; USGCRP, 2014). As a result of this guidance, there is a growing interest, nationally and internationally, in leveraging renewable energy resources. Electricity generated by renewable energy resources constituted 12.7% of the total energy production in the U.S. in 2017 (U.S. EIA, 2018a), and U.S. Executive Order 13693 promoted an exemplary reduction in the greenhouse gas emissions of Federal Agencies and an increase in the percentage of electricity obtained by renewable energy resources.

Globally, solar energy, wind energy, and hydropower (i.e., energy driven by the terrestrial water cycle) have been the leading sources of renewable energy. Ocean wave energy, however, has become increasingly recognized as another promising source of electricity, as waves contain as much as 2 TW of power globally (Gunn and Stock-Williams, 2012), and offer a highly predictable energy resource in comparison to more conventional sources. Ocean waves have been simplistically described as "energy in transition" (McCormick, 2007). Most waves are generated when the wind blows over a distance, or *fetch,* of open water. In general, the wind blows consistently over the open ocean and its energy is transported to the shorelines in the form of wave energy, with little to no loss until the waves reach shallow water.

It has been demonstrated that wave energy can be converted into electricity by wave energy converters (WECs) (EMEC, 2019; Ocean Power Technologies, 2018; Waves4Power, 2017; Wavestar, 2013). WECs extract energy from the motion of surface waves or from fluctuations in the water pressure below the ocean surface (BOEM, 2018). The surface waves or pressure fluctuations drive a generator or a power take-off system, allowing the kinetic energy of the waves to be converted into electricity. There are a variety of types of WECs with various physical

9

principles and efficiencies. For any given location, the most suitable type for deployment should be determined based on the local needs and characteristics of the particular coastal region, such as the bathymetry, wave climate, coastline properties, and marine life.

The installation and maintenance costs of WECs can be very high. Comprehensive assessment of the available wave power for the area of interest is thus an essential component of WEC implementation. Numerous studies have been conducted to estimate wave power potential around the world. Common methods for the assessment of local wave power potential include the use of wave power equations using either measured wave parameters (i.e., wave height, wave period, wave spectrum etc.) based on buoys or satellite data (Defne et al., 2009a; Ozkan and Mayo, 2019; Saglam et al., 2010; Sierra et al., 2016) or numerical wave models (Appendini et al., 2015; Garcia and Canals, 2015; Gunn and Stock-Williams, 2012; Hemer et al., 2017; Iglesias et al., 2009; Jadidoleslam et al., 2016; Kim, 1997; López-Ruiz et al., 2018a, 2018b, 2016; Marta Gonçalves, 2018; Mirzaei et al., 2015; Mota and Pinto, 2014; Reguero et al., 2015; Smith et al., 2013; Van Nieuwkoop et al., 2013; Venugopal et al., 2017). According to the Electric Power Research Institute, the wave power potential in the outer shelf surrounding the United States is 0.30 TW, which is enough energy to power 93,850 homes annually (BOEM, 2018).

It is clear that waves offer an immense amount of clean and renewable energy, however, the energy-harnessing process may have unforeseen environmental impacts. These must be carefully investigated prior to WEC implementation. Like most manufactured devices, WECs cause greenhouse gas emissions during the processes of production, deployment, maintenance, and removal. Several studies have assessed these impacts and most of them have found that the carbon payback can be achieved in a short time relative to the lifetime of the devices (Dalton et al., 2014;

Thomson et al., 2011; Uihlein, 2016). In addition to an acceptable carbon payback time, WECs can also have positive effects on coastal ecosystems. Langhamer (2012) showed that the dynamic underwater mechanisms of WECs can improve water circulation and promote the diversity of marine life by acting as artificial reefs.

The impacts of WECs on coastal hydrodynamics have also been investigated. Wave heights, wave periods, wave directions, longshore current velocity, nearshore circulation, flow conditions, and wave propagation patterns are some of the parameters that can be impacted by WEC operations. Numerical models and in situ observations have been utilized to better understand the potential alterations in these parameters due to the presence of WECs (Atan et al., 2019; Chang et al., 2016; Contardo et al., 2018; Millar et al., 2007; Rusu and Guedes Soares, 2013). Studies have shown up to 30% reduction in significant wave heights in the lee of wave energy farms, and this percentage varies depending on the WEC type, distance from the WEC farm to the coast (i.e., deep water or shallow water deployment), initial wave conditions, and configurations of WECs. In the literature, the effects of the WECs on the hydrodynamics immediately in their lee are commonly studied. However, only in the last decade have effects on the coastline been studied.

Specifically, researchers have recently begun to investigate the impacts of WECs on morphodynamics and coastal erosion. Coastal erosion is defined as the loss or displacement of coastal sediments due to the impacts of storms, strong waves, tides, flooding events, and/or human activities. It is a critical challenge that many urbanized coastal areas face, particularly as the climate changes and global wave power increases (Reguero et al., 2019). Wave attack is one of the main causes of coastal erosion, and a number of studies have begun to investigate how WECs impact wave-induced erosion. We review the findings of these studies here. The main objective of

11

this review is to investigate the interaction between WEC farms and the morphodynamics of the coastal environment. Specifically, we seek to understand the impacts of wave energy conversion on coastal erosion. The rate of erosion is highly dependent on local characteristics of the coastline, the local beach modal state (i.e., size of the sediment particles, wave directions, and tidal regime (Abanades et al., 2015a)) and the local wave climate, therefore we categorize and review the studies by location. We discuss the methodologies and the results of the studies in Section 2 and Section 3, respectively. In Section 4, we provide a critical review of findings in the literature and offer recommendations for future work.

2.2 Approaches

In order to investigate the impacts of WEC farms on coastal erosion, it is necessary to understand the interactions between the local wave climate, the WEC farms, and the coastline. A schematic of these interactions is illustrated in Figure 2-1. For qualitative and quantitative assessments of these interactions and their nearfield (i.e., in the proximity of the WEC farm) and far-field (i.e., in the proximity of the coastline) effects, both numerical modeling approaches and experimental approaches have been implemented. In these approaches, researchers conduct experiments first excluding and then including representations of the WEC farm. The former experiment is referred to as the baseline scenario. The results from the latter experiment can then be compared to the baseline scenario to evaluate the changes induced by the presence of the WEC farm. Here we focus on studies investigating the interactions between the wave climate and the WEC farm, as well as resulting changes to morphodynamics and impacts on littoral sediment transport.
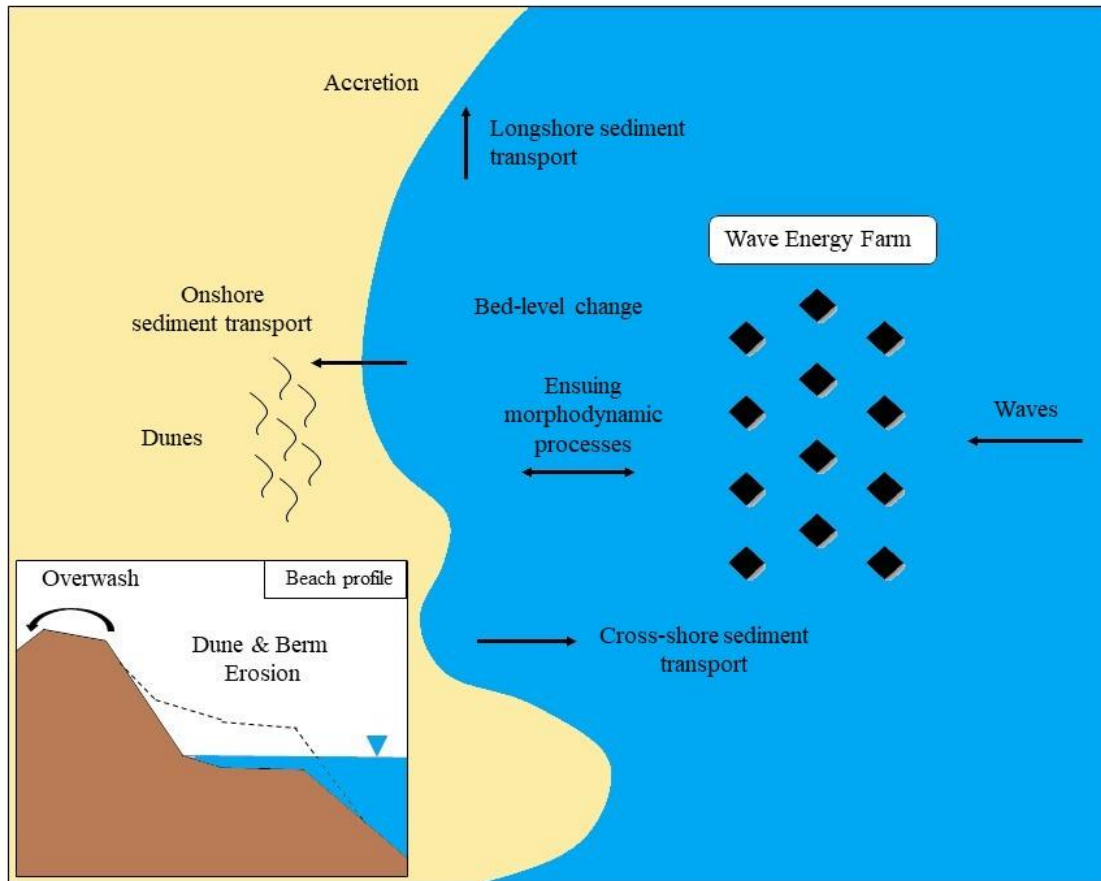
Figure 2-1: Interactions between marine energy farms and coastal processes.
Adopted from (Amoudry et al., 2009)

2.2.1   Numerical Modeling Approaches

Numerical modeling approaches for the investigation of the impacts of WEC farms on coastal morphology have been conducted by coupling wave propagation models with morphodynamic models. The two models are often loosely coupled by using data that describes local wind, bathymetry, and boundary conditions as input to the wave propagation model, and then using the resulting model output (i.e., local wave parameters) as input to the morphodynamic model. The

morphodynamic model outputs data describing the beach profile and sediment transport rates at the coast.

2.2.1.1 Wave modeling

Wave models are used to simulate the behavior of the wave climate (wave heights, wave periods, etc.) in the lee of the WEC farms. The Simulating Waves Nearshore (SWAN) and Delft3D-WAVE models are the most commonly used wave models. Both solve the spectral action balance equation and account for various physics including wave propagation in time and space, diffraction, and transmission through/reflection against obstacles (Booij et al., 1999; Roelvink and Van Banning, 1995). The spatial and temporal resolution is specified by the user. A common assumption when using wave propagation models is that the potential effects of WEC farms on coastal morphodynamics are observed in *shallow water* at the coast only, i.e., that the influence of the waves on sediment is negligible in water depths higher than the depth of closure (Stokes and Conley, 2018a). WECs are frequently represented in these models as partially transmitting and partially reflecting obstacles by using representative transmission (K_t) and reflection coefficients (K_r). K_t is defined as the ratio of transmitted wave heights to incident wave heights $(K_t = {H_t}/{H_i})$ and it ranges from 0 to 1, where $K_t = 0$ represents the complete energy absorption by the WECs (no wave transmission through the WEC farm) and $K_t > 0$ represents partial wave transmission. Similarly, K_r is defined as the ratio of reflected wave heights to the incident wave heights $(K_r = {H_r}/{H_i})$ and it ranges from 0 to 1, where $K_r = 0$ represents no wave reflection by the WECs and $K_r > 0$ represents partial wave reflection (Ergin, 2009). K_t and K_r of WECs are often estimated based on experimental results. They vary depending on the physical and

14

mechanical properties of individual WECs as well as the configuration of the WEC farms. Most of the studies reviewed here use wave reflection and transmission coefficients that are determined from laboratory tests such as those described in (Bergillos et al., 2019a, 2019b; Fernandez et al., 2012a). However, Stokes and Conley (2018) presented a new way of parameterizing the transmission coefficient of the WEC, which does not rely on laboratory tests and can be applied to any WEC type. The authors demonstrated the effectiveness of the derived 'rated power transmission coefficient' through a test case and compared the results to the coastal impacts estimated when using experimentally derived transmission coefficients. They concluded that implementing the rated power transmission coefficient in the wave model realistically represents the amount of energy absorbed by WECs.

Wave to WEC and WEC to WEC interactions within a WEC farm are considered in the impact assessment studies. Rijnsdorp et al. (2017), proposed a non-linear phase-resolving wave model to simulate these interactions. The authors claimed that phase-averaged wave models (spectral models) are not able to represent all of the physical processes when modeling the coastal impacts of WECs such as diffraction and wave to WEC interactions. They validated the Simulating Waves till Shore (SWASH) model to realistically represent the coastal processes involved. Model results were compared to a phase-averaged model (SNL-SWAN), and discrete alterations in wave heights in the lee of the WEC were observed. The authors claimed that the SWASH model has advantages over SNL-SWAN as it accounts for wave scattering and radiation. Simulations showed that the improved SWASH model is able to characterize the dynamic response of a submerged body to wave action. Only a single, submerged WEC was investigated in this paper, however, this study illustrated that there are influential processes that might not be fully represented with phase-

averaged models. This should be considered in future studies, e.g. both submerged and emergent WECs and farms where WEC to WEC interactions are present.

2.2.1.2 Morphodynamic modeling

Among the studies that investigate the impacts of WEC farms on coastlines, XBeach is the most prevalently used morphodynamic model. XBeach simultaneously evaluates the short wave action balance equations, roller energy balance equations, mass and momentum balance equations, nonlinear shallow water equations, sediment transport equations, and bed update processes (Roelvink et al., 2015). The initial beach profile, sediment characteristics, tidal conditions, wave dissipation coefficients, and output of the wave propagation model can all be specified as model input. The model is either run in one-dimensional mode to simulate the beach profile evolution (i.e., changes in bed elevation are simulated along the cross-shore distance) or in two-dimensional mode to additionally simulate the alongshore response. While morphodynamic models have been successfully used for short-term simulations (e.g. duration of one storm event), they are not yet capable of producing output over the temporal and spatial scales that can ideally represent long-term impacts of WEC farms on coastal erosion (Stokes and Conley, 2018).

A small number of studies utilize sediment transport equations in lieu of numerical models to estimate coastal erosion rates and changes to the beach profile (Section 2.3.2 and 2.3.7). Note that this method cannot simultaneously account for the multiple coastal processes described above.

2.2.2   *Experimental Modeling Approaches*

Wave basin and flume experiments have been successfully designed to model the impacts of WECs on coastal processes (Section 2.3.7). These scaled physical models provide a better representation of the many complex processes at play which cannot be explicitly simulated with numerical modeling approaches (e.g. Wave to WEC and WEC to WEC interactions). WECs are represented in experimental set-ups as either simple physical barriers or prototypes of full-scale WECs. The latter more effectively simulate the behavior of the physical processes that develop with real-world implementation. The WEC types considered in the studies differ due to the capacity of the laboratories and testing sites. Floating WECs are commonly modeled as they are relatively easy to deploy for testing purposes.

Experimental modeling protocol prescribes conducting multiple tests with and without the WEC farms. Stabilized beach profiles and sediment transport rates observed in the two cases are compared to assess the impacts of WEC farms.

Experimental modeling approaches have advantages and disadvantages over numerical modeling approaches. Although the beach profile, bathymetry, and wave conditions may be difficult to exactly represent in experiments, experimental studies generally do not require as many simplifying assumptions as numerical models, increasing the applicability of the results. Additionally, the wave transmission and reflection coefficients that represent WECs in numerical studies are often determined through laboratory testing, therefore experimental approaches are a fundamental component of numerical modeling approaches. On the other hand, experimental approaches are subject to observational errors (Muste, 2002; Taylor, 1997). It can also be challenging to introduce and manipulate various physical processes in an experimental setup, such

17

as seasonal variations in the wave climate. Furthermore, it can be difficult to scale the temporal

domain of the prototype to understand longer-term impacts of real-world implementation. Finally,

experimental approaches are often prohibitively costly. Experimental approaches are valuable,

however numerical modeling approaches enable researchers to better control for specific variables

and are thus more commonly found in the literature.

2.3   Findings

Erosion rates vary with the local coastal sediment composition, local dominant wave direction,

local bathymetry, and, if present, local vegetation. Thus, the assessment of WEC impacts on

onshore and alongshore sediment transport should be conducted specifically for each region of

interest. To date, studies have been carried out for coastal regions of the U.K., Spain, Mexico,

Ireland, South Korea, and Romania.

2.3.1   *The U.K.*

The Coastal Processes Research Group and COAST Engineering Research Group from the

University of Plymouth conducted the pioneering research on impacts of WEC farms on coastal

morphodynamics in the U.K. Most of the studies concentrated on the beaches around the Wave

Hub test facility where several WEC arrays were tested (Wave Hub, 2019). The Wave Hub test

facility is located in Cornwall, England where the wave power is high (ABPmer, 2019). Several

studies were carried out for locations in the lee of the Wave Hub test facility, including (Abanades

et al., 2015a, 2015b; Abanades et al., 2014a, 2014b) by the COAST Engineering Research Group.

These studies were primarily conducted at Perranporth Beach, which was selected for monitoring

the potential impacts of WEC farms on beach morphology as part of the Wave Hub project in 2015

(Stokes, 2015). Since becoming a grid-connected operational WEC facility in late 2010, the Wave Hub test facility has provided real-time and quality-controlled wave data at this location.

Perranporth Beach is a 3-mile long sandy beach with medium quartz sand protected by high dunes. The median diameter of the local sediment particles is 0.35 mm (Poate et al., 2012). A typical beach profile in this region has a steep beach face and a gentle slope. There is also an offshore sand bar in the surf zone. Researchers have implemented both numerical modeling and experimental approaches to investigate changes to the beach profile in order to assess the impacts of WEC farms at this location. Onshore and alongshore sediment transport has been assessed with and without representation of WEC farms for comparison. Some of the commonly used assessment metrics are bed level impact, beach face eroded area, erosion reduction, and cumulative eroded area.

Despite several different approaches, the studies in this location (Abanades et al., 2015b, 2015a; Abanades et al., 2014b, 2014a; Gonzalez-Santamaria et al., 2013) concluded that WEC farms do not negatively impact the coastline and in fact, can create a calmer sea-state and reduce the rate of coastal erosion, acting as a method of coastal protection. In an effort to gain stakeholder support, Poate et al. (2012) conducted a similar study with the goal of demonstrating that Wave Hub would not negatively impact shorelines, and ultimately they did show this. They did not explore the potential use of WEC for coastal protection. The results of the studies that were conducted for the English coasts are summarized in Table 2-1

Table 2-1: Methods and the results of the studies conducted for the English coasts

Paper	Methodology	Results
Abanades et al., 2014a	Numerical models SWAN, XBeach, WaveWatchIII	• Over 30% reduction in Hs in the proximity of the wave farm • 10% reduction closer to the shore • Over 0.5 m erosion reduction at the submarine bar, • Over 4 m reduction at the beach face erosion • Over 50% reduction in erosion in the north section of the beach
Abanades et al., 2014b	Numerical models SWAN+XBeach loose coupling	• 12% reduction in wave energy flux. 21 to 35 % reduction in eroded areas
Abanades et al., 2015a	Numerical and conceptual models: SWAN and Conceptual beach model by Masselink and Short (1993)	• At a distance of 2 km from the shoreline the reduction of the significant wave height is 25%, • For the farm at 4 and 6 km, the values are 12% and 5%, respectively
Abanades et al., 2015b	Numerical modeling SWAN+XBeach loose coupling	• Up to 20% of beach erosion reduction
Alexandre, 2013	Numerical Models SWAN + MIKE21 + SCAPE	• Average of 50% reduction in cliff recession and sediment transport rate
Gonzalez-Santamaria et al., 2013	Numerical Models SWAN+ROMS+Sediment transport model (Soulsby and Damgaard, 2005)	• 5 to 10 cm reduction in wave height • Sediment concentration changes up to 0.1 kg/m3 at low tide
Poate et al., 2012	Implementation Wave climate: observations Beach morphology: topographic surveys, remote sensing, digital images	• 6% reduction in the wave height • No significant alteration on the coastal morphology

Most of these studies not only showed a substantial reduction in erosion with the presence of WEC farms but also identified other factors that impact the coastline such as the geometry and layout of the WEC farm and the distance between the farm and the shore. These parameters are studied in more detail in other studies, including several conducted for Spain (Section 2.3.2).

Vögler et al. (2011) carried out a similar study in Isle of Lewis, Scotland. The coastlines of Isle of Lewis have long sandy beaches that are comprised of broken shell pieces with diameters between 0.20- and 2.0-mm. Quartz particles are also predominant in many locations. Vögler et al. (2011) used the software MIKE 21, which offers both a wave propagation model and a morphological model, to assess the impact of WEC for this region. They also carried out an experimental study for coastlines in Scotland by taking sediment samples from several sites to validate the model results. They used a wave tank with a wave generator and point absorber WEC prototype. Matching Froude numbers were used to scale the experimental results to the prototype. A year's worth of wave data was input to MIKE21 and combined with a hydrodynamic, spectral wave, and non-cohesive sediment transport model to compare the bed level outputs of cases with and without the WEC farms. It was assumed that the amount of power that is harnessed by the WEC and removed from the waves is equal to the rated electrical power output. Wave reflection, wave diffraction, and wave transmission were not considered, which potentially resulted in more conservative output (i.e., less reduction in wave heights in the lee of the WEC farm). This study did not provide quantitative results such as percent change in erosion rate or total eroded area with and without the WECs. However, it did qualitatively conclude that less erosion and sand bar formation was observed in the presence of WEC farms due to wave attenuation.

The Ph.D. thesis of A. Alexandre (Alexandre, 2013) provided a long term study using a data set containing significant wave heights, peak period, and peak direction for 140 years. This data set was used as input to a wave propagation model. Alexandre assessed the nearshore impacts of WECs in East Anglia, where soft cliff erosion has been observed, using SWAN, MIKE21, the Soft Cliff And Platform Erosion (SCAPE) sediment transport model, and the Coastal Engineering Research (CERC) formula (Hanson, 1989) to quantify changes in sediment transport rates. The SCAPE model, developed to simulate long-term nearshore dynamics, was given 30 years' worth of data to assess the sediment transport rates and cliff recession rates over that time. An average reduction of 50% in cliff recession and the sediment transport rates was found for some locations due to the presence of WECs. Long term wave climate changes were not considered.

2.3.2 *Spain*

Due to its highly energetic coastlines, Spain is another location where a number of studies on WEC impacts have focused. The Environmental Hydraulics Institute of the University of Cantabria, the Andalusian Institute for Earth System Research of the University of Granada, and the Hydraulic Engineering Area of the University of Cordoba have led much of the work for this region through independent studies and collaborations with the University of Plymouth. The Asturias and Cantabria coasts (Atlantic Ocean) and Playa Granada coast (Mediterranean Sea) are the two predominant study sites (Figure 2-2). Northern Spain has a treacherous rocky shore, whereas Playa Granada is a deltaic coast with gravel beaches. Both regions have experienced critical coastal erosion in recent years (Bergillos et al., 2018). Rodriguez-Delgado et al. (2019a) explained that Playa Granada experiences extra-tropical Atlantic cyclones and Mediterranean storms. The highest

significant wave heights under typical conditions and extreme events exceed 2.1 m and 3.1 m, respectively, which makes this coast prone to coastal erosion.

Wave energy research in Spain has been conducted at several ocean test sites including the Biscay Marine Energy Platform, Plocan test site, and Mutriku Oscillating Water Column plant. Studies surrounding several other individual WEC deployments have also been conducted (Mora-Figueroa et al., 2011). These studies have provided valuable data for both the wave energy industry and academic research.

Figure 2-2: Study locations in Spain
Generated using Google Maps

The idea of using WEC farms as a coastal defense mechanism in Spain emerged in 2014 when Iglesias and Carballo assessed the impacts of a WEC farm on nearshore wave conditions and proposed to investigate the morphological impacts on coastlines (Iglesias and Carballo, 2014). Since then, numerous other studies have been conducted to further develop this idea. Mendoza et

al. (2014) conducted one of the first studies on the impacts of WEC farms on beach morphology in the region. They presented two case studies, one of which was at the Bay of Santander located in Northern Spain. Four different types of WEC devices (the Wave Dragon, Blow-Jet, Sea Breath, and DEXA) were tested in two different locations, under two different wave conditions to observe the influence on the beach morphology. A 1-D elliptic mild-slope equation model and a 2-D modified elliptic mild-slope equation model were used to simulate the behavior with and without the WEC farms. WECs were defined in the models as infinitely high porous boxes, and wave transmission and diffraction conditions due to the presence of WEC farms were considered. The results of this study showed that both devices helped to alleviate current coastal erosion rates. Accretion was also observed over some stretches of the coastline.

Bergillos et al. (2018) observed the most significant reduction in coastal erosion rates for a hypothetical WEC farm deployed near the Guadalfeo Coast. The authors numerically simulated eight different scenarios, varying the alongshore location of a WEC farm consisting of 11 WaveCAT devices under two different wave conditions. Weighted averages of several extreme storms with significant wave heights exceeding 3.1 m over the past 25 years were used as input to the wave propagation and coastal morphology models. This study showed that the WEC farm was able to reduce the coastal erosion rate by 44.5% in Playa Granada. This study contributes to the literature by assessing the impacts of WEC farms on coastal morphology in a *deltaic coast*, linking wave run-up and coastal flooding in the presence of WEC farms, and explaining how the alongshore location of WEC farms changes the extent of coastal protection.

The work of Bergillos et al. (2018) lead to a number of research questions, several of which were recently addressed in studies by the Plymouth University and the University of Granada research

groups. The case study for Playa Granada has been studied further to optimize the coastal protection provided by the WEC farm. Rodriguez-Delgado et al. (2018a) investigated the most effective layout of a wave farm composed of 11 WaveCAT WECs in terms of coastal protection. Staggered placement of eleven WECs arranged in two rows (where the row closer to the shore has five WECs) was found to be the most effective layout for mitigating coastal erosion, reducing significant wave heights and longshore sediment transport rates and increasing dry beach area (which indicates less wave run-up). The same authors studied the impact of the alongshore position of the WEC farm and the spacing between devices on coastal protection in their 2018 and 2019 studies, respectively (Rodriguez-Delgado et al., 2018b, 2019b). They stated that the location of the WEC farm is critical when optimal coastal erosion mitigation is desired, and 180 m spacing between WECs yields the highest level of coastal protection.

Bergillos et al. (2019a) explored the optimal geometry of individual WaveCAT WECs (Figure 2-3) through laboratory experiments for the purpose of decreasing wave heights and reducing coastal erosion rates. Experiments were conducted for the cases of a 30° angle and a 60° angle between the wedges of the WEC. Results showed that no particular configuration outperforms the others. Rather, it was suggested that the WEC geometry be adjusted based on the sea state to attain better performance for protecting the shore. Following this study, the authors investigated the impacts of the WEC geometry (i.e., WaveCAT with a 30° angle or a 60° angle between the wedges) on coastal flooding by additionally using nearshore wave heights, wave run-up, and flooded dry beach area as proxies (Bergillos et al., 2019b). The two models SWAN and XBeach-G (developed specifically for gravel dominated beaches) were implemented. Transmission and reflection coefficients of the WEC were found experimentally in a wave tank and defined in

SWAN to simulate the wave conditions in the presence of WECs. Results indicated that the configuration specifying a 60° angle between the wedges of WaveCAT WECs results in less flooded dry beach area and provides better protection against flooding for long wave periods.
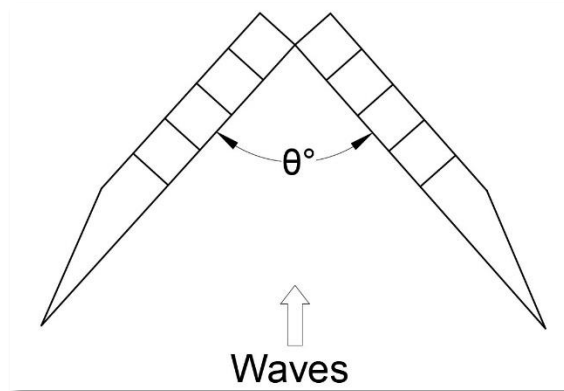
Figure 2-3: Schematic of the WaveCat WEC. Angle between the wedges (θ) can be adjusted. Redrawn from Fernandez et al. (2012, their Fig. 2).

In 2018, another study on the Atlantic coasts of Spain was conducted at Xago Beach, Asturias (Abanades et al., 2018). Xago Beach is a sandy beach, which partially lies in the intertidal zone. A dune area that exists behind the beach has severely eroded in recent years. This specific area is of interest as it is the proposed site for installation of the first WEC farm in the country. This study investigated the impacts of a WEC farm on mitigating coastal erosion by comparing a baseline scenario of a storm condition (maximum significant wave heights exceeding 10 m) with no WEC farm to a storm condition with a WEC farm. Eleven WaveCAT devices were modeled in a wave propagation model with transmission coefficients obtained from laboratory experiments. The authors used impact indicators, such as bed level impact, beach face eroded area, and non-dimensional erosion reduction, to assess the effects of WEC farms on beach morphology. The authors found a reduction in significant wave heights as high as 50% when WECs were present.

Bed level impact, which characterizes the difference in seabed elevation at a point in the beach profile between the baseline and the wave farm scenarios, was found to be over 2 m in the east section of the Xago beach. Non-dimensional erosional reduction, which represents the changes in the eroded area of a standard beach profile with and without the wave farm as a ratio of the total eroded area compared to the initial state of the beach, was found to be 17.64% on average throughout the region. These findings support the idea that wave farms do not negatively impact coastal morphodynamics, and can be used to alleviate severe erosion conditions.

Rodriguez-Delgado et al. (2019c) used artificial neural networks (ANNs) to analyze the impacts of wave farms on coastal erosion in Playa Granada, Spain. The authors aimed to determine the optimal wave farm layout and position for the maximum coastal protection using ANNs, which have lower computational costs than physically-based wave propagation and morphodynamic models. The ANNs were trained with data obtained using SWAN, a longshore sediment transport equation, and a shoreline evolution model. High and low wave energy conditions were represented with corresponding high and low significant wave heights. Two different mean wave directions (east and west) were also considered. The model was applied to various layouts and positions of WECs along the shoreline for 48 hours of wave attack under a combination of wave conditions. Change in the dry beach area was used as a proxy for coastal erosion in applications with and without wave farms. The authors found an increase of approximately 30 m^2 in the dry beach area with the presence of WECs over 48 hours, which translates to ~5400 m^2 increase per year. While most cases resulted in beach accretion with the presence of the WECs, an increase in erosion was also observed for some conditions, demonstrating the importance of thorough, local analyses and optimization studies prior to the deployment of wave farms.

Finally, Bergillos et al. (2019c) and Rodriguez-Delgado et al. (2019a) assessed the performance of WaveCAT WECs under various SLR scenarios. Both studies indicated that WEC farms perform well, if not better with increasing sea levels. WEC farms were found to reverse erosive trends and enable accretion even for the moderate SLR scenario of 0.65 m projected for the year 2100. These studies opened up key discussions of the role of climate change in WEC farms and their morphodynamic impacts, however, the authors called for further research on different types of WECs (i.e., non-floating). Floating WECs move freely with the oscillations of the sea level (Zanuttigh and Angelelli, 2013), and are therefore difficult to use in assessing the impacts of SLR in this context.

The results of the above-mentioned papers are summarized in Table 2-2.

Table 2-2: Methods and the results of the studies conducted for the Spanish coasts

Paper	Methodology	Results
Iglesias and Carballo, 2014	Numerical model (SWAN) and Impact Indicators	• Reduction in wave height and wave power • Impacts of wave farm on the coast vary based on distance to the coast
Bergillos et al., 2018	Numerical models Delft3D-Wave + XBeach-G	• 18.3% and 10.6% reductions in Hs at 10 m water depth and on the coast respectively • 44.5% reduction in erosion in part of the beach and 23.3% in the entire coast
Mendoza et al., 2014	Numerical and Conceptual models WAPOQP by Silva et al. (2006) Long-shore Sediment Transport (LST) equation by Kamphuis (1991)	• Overall reduction in wave height and wave power. • Negative erosion (accretion) observed
Abanades et al., 2018	Numerical models	• 17.64% non-dimensional erosion reduction

28

Paper	Methodology	Results
	SWAN (The deepwater boundary conditions from WaveWatch III) + XBeach	
Bergillos et al., 2019a	Numerical and Conceptual models SWAN + LST equation by van Rijn (2014) + One-line model (Pelnard-Considère, 1956)	• Two WEC configurations under two different storm directions • Concluded that WEC geometry should adjusted based on the sea state
Bergillos et al., 2019b	Numerical models SWAN + XBeach-G loose coupling	• Less flooded dry beach area and better protection against flooding with a 60° angle between the wedges of WaveCAT WECs
Bergillos et al., 2019c	Numerical modeling SWAN + XBeach loose coupling	• Reduction in breaking wave heights: 10% (25%) under westerly (easterly) storms • Reduction in flooded dry area up to 5.7%
Rodriguez-Delgado et al., 2019a	Numerical and Conceptual models SWAN+ LST equation by van Rijn (2014)	• Increase in subaerial beach area (accretion) observed
Rodriguez-Delgado et al., 2019c	Artificial Neural Network (ANN) Validated by SWAN+ LST equation by van Rijn (2014) + One-line model (Pelnard-Considère, 1956)	• 29.59 m² increase in dry beach surface with WECs (5400 m² per year)

2.3.3   *Mexico*

Mendoza et al. (2014) assessed the impacts of a WEC farm for Las Glorias Beach, Mexico in addition to Santander Bay, Spain. Las Glorias Beach is a straight, sandy beach with a short fetch length, resulting in short wave periods and wave heights (Mendoza et al., 2014). Two different WEC types, the Sea Breath and DEXA, were tested in this location under varying wave periods for constant wave heights and wave directions. Similar to the experiments for Santander Bay, a 1-

D elliptic mild-slope equation model, and a 2-D modified elliptic mild-slope equation model were used to simulate the morphodynamics in Las Glorias Beach with and without WEC farms. In addition to the general results discussed in Section 3.2, it was shown that greater wave energy reduction in the lee of WEC farms does not guarantee more accretion on the coast. Comparing the two sites and four WEC types (in total), the authors provided recommendations to assist in the selection of a suitable WEC, placement, and layout for potential WEC farm implementations.

2.3.4 *Ireland*

Irish Atlantic coasts are known to have one of the most energetic wave climates in the world. Ocean wave energy has consequently been recognized as an important renewable energy resource for Ireland. Several marine energy test facilities including the Atlantic Marine Energy Test Site and SmartBay have been actively working to improve marine energy technology (SEAI, 2019). A new test facility called Westwave was proposed for installation off the south-west coast of Ireland and a coastal impact assessment was done as a part of the permitting process. Among the methodologies used in this impact assessment, the ones regarding the impacts of WEC operations on the shores were summarized by Stokes and Conley in their 2018 paper (Stokes and Conley, 2018a). Through a case study in Doughmore Beach in Ireland, the authors also presented a new way of parameterizing the transmission coefficient of WEC arrays (see Section 2.2.1.1) in order to assess the maximum possible energy that can be harnessed. The numerical models SWAN and XBeach were used to simulate two different wave conditions when WECs are operating, i.e., the highest-occurrence wave condition and the 1-year return period wave condition. The authors found a decrease in wave heights under both of these scenarios when three different transmission coefficients (0.00, 0.58, and 0.9) were tested. It was predicted that the beach profile has a higher

sediment volume when the WECs were operated, indicating that the presence of the WEC farm reduced coastal erosion to some degree at Doughmore Beach.

2.3.5   South Korea

Coastal erosion rates are increasing in the eastern coasts of South Korea (Song et al., 2016). Concurrently, the government has been lead to seek renewable energy resources, as South Korea has become one of the world's leading energy importers due to depleting domestic energy resources (U.S. EIA, 2018b). Lee et al. (2011) addressed both of these problems and explored the potential impacts of a wave farm for reducing coastal erosion rates. Donghae City, located on the northeastern coast of South Korea, was selected as a study area. The authors used numerical modeling to simulate the morphodynamic response of the beach with and without the wave farm under winter storm conditions. The represented wave farm consisted of 36 PowerBuoys that were arranged in a 6x6 configuration, with 28-meter spacing between them. The reflection and transmission coefficients, K_r and K_t, were assumed to be 0.5 and 0.74, respectively. Results of the analysis showed a 10% reduction in wave heights when the wave farm was present. A subsequent decrease in the rate of coastal erosion in the area was inferred, and wave farm deployment was proposed as an alternative to hard coastal structures for coastal protection.

2.3.6   Romania

Over the last 30 years, the Romanian shore by the Black Sea has been affected by coastal erosion. There has been a significant loss in the beach face area despite a number of beach nourishment projects (Policy Research Corporation, 2011). The first effort to assess whether a wave farm could help reduce the rate of erosion in this area was made by Zanopol et al. (2014). The authors used

the SWAN model for their assessment, simulating three scenarios with variable depictions of the wave climate (i.e., average conditions, energetic conditions, and extreme events). Four types of WECs were considered (Pelamis, Wave Dragon, Archimedes Wave Swing, and AquaBuoy), along with five different wave transmission conditions ranging from 0% to 100%. Results of the analysis showed that the Wave Dragon is the most effective WEC type for the study location. It had the highest daily energy production with an average value of 13.9 MWh. The authors showed that wave heights can be reduced up to 30% in the nearshore when the wave farms are present, and concluded that lower rates of sediment transport could be expected due to reduced mechanical abrasion.

2.3.7 *Others*

2.3.7.1 Innovative Technologies for Safer European Coasts in a Changing Climate (THESEUS) Project

The Innovative Technologies for Safer European Coasts in a Changing Climate (THESEUS) Project was designed for coastal risk assessment and mitigation in participating European countries (Figure 2-4). It was funded by the European Commission and conducted from December 1, 2009 to November 30, 2013 (THESEUS, 2009). One of the objectives of this comprehensive project was "to propose and analyze a completely innovative solution such as the use of WECs close to the shoreline for contemporary [attenuation of] wave attacks while producing a secondary benefit." In the final report of the project, it was noted that WECs reduce wave heights at the coastline and that utilizing an array of WECs instead of one individual device results in better coastal protection.

Figure 2-4: THESEUS Project Study Sites

2.3.7.2 Streamlining of Ocean WEC farms Impact Assessment (SOWFIA) Project

The European Commission-funded Streamlining of Ocean WEC Farms Impact Assessment (SOWFIA) Project was conducted from October 01, 2010 to September 01, 2013. The aim of SOWFIA was "to achieve the sharing and consolidation of pan-European experience of consenting processes and environmental and socio-economic impact assessment best practices for offshore wave energy conversion developments" (Greaves et al., 2013). Several WEC farm applications and studies were conducted in the participating E.U. nations, each contributing to the outcomes of the project. Objectives, results and expected impacts are summarized in Figure 2-5.
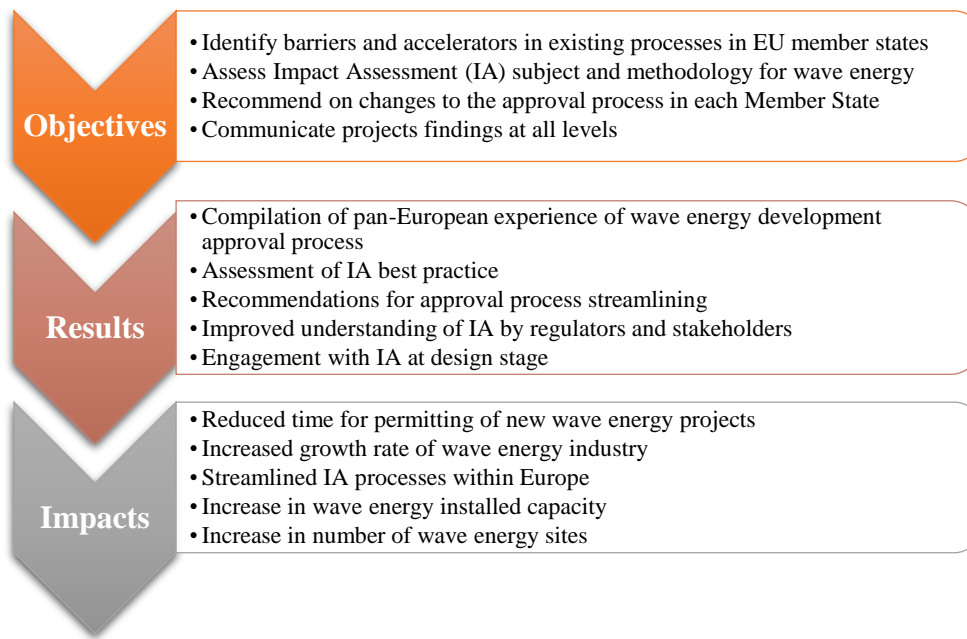
Figure 2-5: Objectives, results, and proposed impacts of the SOWFIA project. Adapted from Greaves et al. (2013, their Fig. 1)

Impacts of the wave farms on coastal geomorphology were assessed at four test centers: the Atlantic Marine Energy Test Site in Ireland (SEAI, 2019), Ocean Plug in Portugal ("Ocean Plug," 2019), SEM REV in France ("SEM-REV," 2019), and Wave Hub in the U.K. (Wave Hub, 2019). This project did not consider wave farms as a coastal defense mechanism, but instead aimed to show that wave farms do not pose harm to the wave climate and/or coastlines, nor do they otherwise disrupt common uses of the beach. It was concluded that the potential impacts of WEC farms would be insignificant compared to naturally occurring coastal processes (Conley et al., 2013). The authors discussed that wave farms potentially alter beach morphology only if the reduction in the wave heights due to the presence of WECs exceeds 30% but predicted a reduction of only 6%. The findings of this study are not in agreement with many others. For example, more recent studies in Europe (Sections 2.3.1, 2.3.2, 2.3.6) have shown that WECs can reduce wave

34

heights by approximately 30%. Furthermore, this percentage can potentially be increased by improved efficiency in WEC technology, which would likely result in amplified impacts on coastal processes.

2.3.7.3 Experimental studies

In addition to the internationally funded projects, several experimental studies, not necessarily specific to any particular location, have also been conducted (Ruol et al., 2010; Xu and Huang, 2018; Zanuttigh and Angelelli, 2013). Xu and Huang (2018) focused on implementing WECs as a way of shoreline protection. The WEC type used in their study was an oscillating water column (OWC) integrated into a pile breakwater, as it was found to be the most optimal choice in terms of safety and costs. An OWC is a bottom-sitting, fixed WEC type which is positioned outside the surf zone for better extraction of wave energy. The experimental study used a wave flume in the Hydraulic Modeling Laboratory at Nanyang Technological University in order to model conditions with and without the OWC. It was determined that some wave parameters and coastal conditions were not affected by the presence of the OWC, however, changes in the wave height and wave period were observed. The authors concluded that embedding OWCs into pile breakwaters provides clean energy and reduces the cross-shore sediment transport that causes erosion.

Zanuttigh and Angelelli (2013) used a wave basin at the University of Aalborg to test floating WECs for coastal protection. The wave basin was 15.7 x 8.5 x 1.5 m and used to generate short-crested waves. This allowed researchers to test WECs under both deep and shallow water conditions. A single DEXA WEC device was deployed in the wave basin at two different model prototype scales, 1:30 and 1:60. The experimental results showed a decrease in wave power in the

lee of the WEC. Changes in wave direction in the presence of the WEC were also observed, which has implications for the direction of sediment transport. It was stated that the depth of the WEC did not significantly alter the hydrodynamics, and the authors concluded that the impacts of a floating WEC would not be altered by potential changes in the water depth due to sea level rise. Thus, floating WECs have the potential to provide coastal protection, and adapt to climate change conditions.

Ruol et al. (2010) used an experimental approach to assess how the implementation of a DEXA WEC array in Marina di Ravenna beach (Italy) could affect the coast in the context of sediment transport. Experiments were conducted in the wave basin of Aalborg University. The DEXA model was reproduced at a 1:20 model:prototype scale. The transmission coefficient and the device efficiency were determined to range from 10 – 35% and 0.6 - 0.9, respectively. The results of the experiments were then used to calculate the alongshore sediment transport in the presence of the representative wave farm via the CERC formula (Hales, 1981). Comparison of the amount of alongshore sediment transport with and without the wave farm showed a clear difference between the two scenarios. When the transmission coefficient was assumed as 0.8, the alongshore sediment transport in the wave farm scenario was reduced by 43% relative to the baseline scenario. In other words, the WEC farm reduced alongshore erosion, providing increased coastal protection. The authors also noted that the reduction in sediment transport is variable depending on wave conditions (e.g. wavelengths).

2.4   Conclusions

In this paper, we have reviewed a number of recent studies that have assessed the impacts of WEC farms on coastal morphodynamics. We have discussed common methodologies as well as the findings of individual studies. Numerical modeling is the most prevalent approach to the reviewed impact assessments, with SWAN (a wave propagation model) and XBeach (a morphodynamic model) being the most widely used models. Results of the reviewed studies show that WEC farms do not negatively impact coastal morphodynamics, and in fact often reduce coastal erosion, as they act as a physical barrier against wave attack (i.e., they have breakwater behavior due to induced wave reflection) and also reduce wave heights by extracting wave power. Moreover, multiple studies concluded that sediment deposition increases near the shore due to the ensuing lower energy waves. It is noted that the distance between the WEC farm and the shoreline, as well as the configuration of the individual devices, plays a major role in the extent of erosion reduction.

The reviewed studies contribute to renewable energy research and practice in substantial and unique ways, however, we have identified several research gaps. A number of the reviewed studies aimed to demonstrate that WEC farms can be used for coastal protection, however, it is unclear whether the suggested optimal conditions for reducing coastal erosion (i.e., the location and layout of the WEC farm) also maximize wave power generation. Further study is needed to determine the optimal design and position of WEC farms so that both the wave energy conversion and the coastal protection capacities are maximized in order for deployments to be practical. Additionally, the duration of each of the studies reviewed was less than one year with the exception of the Ph.D. thesis discussed in Section 2.3.1, and in most cases only one storm condition (1-2 days) is simulated. Since a typical WEC farm installation has a design life of approximately 25 years,

longer-term studies are needed to comprehensively assess the impacts of WEC farms on coastal erosion. As discussed in Section 2.2.1.2, current numerical morphodynamic models are not capable of simulating the long-term impacts of WEC farms on coastal erosion, therefore, there is an illustrated need for numerical morphodynamic model development. Conceptual models may be an appropriate alternative in the meantime. In general, impacts of climate change were not considered. In two of the studies discussed in Section 2.3.2 coastal morphodynamics were simulated under three different sea-level scenarios. While this approach provides some insight into potential effects of sea level rise, it neglects other factors (such as long-term changes in wave climate, as discussed in Bergillos et al., 2019c; storm climatology; land subsidence; and also WEC efficiency) that will likely affect relevant hydrodynamics and morphodynamics in the coming decades. Thus, longer-term studies that more fully account for the impacts of climate change are needed. Finally, the existing studies primarily focused on European coastlines. The Americas have not been studied with the exception of one study that included a beach in Mexico. The U.S. and Canadian coastlines have considerable wave power (particularly along the North Pacific coast) and also suffer from coastal erosion. WEC farms could thus provide a viable alternative to traditional methods of energy generation and coastal protection in these regions. Future studies should more adequately assess the effects of WECs on morphodynamics in the Americas.

2.5   Acknowledgements

represent the official views of the Gulf Research Program of the National Academies of Sciences,

Engineering, and Medicine.

CHAPTER 3: THE POTENTIAL OF WAVE ENERGY CONVERSION TO MITIGATE COASTAL EROSION FROM HURRICANES

The content in this chapter is submitted as: Ozkan, C., Mayo, T., & Passeri, D.L., (2020). Potential of Wave Energy Conversion to Mitigate Coastal Erosion from Hurricanes. *Renewable Energy, Submitted*

3.1 Introduction

Beach erosion is a global coastal hazard with catastrophic consequences due to the land and property loss that can ensue. Of the world's sandy beaches, 24% of them are experiencing erosion rates exceeding 0.5 m/yr (Luijendijk et al., 2018). In the U.S., environmental agencies have described stretches of the Gulf of Mexico (GOM) and Atlantic coastlines as critically eroding, which is defined as "*a segment of the shoreline where natural processes or human activity have caused or contributed to erosion and recession of the beach or dune system to such a degree that upland development, recreational interests, wildlife habitat, or important cultural resources are threatened or lost*" by Florida Department of Environmental Protection (2019). The average coastal erosion rate along the Atlantic coast of the U.S. is reported to be 0.6 to 0.9 m/yr (National Ocean Service, 2020). Coastal erosion rates are expected to increase in the coming years, and even those coastlines that are currently stable or accreting may begin to experience erosion (Masselink et al., 2020). Furthermore, coastal regions are often heavily urbanized and densely populated, comprising nearly 40% of the U.S. population (NOAA, 2016). The population in coastal areas increased by 39% from 1970 to 2010, and this upward trend is projected to continue (NOAA, 2013). The growing coastal population and climate change impacts (e.g., rising sea levels and increasing severity of tropical cyclones) make coastal regions increasingly vulnerable to erosion.

An increase in coastal flood frequency and extreme events is expected over the coming decades, which will accelerate beach and cliff erosion (Taherkhani et al., 2020).

As a result, efforts to mitigate the effects of coastal erosion have intensified. The construction of seawalls, breakwaters, revetments, and jetties, in addition to beach renourishment projects are some of the more traditional coastal engineering approaches to mitigation. However, these conventional methods may not adapt well to the changing climate, and nature-based solutions may be a better alternative (Morris et al., 2020). Greener alternatives, including wetland protection and construction of living shorelines have been explored in recent years (Kibler et al., 2019; Seddon et al., 2020; Temmerman et al., 2013). While these strategies provide solutions to coastal erosion, they fail to address the root causes of the hazard and often require substantial maintenance. For example, beach nourishment projects in Sand Key, FL have been implemented 26 times since 1961 with a total cost of $142 million (ASBPA, 2019). A seawall repair project in Ellis Island, NY proposed in 2010 is expected to cost stakeholders a total of $29 million in addition to the initial cost of construction (US Department of the Interior, 2016). In this study, we explore a sustainable approach to mitigating coastal erosion through wave energy conversion.

Wave energy conversion is the process of converting the kinetic and potential energy of ocean waves into mechanical or electrical energy. Ocean wave energy is abundant, consistent, and highly predictable and is an emerging source of renewable energy (Ozkan and Mayo, 2019). Energy in the waves can be harnessed and converted into electricity through devices known as wave energy converters (WECs). WECs are commonly configured in arrays, i.e., wave farms, in order to increase the span across which waves can be captured and to optimize the use of materials such as underwater cables that are used to transfer the generated electricity to the shore. Although the

initial cost of wave farms can be high (Dalton et al., 2009; Rusu and Onea, 2018), coastal communities can doubly benefit from them because they not only provide electricity but also have the potential to reduce coastal erosion. An increasing number of studies have begun to explore the impacts of WECs on coastal morphodynamics and have illustrated that they often mitigate coastal erosion for gravel and sandy beaches through wave dampening (i.e., removing the energy of the waves), wave reflection (i.e., acting as a physical barrier), and reducing the bottom shear stress (Abanades et al., 2018, 2015a; Abanades et al., 2014b; Abanades et al., 2015b; Abanades et al., 2014a; Bergillos et al., 2020, 2019a, 2019c, 2019b, 2018; Gonzalez-Santamaria et al., 2013; Jones et al., 2018; Ozkan et al., 2020; Rijnsdorp et al., 2020; Rodriguez-Delgado et al., 2019a, 2019b, 2018b, 2018a; Rusu and Onea, 2018; Stokes, 2015; Stokes and Conley, 2018b; Xu and Huang, 2018). Studies to date have been focused mostly in Europe, with one study in the U.S. carried out for Newport, OR (Jones et al., 2018).

In this study, we use the numerical morphological model XBeach to simulate the impacts of wave energy conversion on coastal erosion on a barrier island on the U.S Gulf Coast. We perform a case study focused on Dauphin Island, AL, where we used XBeach to simulate baseline (i.e., with no wave farm) and wave farm scenarios under severe storm (Hurricane Ivan and Hurricane Katrina) conditions and analyze the impact of WECs on beach profiles, dune heights, total water levels (TWL), bottom shear stresses, and total sediment volume/area of the coastline.

3.2 Case Study

3.2.1 Location

Dauphin Island is located in the Gulf of Mexico off the coast of mainland Alabama (Figure 3-1). It is a narrow, 25 km long, low-lying barrier island with an average elevation of 2.18 m above mean sea level (USGS, 2017). Dauphin Island has a diverse topography with beaches, dunes, wetlands, maritime forests, and freshwater ponds. The eastern portion of the island has a double-dune structure, and the middle and western parts of the island have relatively lower elevations.

Figure 3-1: Study location; Dauphin Island, AL.

The average annual offshore wave power density in this region is approximately 1.7 kW/m (NREL, 2020). This wave action, along with the regular occurrence of tropical cyclones, has made Dauphin

Island especially vulnerable to coastal erosion. The rate of coastal erosion was estimated as 4.7 m/yr at the beginning of the century (Morton et al., 2004). Dauphin Island has undergone substantial morphological changes over the past century due to coastal processes and extreme events, causing breaches and island migrations (Givens, 2019). Specifically, Dauphin Island has experienced each of the Sallenger storm impact scale categorizes, i.e., swash, collision, overwash, and inundation (Sallenger, 2000). Swash (i.e., when TWL is lower than the dune toe) and collision (i.e., when TWL exceeds the dune toe) regimes can be observed under fair weather conditions across the island. On the western portion of the island, overwash regime (i.e., when water levels gradually increase and exceed the dune crest) and inundation (i.e., when the TWL exceeds the height of the entire beach system) have also been experienced historically under storm conditions due to lower elevations. On the East portion island, however, the collision regime is more prevalent due to higher elevations and double dune structure.

There have been substantial efforts to protect and stabilize the inhabited eastern and middle portions of Dauphin Island through the construction of groins and breakwaters (Cebrian, 2019; Morton et al., 2004). Dunes have also played an essential role in regulating storm impacts. In the eastern portion of the island, dune heights reaching up to 3 m have been constructed and fortified to defend the homes and infrastructure behind them; however, this region remains subject to significant morphological change. The low elevation of the middle portion of the island makes it particularly susceptible to breaching (Hansen and Sallenger, 2020). During Hurricane Katrina in 2005, a breach was generated in the middle of the island (known as "Katrina Cut") and has since been restored with rocks, but the area remains vulnerable to substantial wave attack and storm surges. The uninhabited western portion of the island is the most susceptible to collision, overwash,

and inundation during storm events due to the low dune heights (less than 1.5 m) and the absence of protective structures. Figure 3-2 shows the pre-storm bed elevations at three cross-shore transects along the island.
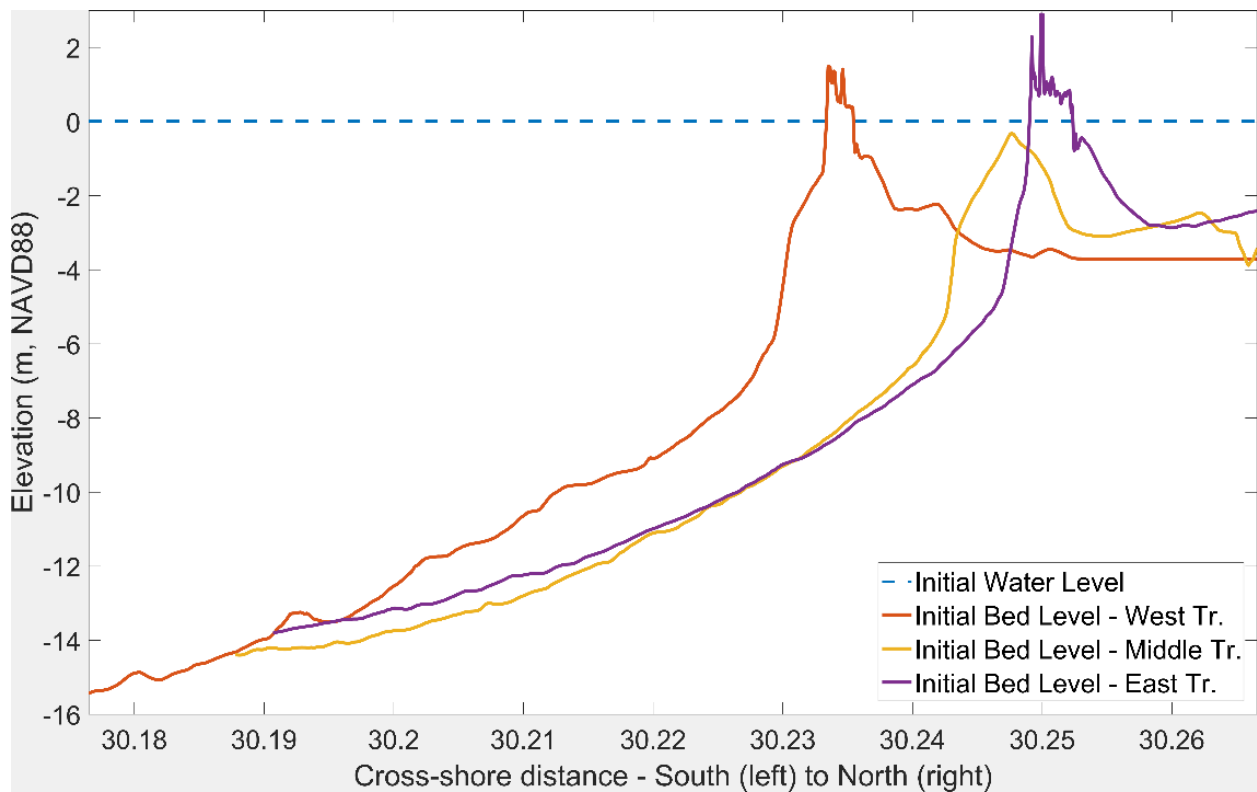
Figure 3-2: Initial Profiles (Pre-storm Bed Levels) and Water Level (dashed line) for West, Middle, and East transects shown in Figure 3-4.

3.2.2   *Hurricanes*

Dauphin Island has been impacted by ten major hurricanes in the past 25 years. For this study, we focused on simulating the impacts of two major hurricanes that affected Dauphin Island, AL during this time period: Hurricane Ivan and Hurricane Katrina. Hurricane Ivan occurred in 2004 and was one of the most catastrophic storms in U.S. history (FEMA, 2016; National Hurricane Center - NOAA, 2018). After peaking in strength, Ivan traveled northward across the GOM and made

45

landfall in Gulf Shores, Alabama as a Category 3 (Figure 3-3). It was ultimately responsible for

$20.5 billion in property damage (National Hurricane Center - NOAA, 2018) and 32 confirmed

deaths in the U.S. (FEMA, 2016). Hurricane Katrina made landfall in southeast Louisiana as a

Category 3 hurricane (Figure 3-3); and became the costliest natural disaster in U.S. history at that

time, causing $125 billion in property damage (National Hurricane Center - NOAA, 2018). To

compensate for the losses, The National Flood Insurance Program funded nearly $15 million to

insurers in Dauphin Island alone (Gaul, 2019). Katrina was also responsible for 1833 confirmed

deaths, including two that occurred in Alabama (Knabb et al., 2005).
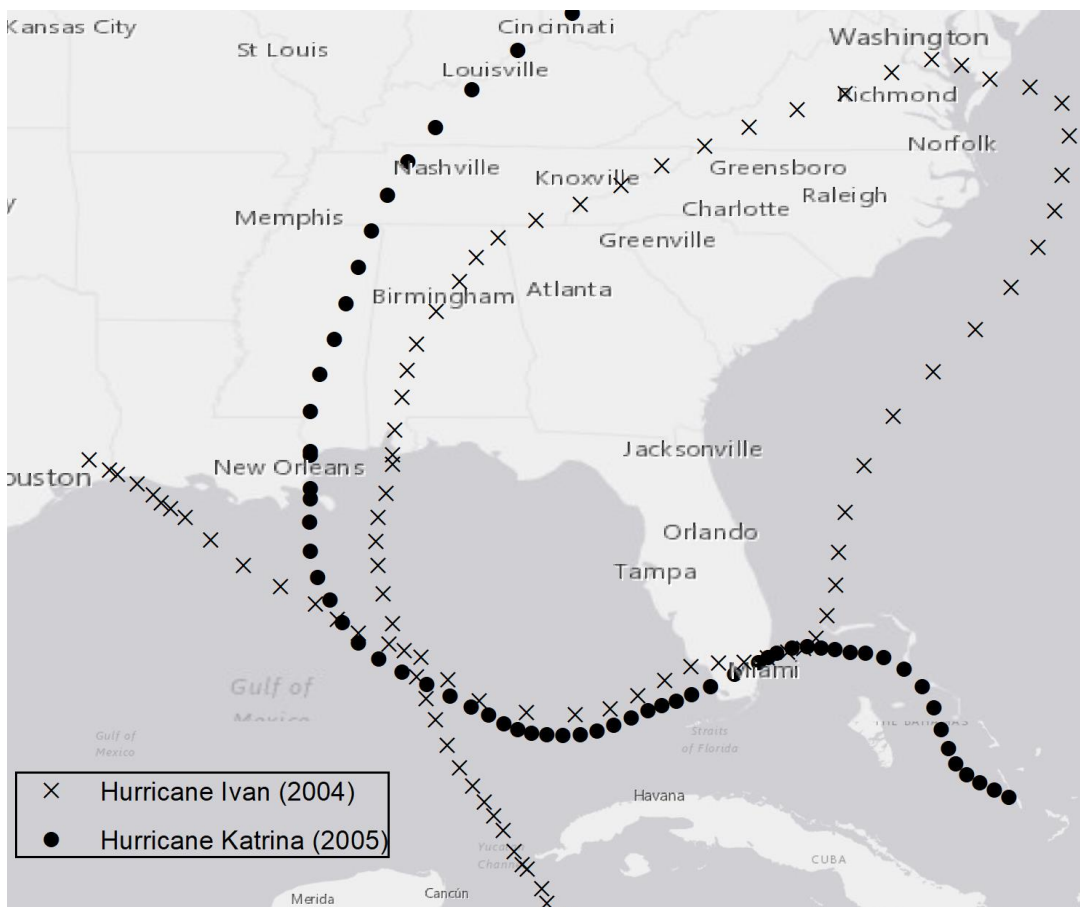
Figure 3-3: Hurricane Tracks of Ivan and Katrina

3.3   Methodology

XBeach is an open-source, process-based numerical model, and here we use version 1.23.5527 (Roelvink et al., 2009). This model was developed to simulate hydrodynamic and morphodynamic processes and their impacts on sandy coastlines. Specifically, it can simulate wave-induced currents and the consequential sediment transport and morphological changes. It simultaneously solves equations defining the short wave action balance, mass and momentum balance, roller energy balance, nonlinear shallow water flow, sediment transport, and bed update processes (Roelvink et al., 2018). The spatial scale of XBeach can be on the order of several kilometers, and its time scale is on the order of several days, i.e., the duration of a typical severe storm. XBeach resolves the hydrodynamic processes of short and long wave transformation, wave-induced setup, and overwash and inundation across a user-specified grid. Morphodynamic processes, including bedload and suspended sediment transport, bed update and breaching, and dune face avalanching are also resolved. XBeach has been effective in modeling hydrodynamics and storm-induced beach and dune evolution in 1D and 2D on a variety of coastlines (Abanades et al., 2014; Abanades et al., 2014a; Bergillos et al., 2018; Enríquez et al., 2019; Passeri et al., 2018a; Stokes and Conley, 2018a), making it a useful tool for investigating the morphological changes induced by the hydrodynamic effects associated with wave farms.

3.3.1   Model Setup and Assumptions

Here, we use a previously validated two-dimensional model domain for Dauphin Island (Passeri et al., 2018b). It covers approximately 6 km seaward, 3.5 km landward, 3.5 km westward, and 2 km eastward of the island's extent (Figure 3-4). The alongshore spatial resolution is 25 m, and the

variable cross-shore spatial resolution ranges from 12.5 m in the offshore to 3 m across the subaerial island.
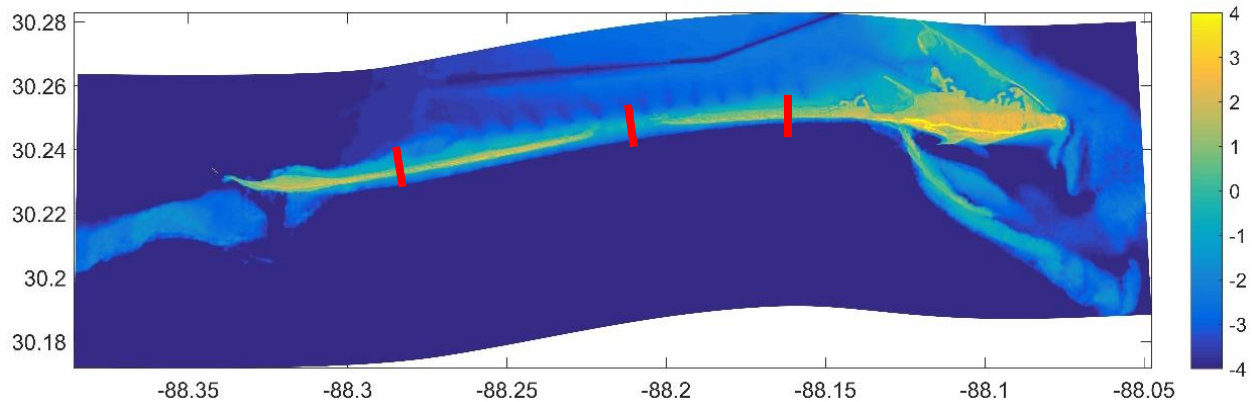
Figure 3-4: XBeach model domain, pre-Ivan elevations (m, NAVD88), and cross-shore transects (red lines) analyzed in this study. The Latitude and Longitude coordinate system is used.

The topographic and bathymetric data were derived from a post-Katrina digital elevation model (Danielson et al., 2013). This dataset describes the Katrina Cut, i.e., the breach that occurred in the middle of the island after Hurricane Katrina in 2005 (Figure 3-4, middle transect). Using this data set allows us to simulate the impacts of Hurricane Ivan and Hurricane Katrina under present-day conditions with and without the wave farm. Bed friction coefficients were parameterized using spatially variable Chezy coefficients based on land use/land cover data (Passeri et al., 2018b).

A number of previous studies have used numerical wave models such as Simulating Waves Nearshore (SWAN) to investigate hydrodynamic impacts of WECs, specifically the behavior of the wave climate in the lee of the wave farms. WECs are often represented as partially transmitting and partially reflecting obstacles through transmission and reflection coefficients (K_t and K_r, respectively), which define the ratio of transmitted or reflected wave heights to incident wave heights (Ergin, 2009). These coefficients are specific to individual WEC devices and also the

48

configuration of the wave farm and are generally estimated from laboratory experiments (Bergillos et al., 2019b, 2019a; Fernandez et al., 2012b). Both K_t and K_r range from 0 to 1, where $K_t = 0$ represents complete energy absorption by the WECs (no wave transmission through the WEC farm) and $K_t > 0$ represents partial to full wave transmission. Similarly, $K_r = 0$ represents no wave reflection by the WECs and $K_r > 0$ represents partial to full wave reflection (Ergin, 2009). The presence of a wave farm can also be represented through wave parameters, such as wave heights and wave periods, obtained from the wave model, and are then used as input to morphological models to investigate the morphological changes caused by WECs (Abanades et al., 2014a, 2014b).

In this study, WECs are represented in the XBeach model through adjustments to the offshore boundary conditions, which are extracted from a coupled Advanced Circulation (ADCIRC)+SWAN model (Bilskie et al., 2016; Luettich et al., 1992). A hypothetical wave farm is assumed to be located along the offshore boundary since the adjustments to boundary conditions are made to the offshore boundary. JONSWAP (Joint North Sea Wave Project) wave spectra data describing the wave climate (i.e., significant wave heights, peak frequencies, directional spreads, and main wave angles) during Hurricane Ivan and Hurricane Katrina are applied uniformly to the offshore boundary. Time-series of hourly water levels are forced uniformly across the onshore and offshore grid boundaries for Hurricane Ivan. For Hurricane Katrina, water levels are forced at the four corners of the XBeach grid (Passeri et al., 2018b). The XBeach model is executed in surfbeat (instationary) mode to develop the baseline scenario (i.e., the case without WECs). Next, the significant wave heights are reduced by 30% to represent the hydrodynamic effects of WECs based on recent estimates of WEC efficiency (Abanades et al., 2014a; Rijnsdorp et al., 2020), while water

levels, wave directions, and peak wave periods remain the same. The XBeach model is then simulated for the wave farm scenario, and differences between the two cases are investigated. With this approach, physical wave to WEC or WEC to WEC interactions are not captured, i.e., we only represent the energetic effects of wave farms. It should also be noted that since the waves are forced on the offshore boundary, the effects of any localized wind waves are not resolved, i.e., we are only assessing the effects of the wave farm on the offshore waves that propagate landward. This serves as a fundamental step in understanding the minimum potential of WECs to reduce coastal erosion, as including physical effects would likely cause an additional reduction.

3.4 Results

3.4.1 Hurricane Ivan

3.4.1.1 Response of Water Levels and Nearshore Wave Climate to Simulated Wave Farms

Here we compare the output of the baseline (i.e., significant wave heights (Hs) unchanged) and wave farm (Hs reduced by 30%) simulations to assess the impact of WECs. Peak water levels during Hurricane Ivan, and the pre- and post-storm bed levels for the baseline and wave farm scenarios are presented in (Figure 3-5). The TWL exceeds most dune heights and inundates a significant portion of the island in both the baseline and wave farm scenarios. Peak water levels measured at the beach face for the baseline scenario are higher than those observed in the wave farm scenario along the west and middle transects, by 0.3 m and 0.1 m, respectively (Figure 3-5a and b). Along the east transect, however, the peak offshore water level in the wave farm scenario (where the Hs is lower) is ~0.5 m higher than that in the baseline scenario, and overtops the primary dune causing erosion with sand deposited in the nearshore (Figure 3-5c). This is in contrast to the

baseline scenario, where the collision regime is observed at the primary dune, which causes avalanching. This is likely due to nonlinear superposition of swell waves and wind waves, which can create higher TWL at irregular locations (Badulin et al., 2008; Vethamony et al., 2011). Additionally, the impact of the reduction in wave heights due to WECs on TWL varies in the north-south direction, as the hydrodynamics are also influenced by the bottom surface (i.e., friction and topography) and geometry of the island. This illustrates that the TWL is not always directly related to the wave heights defined on the offshore boundary. In other words, the role of WECs in potentially changing the TWL or the regime varies across the coast. The maximum water levels reached at each grid cell during the simulation for the baseline and wave farm scenarios, as well as the difference between the two scenarios, are illustrated in Figure 3-6. Overall lower maximum water levels are observed in the wave farm scenario (Figure 3-6b) compared to those observed in baseline scenario (Figure 3-6a). Calculating the difference in maximum water elevation of the two model scenarios illustrates the alongshore variability in maximum TWLs, where the wave farm scenario had high water levels compared to the baseline scenario near the eastern portion of Dauphin island (Figure 3-6c). Conversely, the opposite is illustrated for the western portion; therefore, it should not be assumed that reduced wave heights offshore will result in uniformly lower total water levels across the whole domain. For this storm, the wave farm is more effective in reducing the TWL in the western part of the island where the water levels are the highest in both baseline and wave farm scenarios, which may have implications for the ideal configuration of wave energy converters to achieve similar efficacy in the eastern region. Also, this may mean that WECs make a bigger impact on the areas with high max water levels. Focusing on the western portion of the island, Figure 3-6d and Figure 3-6e show that the dry areas are more prevalent for

the wave farm scenario than the baseline indicating that the presence of wave farms reduces overtopping and inundation at this location.
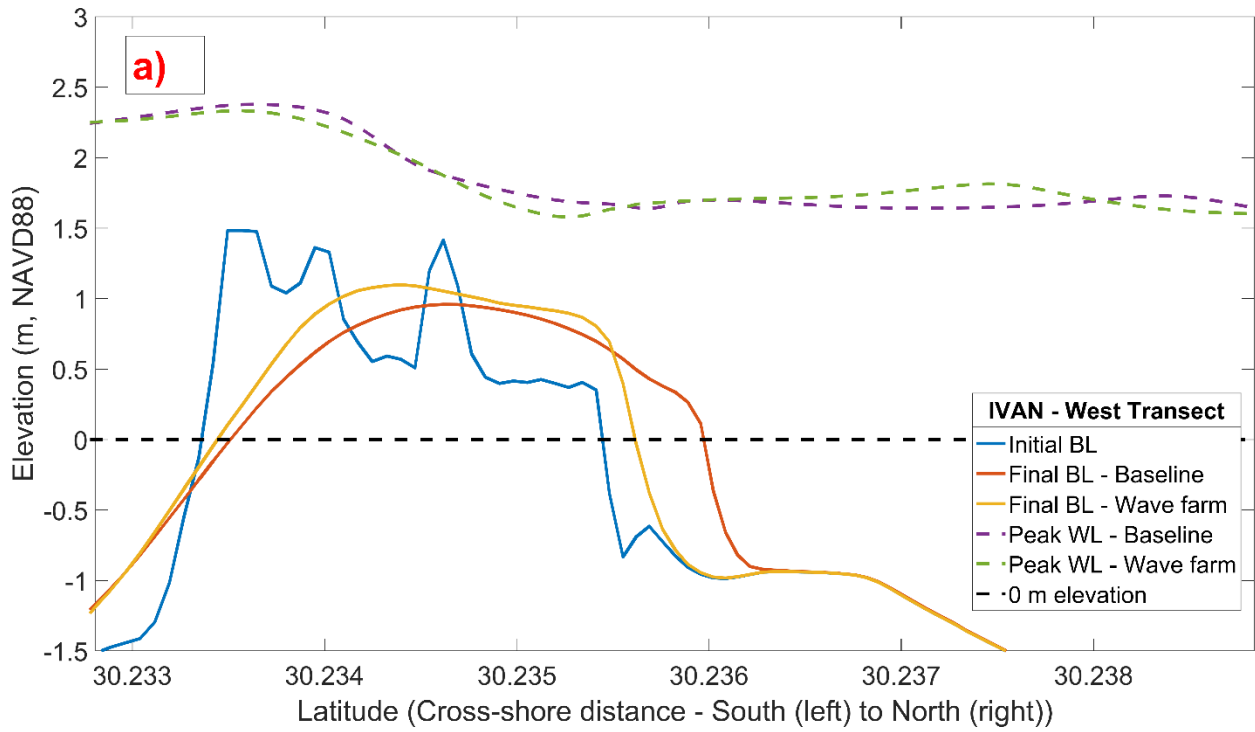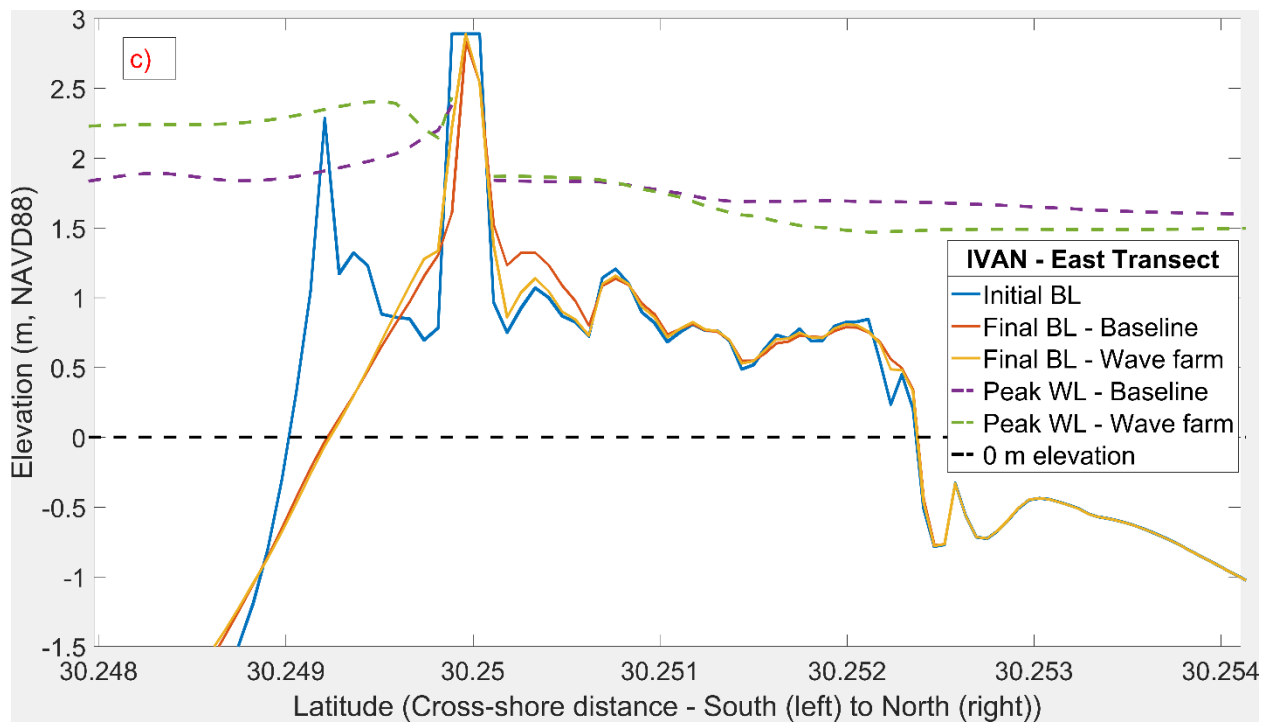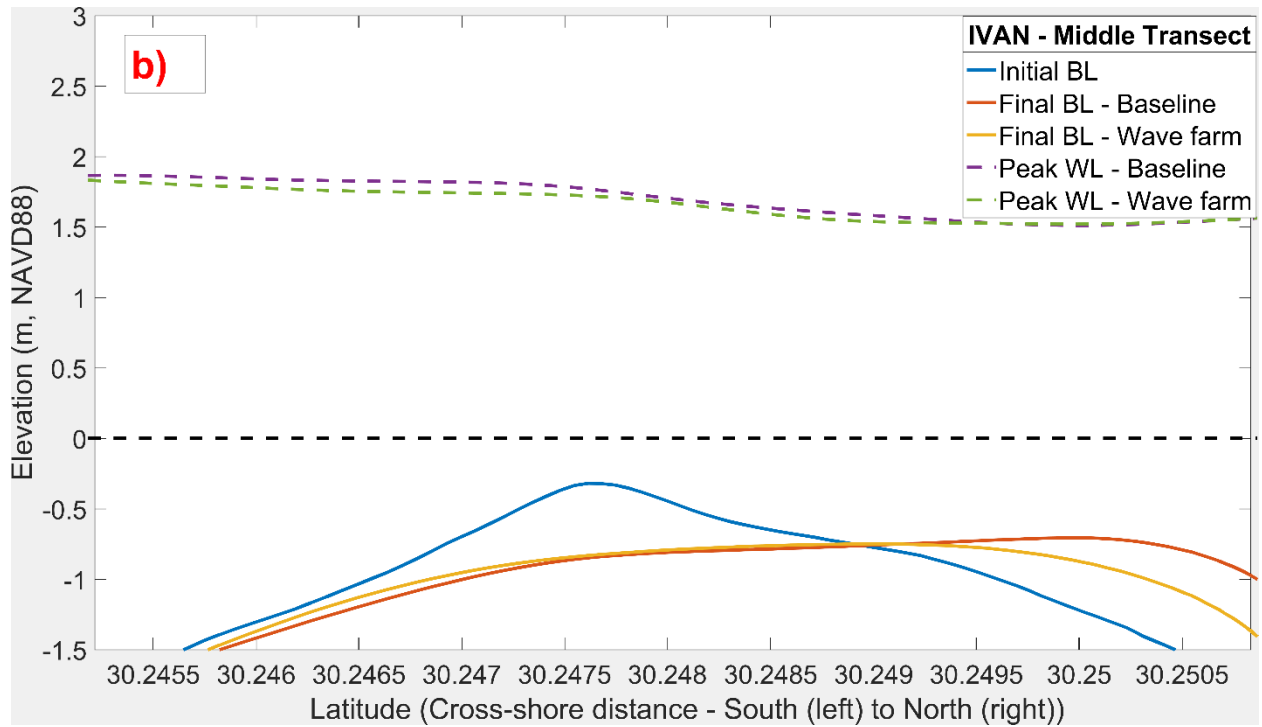
Figure 3-5: Hurricane IVAN Bed levels (BL) and water levels (WL) under baseline and wave farm scenarios. Note that the figures are zoomed in for readability. Initial WL is at the zero-level for all transects.
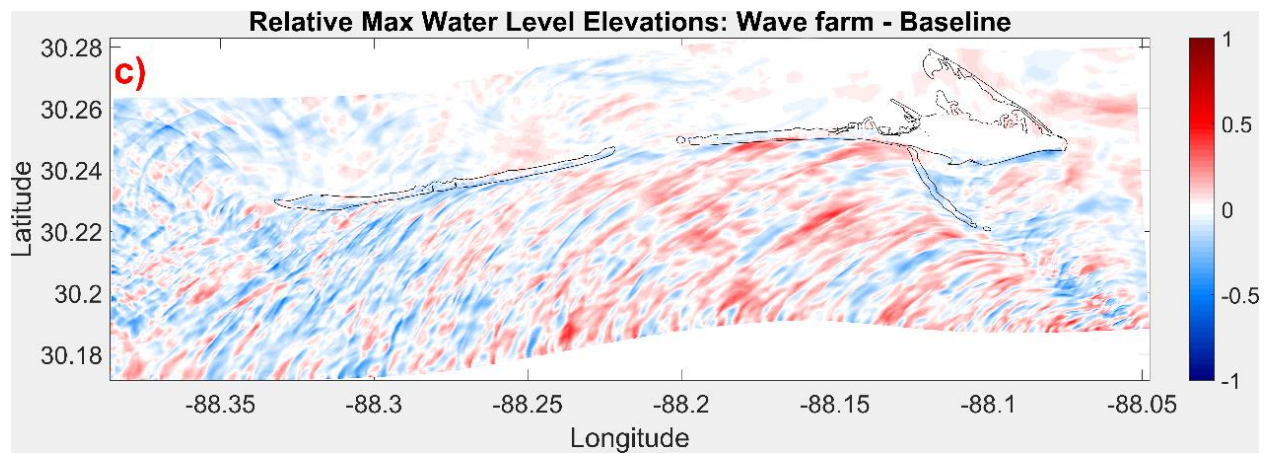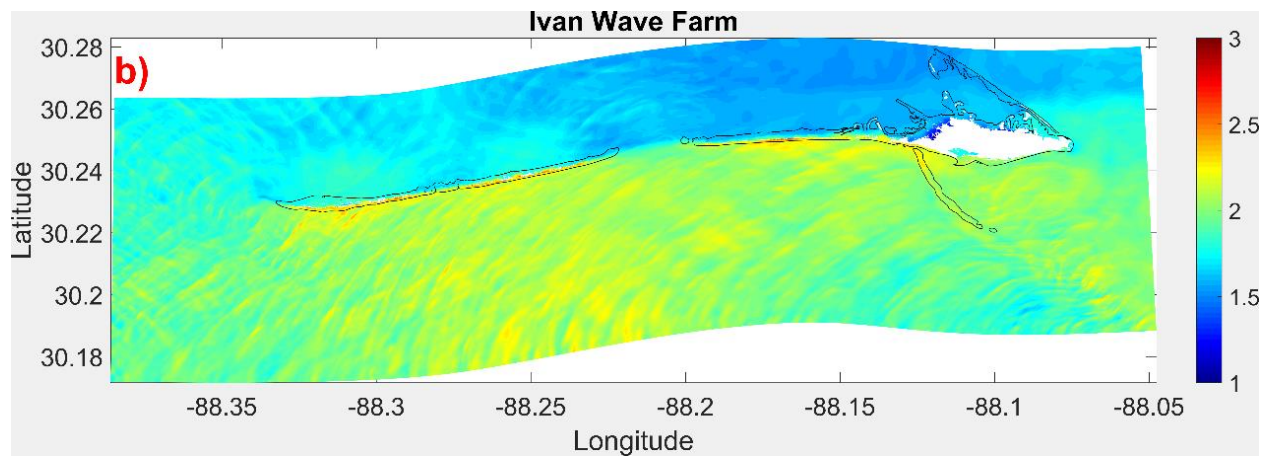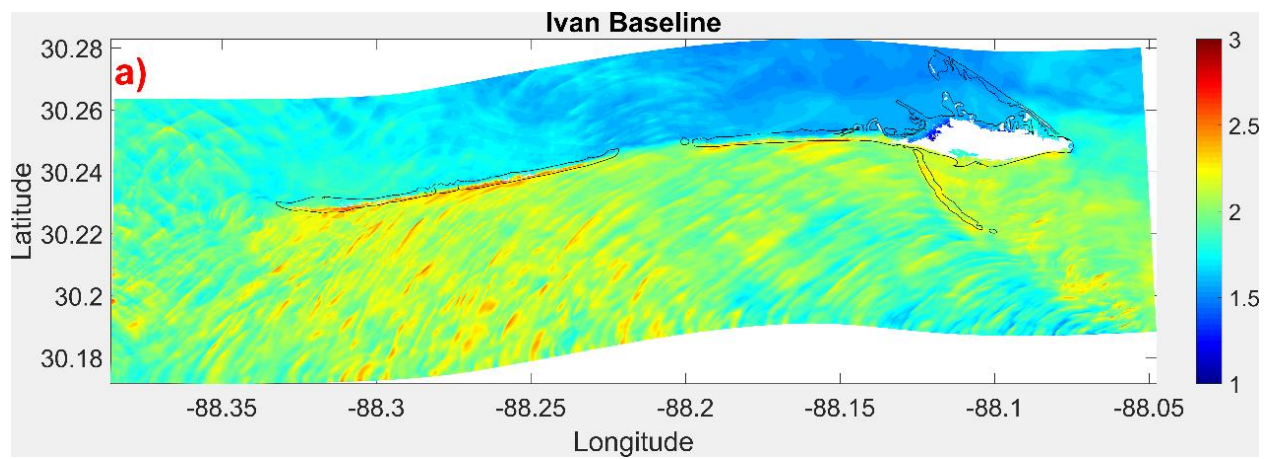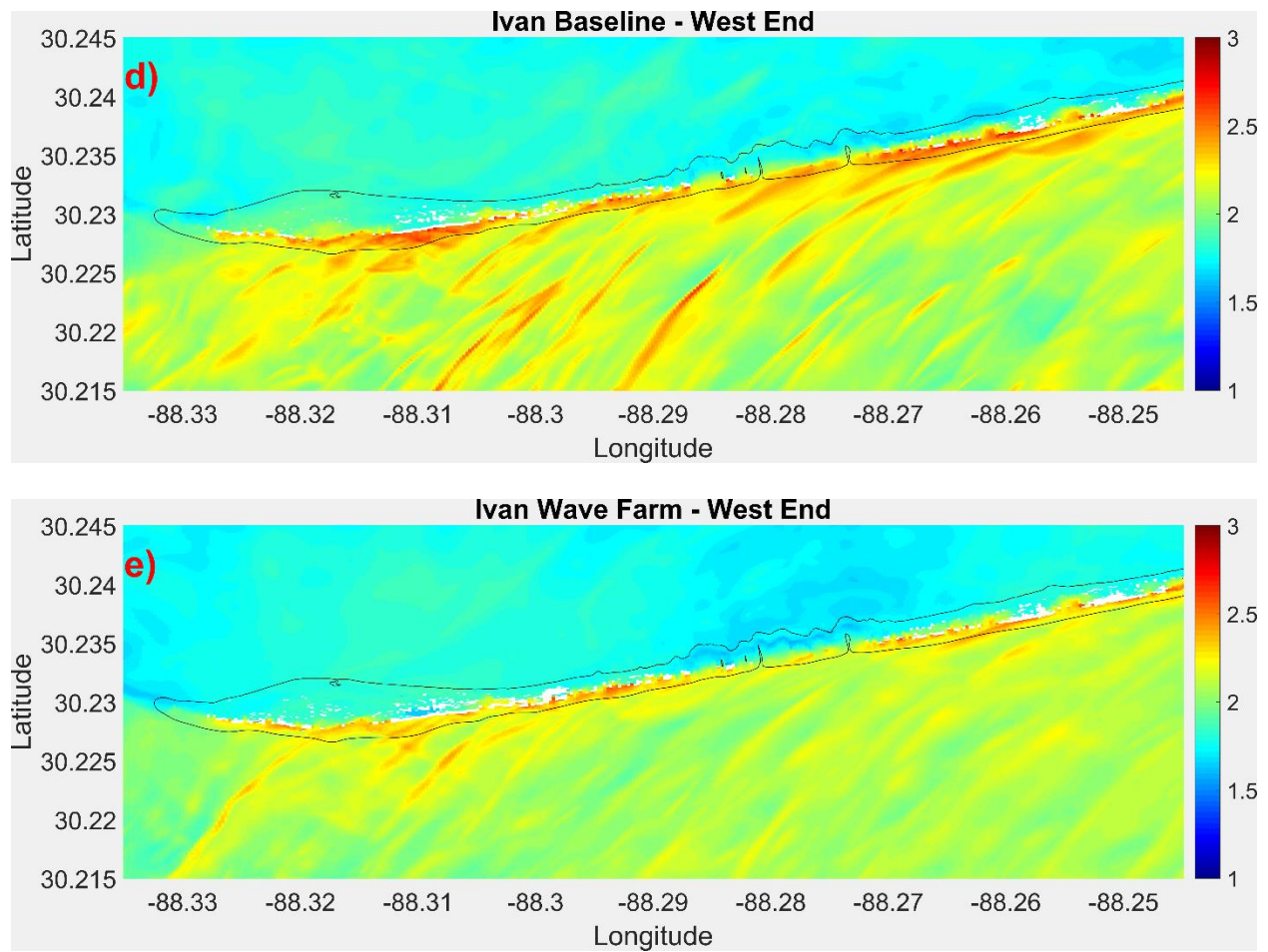
Figure 3-6: Hurricane Ivan - Max Water Levels observed at each grid cell throughout the storm for baseline (a) and wave farm (b) scenarios (c) Difference between the two scenarios: b subtracted from a. (d) and (e) Magnified versions of (a) and (b), respectively. White patches are the dry areas, and the black line is the post-storm zero-meter contour of the island.

We examined how WECs impact wave-induced erosion by analyzing the maximum Hs across the domain in both scenarios (Figure 3-7). It is observed that the Hs in the wave farm scenario is lower for the wave farm scenario as expected due to the adjustment in Hs on the offshore boundary condition to represent the wave farm. On average, the nearshore wave heights in the wave farm scenario were found to be 0.3 m lower than the baseline scenario, which results in lower potential erodibility due to decreased wave action (Figure 3-7c). There are some areas where the wave farm

did not make any impact, i.e., the white areas indicating the same Hs for both scenarios. Also, Hs in the wave farm scenario appears to be slightly higher in the east and west of the island compared to the baseline scenario, indicating that the impact of WECs on wave height is reversed in the sheltered areas (east of the island) and landward of breaches. Figure 3-7c illustrates that the impacts of WECs on Hs are not uniform, and we see pockets of no differences due to the complex hydrodynamics. We mostly see no change in Hs behind the island with the exception of the Katrina Cut; here, we again see higher wave heights in the wave farm scenario, likely due to the channeling that is discussed in Section 3.4.1.2. In Figure 3-7d, the percent difference in Hs is presented, and although the wave heights at the offshore boundary are reduced by 30% to represent the wave farm, this percent change was not constant as waves propagate to the coast. In some areas, up to 50% reduction in Hs is observed (circled locations in Figure 3-7d) in the wave farm scenario. This suggests that the impacts of a wave farm on Hs are broader than its local circumference (i.e., the offshore boundary in this case).
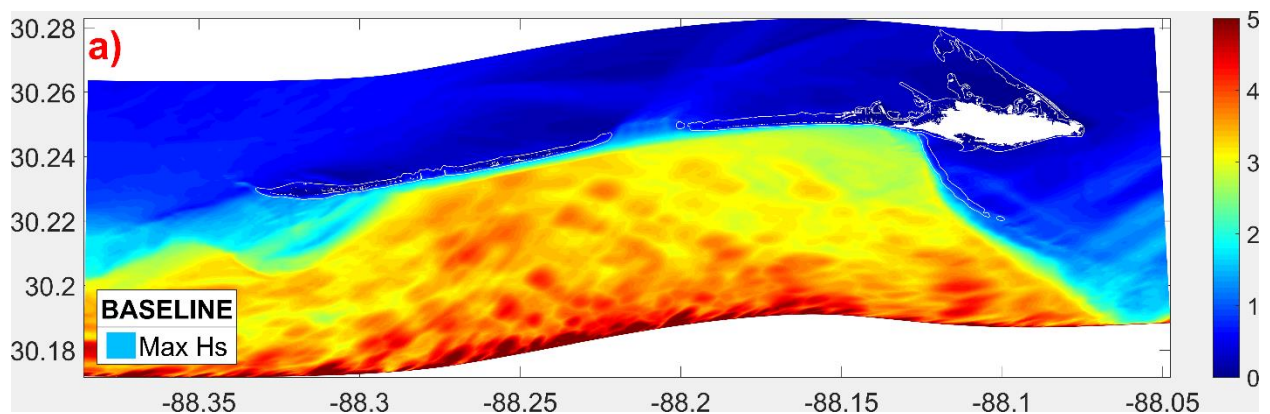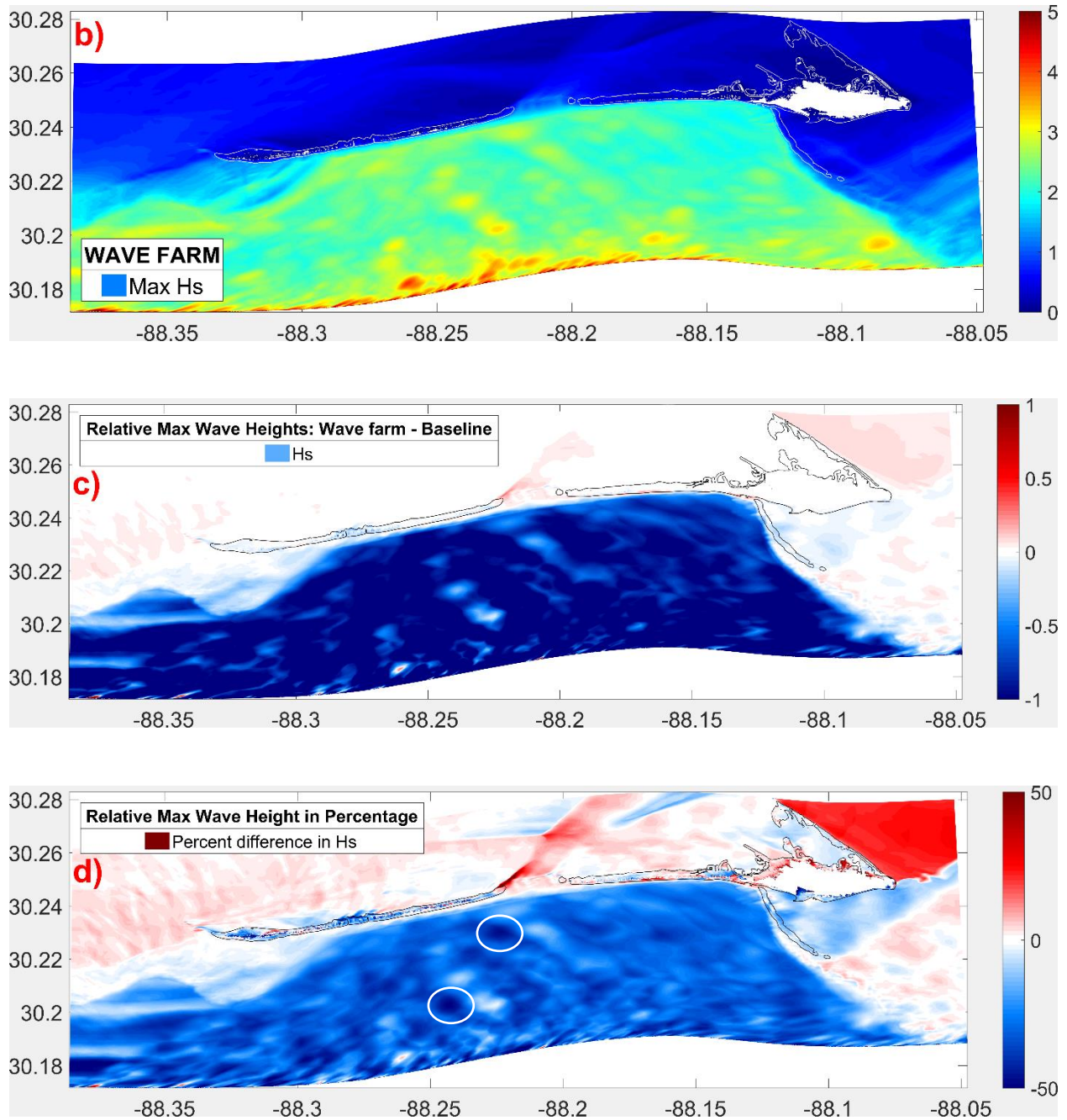
Figure 3-7: Hurricane Ivan - Maximum wave heights (Hs) across the domain: (a) baseline scenario, (b) wave farm scenario (c) Hs difference between the two scenarios in [m] Baseline values are subtracted from wave farm values. (d) Hs difference in [%]. White circles are some of the locations where the reduction in Hs exceeds 50% in the wave farm scenario. The blue color represents the reduction in Hs due to WECs, and the red color represents the increase in Hs due to WECs. White and black lines are the post-storm zero-meter contours of the island.

3.4.1.2 Response of Morphology to Simulated Wave Farms

To relate the impacts of water levels to coastal morphology, we examine the dune heights, bed elevations, inundated area, and bed shear stress across the island. Initial and final beach profiles are extracted from transects located on the east, middle, and west regions of the island (Figure 3-4). Morphologic changes to the beach, dune face, and dune heights are used as proxies for coastal erosion and bed level change.

The average dune crest heights across the island are 3.24 m and 3.33 m for baseline and wave farm scenarios, respectively. This shows a 3% reduction in the dune loss across the island with the presence of WECs The maximum dune height difference between the two scenarios occurs at 825 m west to the western transect, where the dune height in the wave farm scenario is 1.77 m higher than in baseline scenario (see Figure 3-8). These results illustrate how wave dampening by wave farm presence can help diminish the damage due to inundation and overtopping.
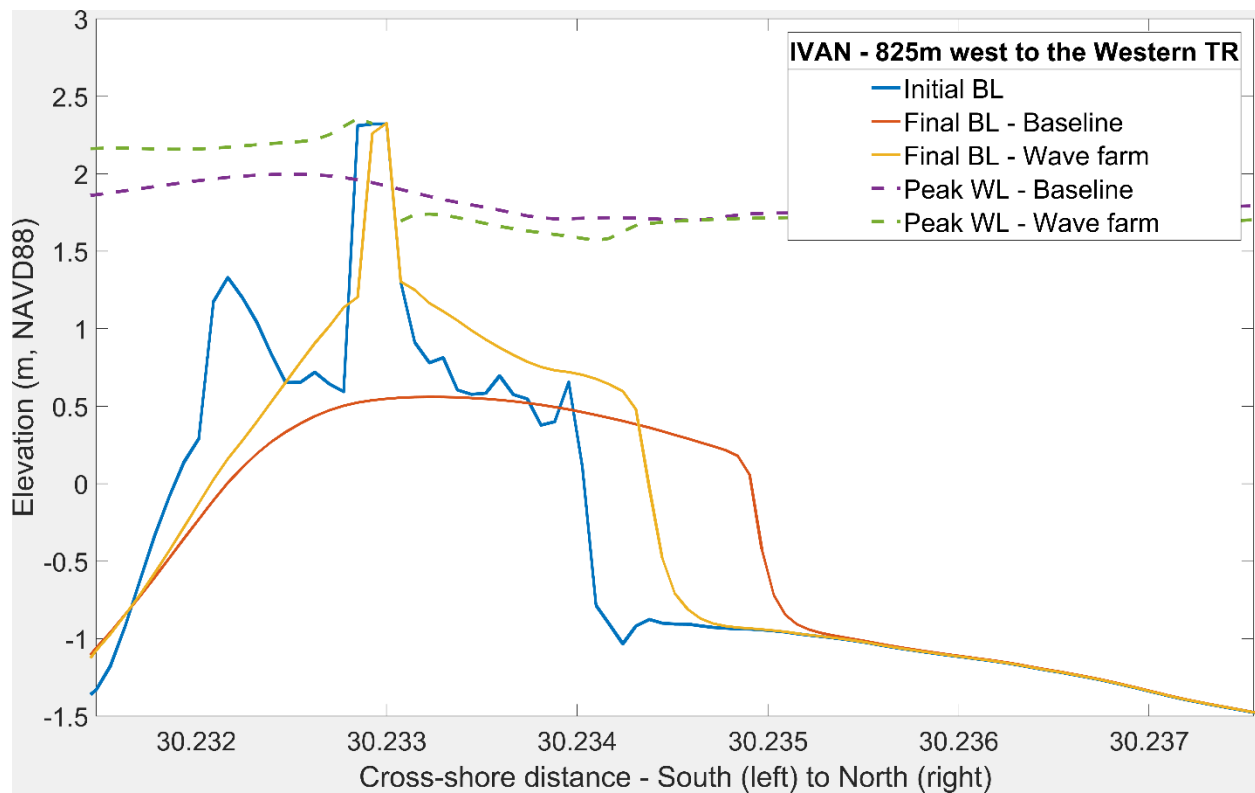
Figure 3-8: Bed levels (BL) and water levels under baseline and wave farm scenarios at the location where the max dune height difference between the two scenarios occur.

We also investigate the changes in the dune heights and beach profile for west, middle, and east transects shown in Figure 3-4 to better understand the morphological response at different portions of the island. At the west transect (Figure 3-5a), the inundation caused by Hurricane Ivan causes sediment to be mobilized at the dune face and deposited behind the dune structure in the baseline scenario, and the dune height is reduced by 0.75 m. In the wave farm scenario, the dune height is only reduced by 0.5 m, i.e., the erosion is mitigated by 33% when the hydrodynamic impacts of wave farms are represented. The differences in dune heights in the two scenarios are not as pronounced for the middle and east transects. The middle transect is located at the breach of the island (i.e., it is initially underwater); therefore, the changes in the surface wave heights do not substantially alter the underwater bathymetry (Figure 3-5b). The east transect is prevented from

59

complete inundation by the high double-dune structure (Figure 3-5c). The primary dune takes on

the impacts of the storm and is eroded, while the secondary dune stays intact in both scenarios.

The difference between the final dune heights in the two scenarios is not substantial, most likely

due to the wave action being dissipated on the first dune and the high water levels dominating the

erosion process in the second dune. However, the height of the second dune is slightly (5.5 cm)

higher in the wave farm scenario in contrast to the baseline scenario. For both scenarios, the bed

elevations are unchanged from the initial (pre-storm) profile in both the seaward and landward

ends of the transects. At all three transects and for both scenarios, the sediment in the beach face

is transported and deposited onshore post-storm (i.e., immediately behind the pre-storm dunes),

creating irregular and shallow sand dunes. Figure 3-5 shows that in the baseline scenario, the

sediment is transported 5 to 50 m further inland than in the wave farm scenario for all three

transects.

The differences in the final bed elevations across Dauphin Island post-Ivan under the baseline and

wave farm scenarios are shown in Figure 3-9. On the western portion of the island, higher accretion

in the west most point and lower cross-shore sediment transport are observed in the presence of

the wave farm compared to the baseline scenario. Also, there are fewer channels cut through the

island in the wave farm scenario (Figure 3-9d). This substantially reduces the breaching tendencies

in the area where the island is the narrowest with a width of ~230 m. In Pelican Island, however,

slightly lower bed elevations (i.e., more erosion) are observed in the wave farm scenario. This can

likely be attributed to the dominant swell wave angle coming from the southeast (SE 144.05°),

which causes the sediment to be transported to the west (Buhring, 2017). The lower elevations at

the Katrina Cut and behind the western channels in the wave farm scenario (i.e., red areas in Figure

3-9c) indicate less cross-barrier (towards mainland Alabama) sediment transport and deposition in the back-barrier in the wave farm scenario. The middle breach shifts westward in the presence of the wave farms, and the width is 200 m smaller than in the baseline scenario (the breach width is 2.4 km in the baseline scenario and 2.2 km in the wave farm scenario). A smaller breach opening and lower bed levels underwater in the presence of WECs indicate that wave farms can cause more precise erosive action at a breach.
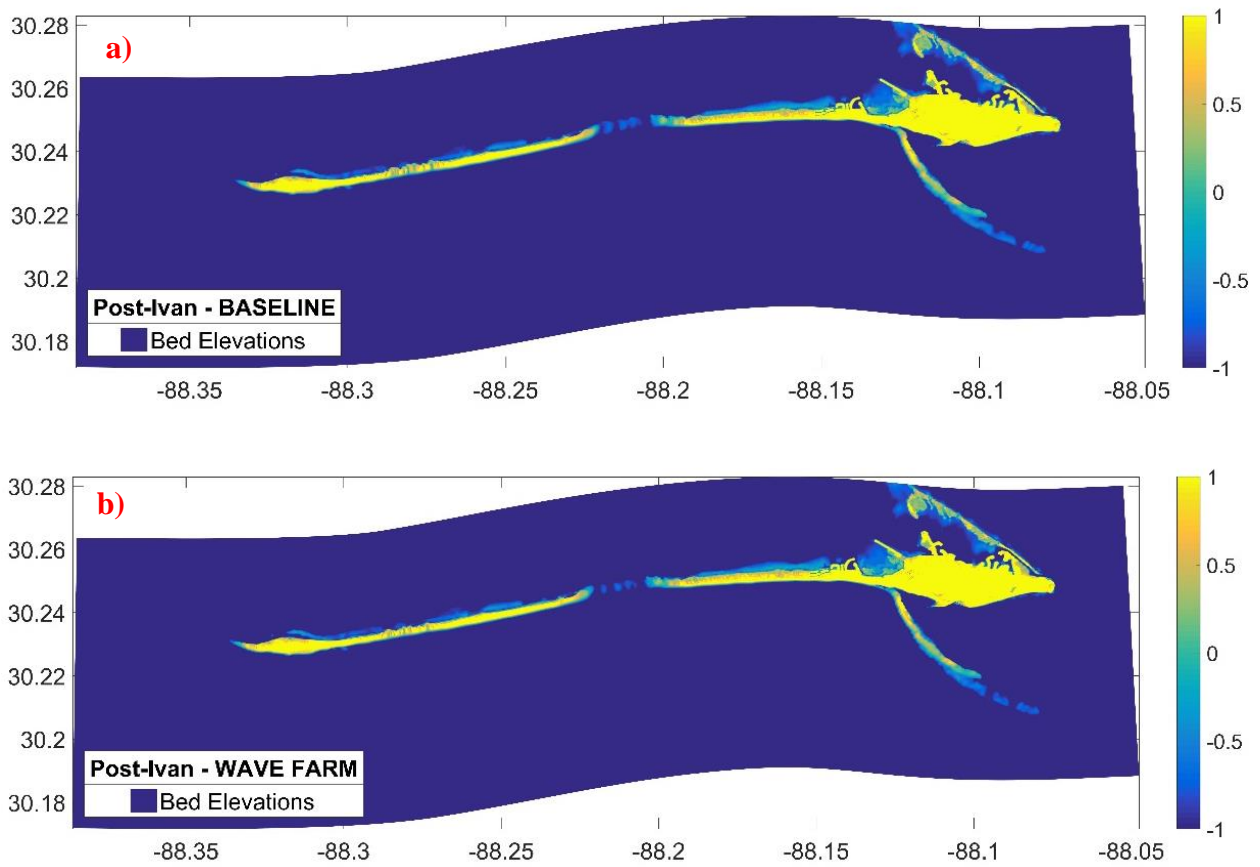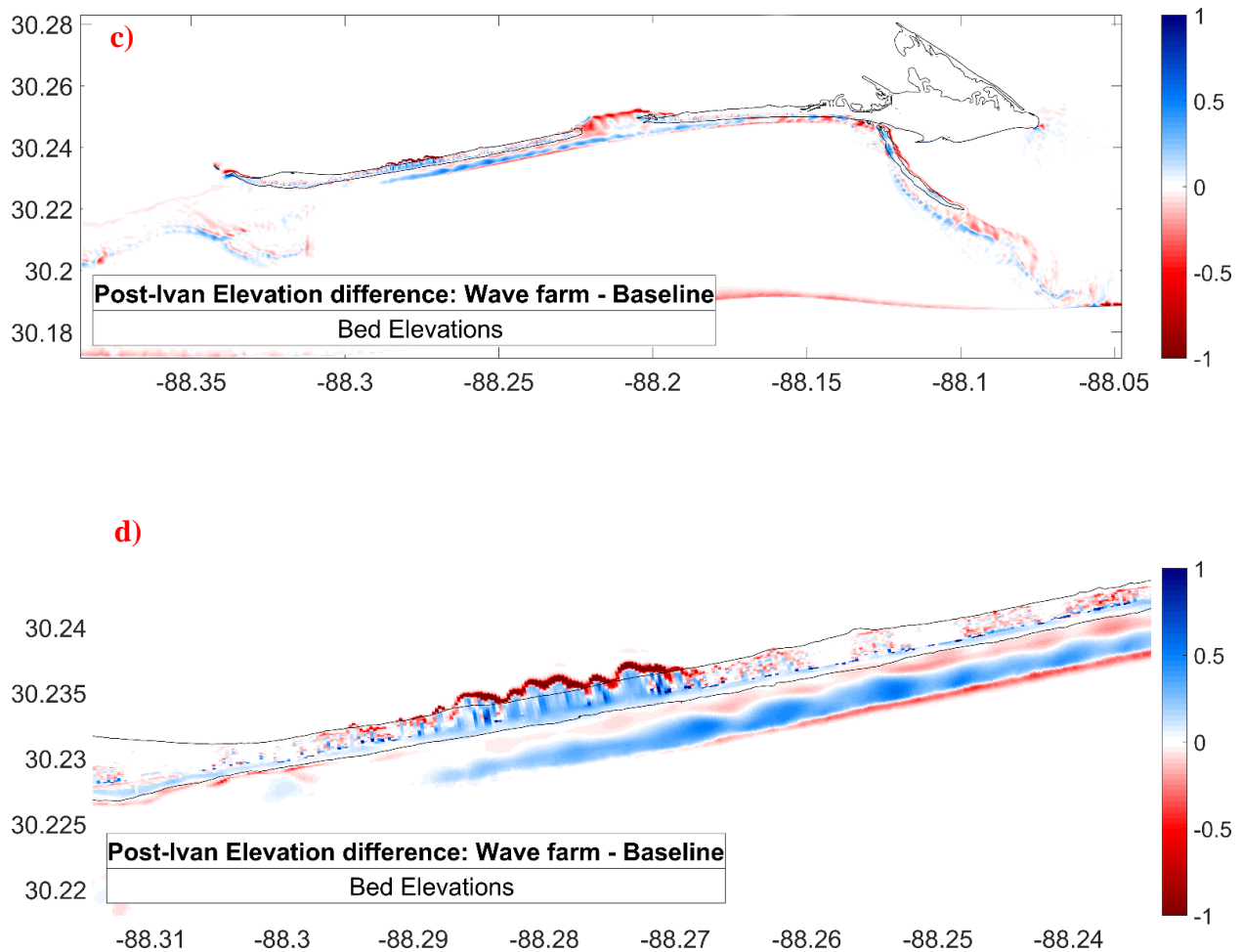
Figure 3-9: Hurricane Ivan - Final bed elevations [m] for baseline (a) and wave farm (b) scenarios (c) Difference between the two scenarios (d) Magnified version of (c) showing the channels in the western portion – Positive (blue) values show the locations where the final elevations are higher in the wave farm scenario. The black line is the post-storm zero-meter contour of the island.

To quantify the impacts of the wave farm on coastal sediments, we present the results of the inundated area, volume loss, and bed shear stress calculations for both scenarios in Table 3-1. The post-storm subaerial island area and subaerial sand volume are higher when the WECs are present. Also, the total inundated area and net loss in the sand volume are lower in the wave farm scenario. Results indicate a 15% reduction in the net loss of sand volume due to the wave farm.

Bed shear stress is used as another indicator of erosion at the bed level, as the likelihood of ocean bottom sediment to be mobilized is directly correlated to the intensity of bed shear stress (Jones et al., 2018; Wang et al., 2011). XBeach calculates the bed shear stress associated with the long waves and mean currents using the following formulation in the cross-shore; x- (τ_{bx}) and alongshore; y-(τ_{by}) directions (Roelvink et al., 2018) :

$$\tau_{bx} = c_f \rho u_E \sqrt{(1.16\, u_{rms})^2 + (u_E + v_E)^2}$$

$$\tau_{by} = c_f \rho v_E \sqrt{(1.16\, u_{rms})^2 + (u_E + v_E)^2},$$

where c_f is the dimensionless friction coefficient, ρ is the density of water, u_E, and v_E are the Eulerian east-west and north-south velocities, respectively, and u_{rms} is the root-mean-square velocity. In this study, the average maximum bed shear stress in the x- and y- directions over the duration of the storm in the mid-domain nearshore area (i.e., where the water depths are low and bed shear stress is responsive to the changes in the wave heights) is calculated. The maximum shear stress in the wave farm and baseline scenarios, as well as the differences between them, are listed in Table 3-1. The maximum averaged bed shear stress values are reduced from 206.79 to 144.71 N/m^2 for the baseline and wave farm scenarios, respectively (30% reduction). It is observed that the reduction in the y-direction (alongshore) (11%) is lower than the reduction in the x-direction (cross-shore) (38%), indicating that the presence of wave farms impacts the bottom sediment transport more in cross-shore direction and less in alongshore direction.

Table 3-1: Inundated and dry areas, initial and final sand volume, net loss in sand volume, and max bed shear stress values in x- and y- directions [N/m2] averaged over time in the mid-domain nearshore area for Hurricane Ivan under baseline and wave farm scenarios

IVAN	Baseline	Wave farm	Difference	Impacts of WECs
Initial island area (millions of m^2)	14.19	14.19	-	-
Total dry area (millions of m^2)	4.49	4.59	0.10	More dry area w/ WECs
Total inundated area (millions of m^2)	9.69	9.59	- 0.10	Less inundation w/ WECs
Initial sand volume (millions of m^3)	19.73	19.73	-	-
Final sand volume (millions of m^3)	19.00	19.10	0.10	More sand volume w/ WECs
Net loss in sand volume (millions of m^3)	0.73	0.62	- 0.11 (15%)	Less sand loss w/ WECs
Max τ_{bx}	192.24	118.69	-38%	Less τ_{bx} w/ WECs, less sediment mobilization
Max τ_{by}	76.19	67.81	-11%	Less τ_{by} w/ WECs, less sediment mobilization
Max $\tau_b = \sqrt{\tau_{bx}^2 + \tau_{by}^2}$	206.79	144.71	-30 %	Less τ_b w/ WECs, less sediment mobilization

3.4.2 *Hurricane Katrina*

In order to investigate the applicability of our results to other storms, we repeat the methodology described in Section 3.4.1 with storm data from Hurricane Katrina.

3.4.2.1 Response of Water Levels and Nearshore Wave Climate to Simulated Wave Farms

Results of the simulations of Hurricane Katrina showed patterns similar to those seen for Hurricane Ivan in terms of the water levels and inundation/overwash regimes experienced along the transects, with the west and middle transects being entirely inundated. However, Hurricane Katrina was a stronger storm and also coincided with high tides, causing peak water levels to exceed 3.5 m and inundate the eastern portion of the island compared to Hurricane Ivan. Peak water levels are observed to be consistent between the baseline and wave farm scenarios (Figure 3-12). This indicates that wave farms are not as effective in changing the regime (e.g., collision, overwash) during intense storms when TWL is high.

Figure 3-10 illustrates the maximum water levels across the domain for both scenarios and the difference between them. As discussed in the case of Hurricane Ivan, Figure 3-10 indicates overall lower max water elevations in the wave farm scenario. In Figure 3-10c, the areas where maximum TWLs are lower in the wave farm scenario (i.e., areas denoted with blue color) is dominant across the domain, unlike the Ivan case (see Figure 3-6c). It should be noted that the difference between the TWLs for the two scenarios is in the order of centimeters for Katrina; therefore, it may not be accurate to conclude that the wave farm is more effective in reducing the TWL across the domain for the Katrina case.
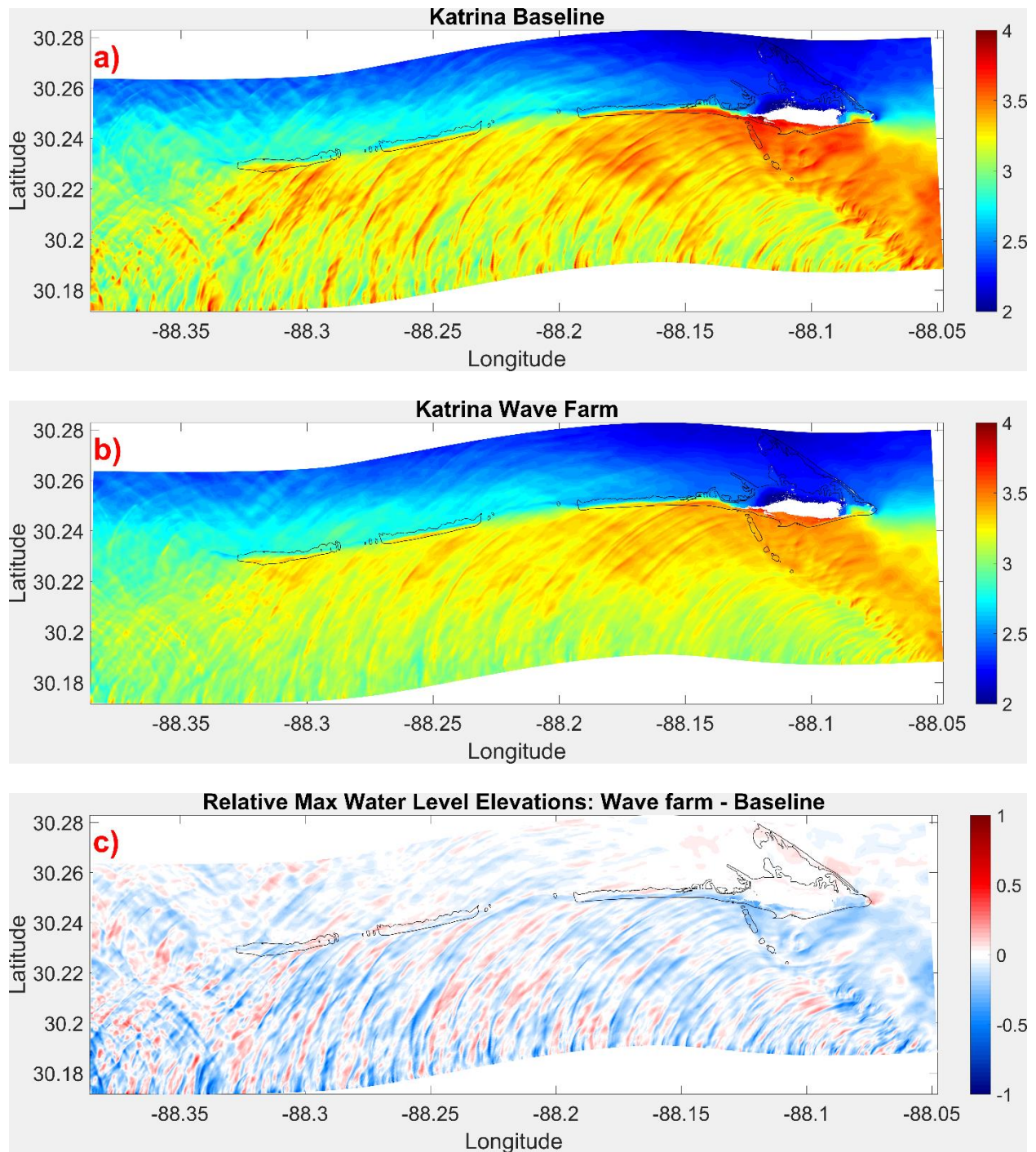
Figure 3-10: Max Water Levels observed at each grid cell throughout the storm [m] for baseline (a) and wave farm (b) scenarios under Hurricane Katrina conditions (c) Difference between the two scenarios: b subtracted from a. The black line is the post-storm zero-meter contour of the island.

66

As expected, the maximum Hs is lower in the wave farm scenario compared to the baseline scenario due to the adjustments made in Hs at the offshore boundary to represent the wave farms (Figure 3-11). The response of the Hs to this adjustment dissipates as the waves propagate towards the shore. On average, the nearshore wave heights in the wave farm scenario are found to be ~0.2 m lower than the baseline scenario.
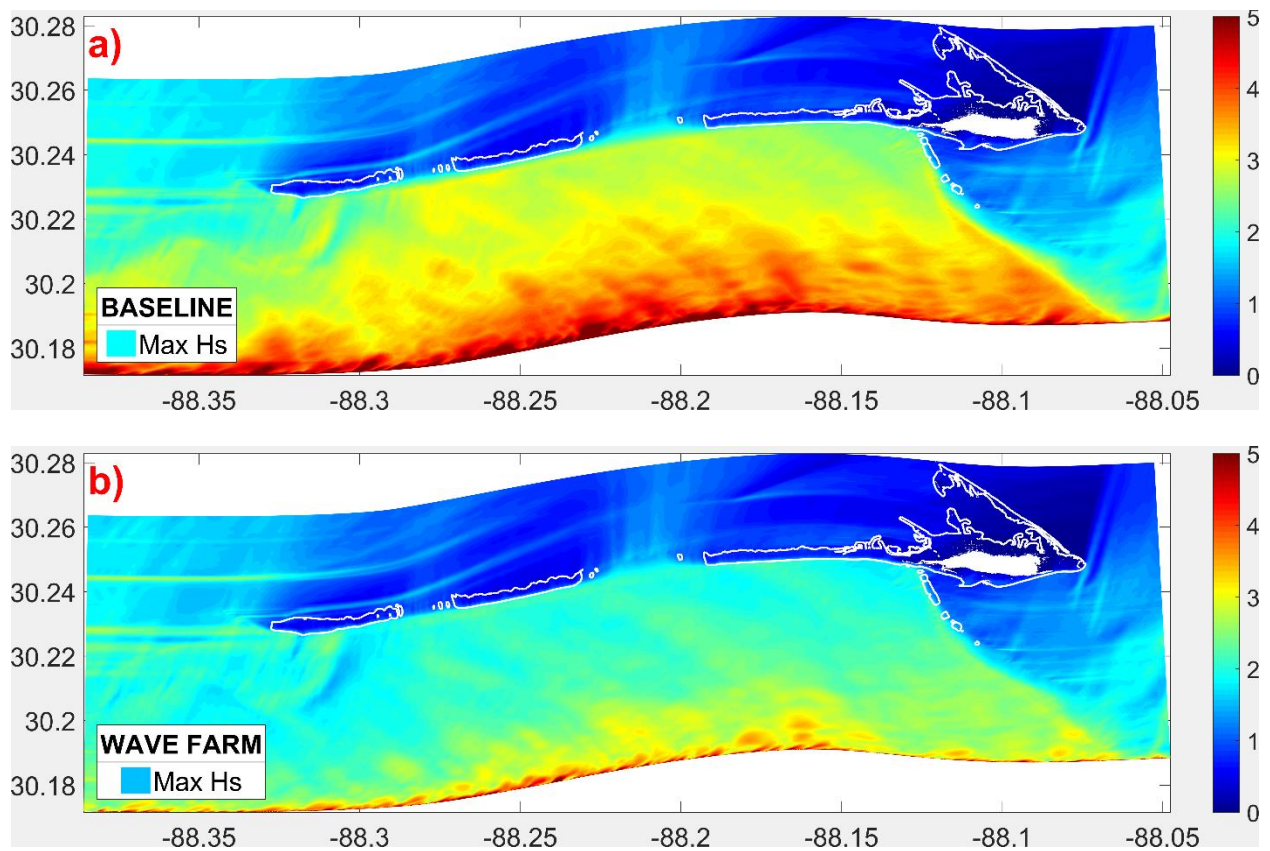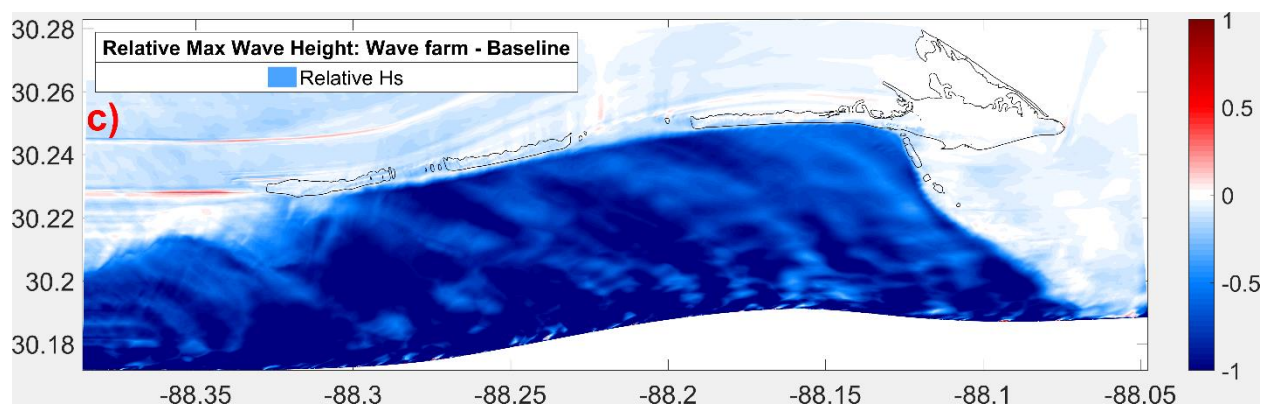
Figure 3-11: Hurricane Katrina - Maximum wave heights (Hs) across the domain: (a) baseline scenario, (b) wave farm scenario (c) Hs difference between the two scenarios in [m] Baseline values are subtracted from wave farm values. The blue color represents the reduction in Hs due to WECs, and the red color represents the increase in Hs due to WECs. Values on the x-axis and y-axis show the longitude and latitude, respectively.

3.4.2.2 Response of Morphology to Simulated Wave Farms

The impacts of WECs to dune heights, bed elevations, and beach profiles shown in the Hurricane Katrina case study are similar to those observed with Hurricane Ivan. Hurricane Katrina fully erodes the dune systems in all three transects; however, like Hurricane Ivan, the final bed levels are generally higher in the wave farm scenario than the baseline scenario (Figure 3-12). Discussions in Section 3.4.1.2 related to the complete beach profiles and the dune heights across the island are applicable for the results of the Hurricane Katrina case, i.e., the bed elevations are unchanged from the initial (pre-storm) profile in both the seaward and landward ends of the transects and the sediment in the beach face is transported and deposited onshore post-storm further inland in the baseline scenario in all three transects. The average of subaerial dune heights across the island is found to be 2.46 m and 2.55 m for baseline and wave farm scenarios, respectively (i.e., 4% reduction in dune erosion with WECs). The maximum dune height difference

between the two scenarios occurs at the eastern end of the island, where the dune height in the wave farm scenario is 1.6 m higher than that is observed in the baseline scenario (see Figure 3-13).
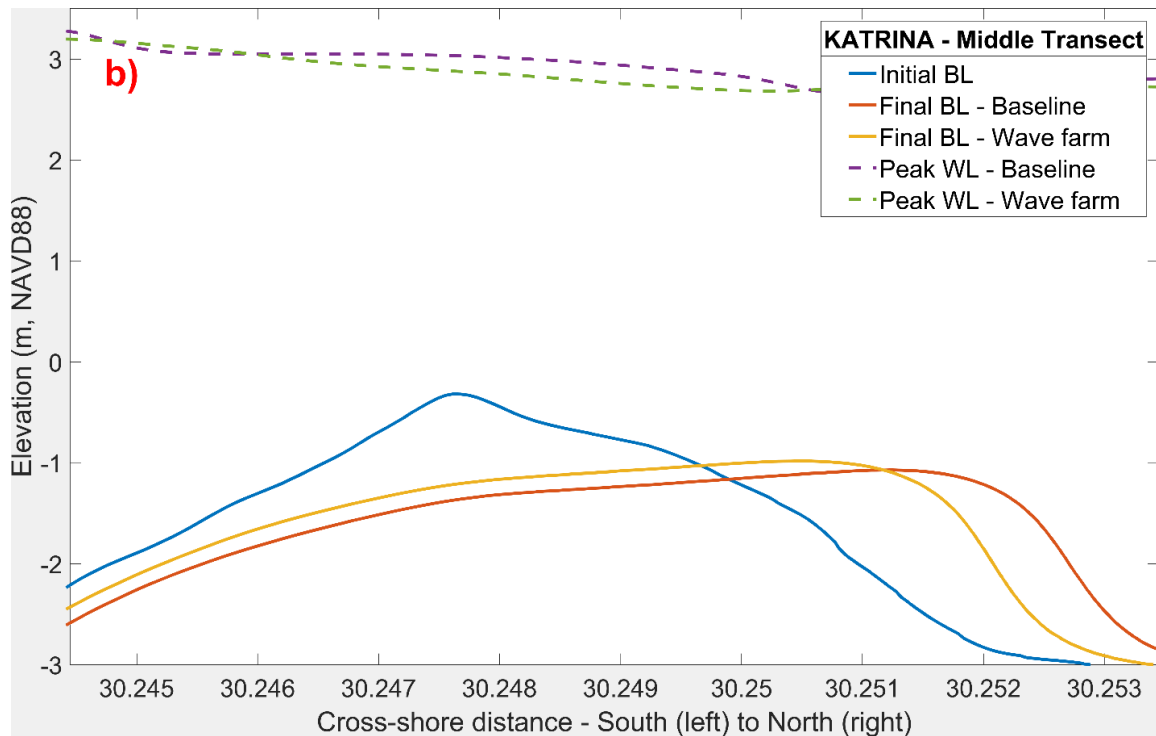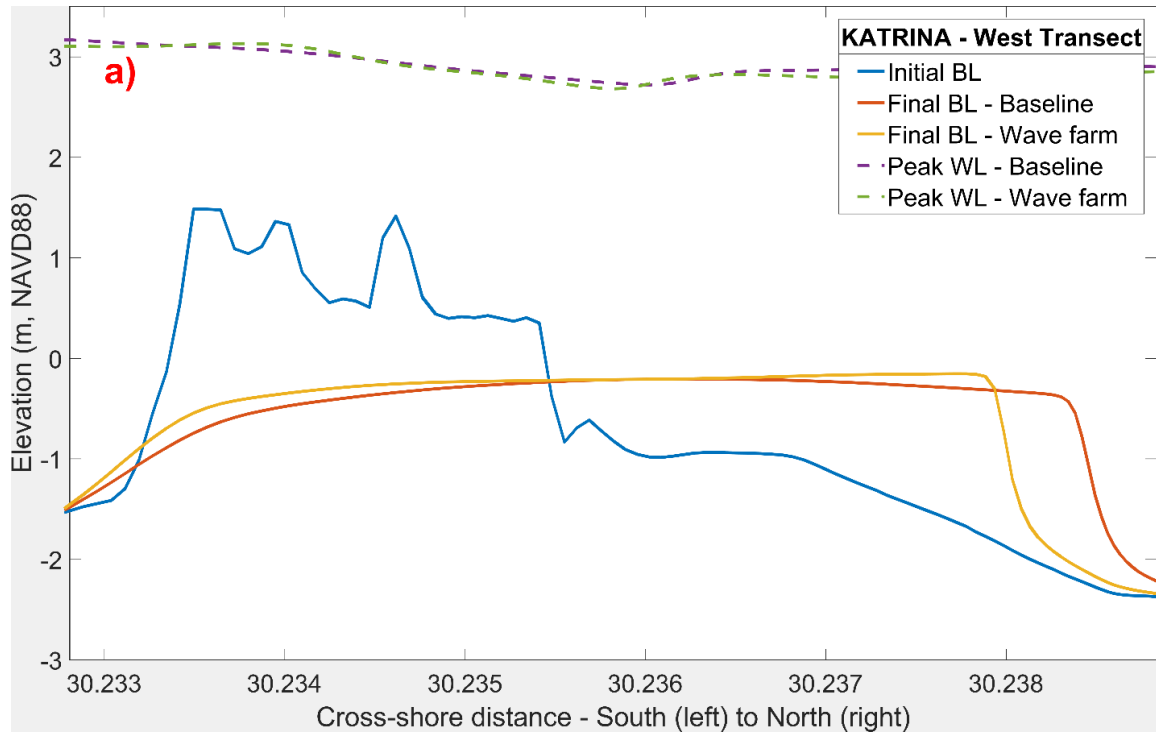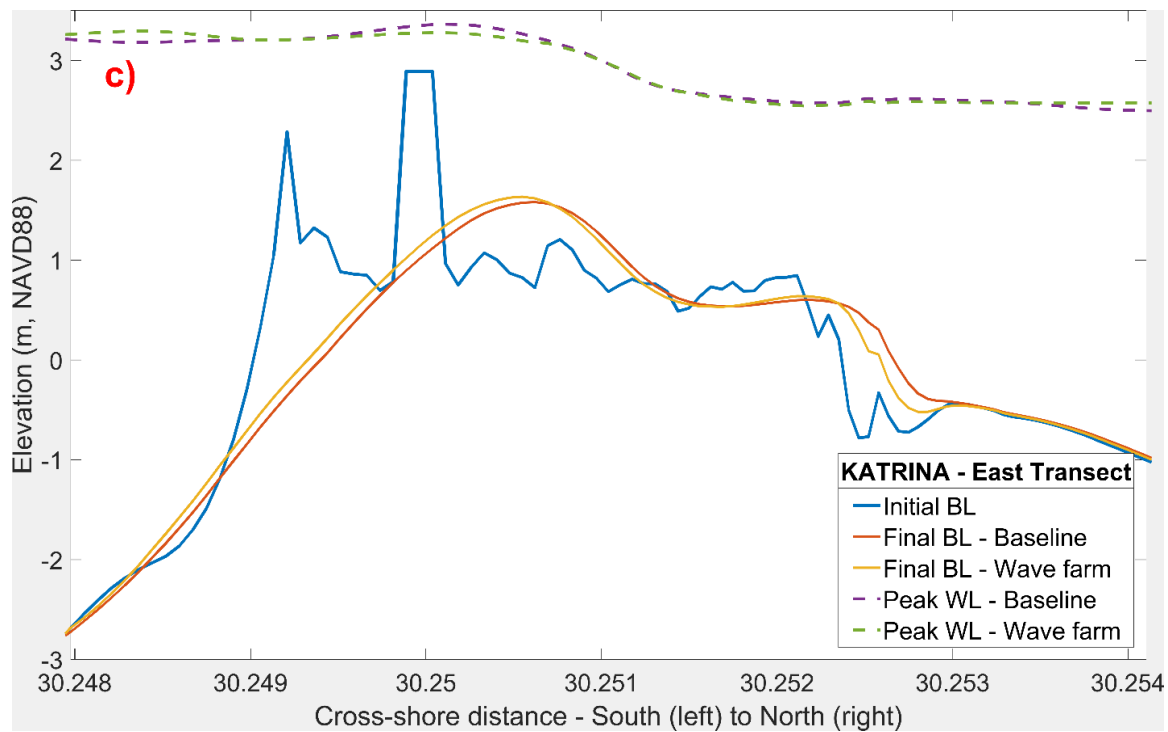
Figure 3-12: Hurricane Katrina - Bed levels (BL) and water levels (WL) under baseline and wave farm scenarios. Note that the figures zoomed in for readability. Initial WL is at the zero-level for all transects.

Figure 3-14 shows the bed levels post-Katrina, where a second breach is observed in the western portion of the island in both scenarios. The difference between the two scenarios is not as pronounced as the Ivan case; however, we observe more landward overwash deposition in the baseline scenario. Even though the dunes are still being overwashed, the wave farm is reducing cross-barrier sediment transport.

70
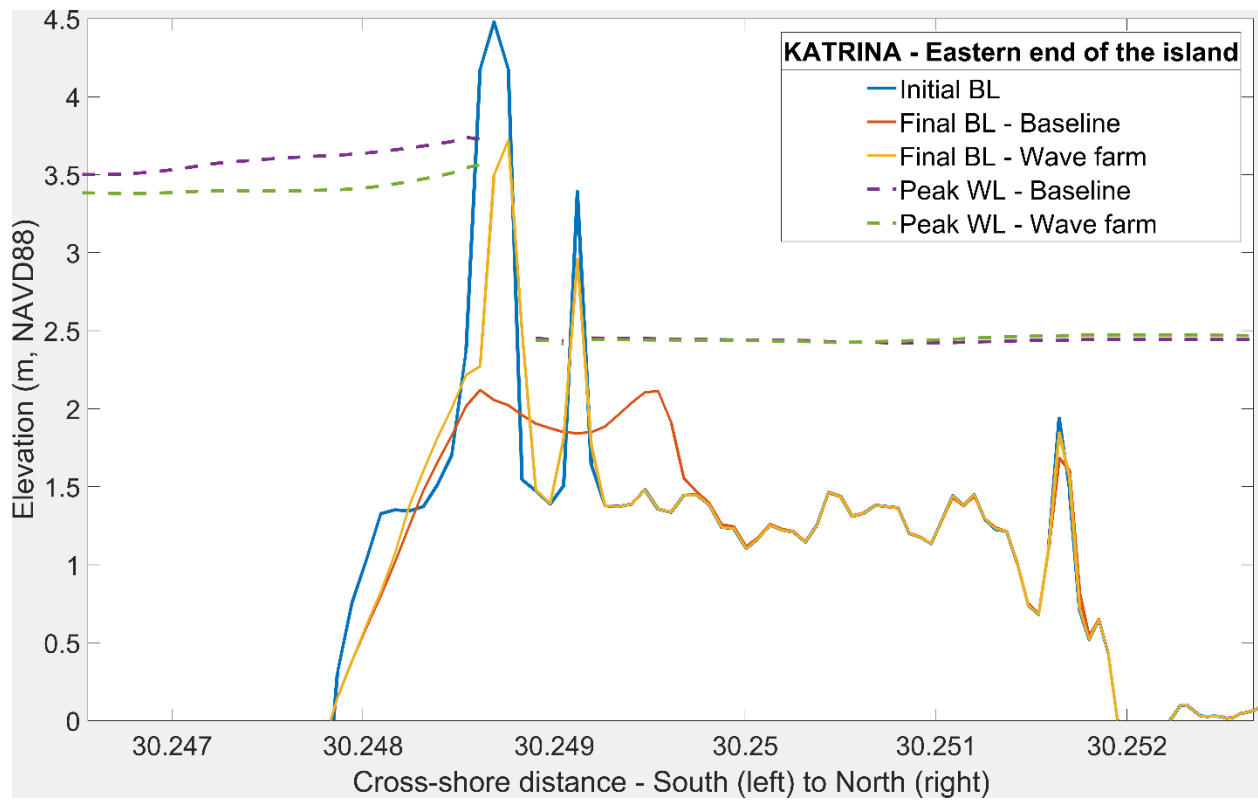
Figure 3-13: Bed levels (BL) and water levels under baseline and wave farm scenarios at the location where the max dune height difference between the two scenarios occur.
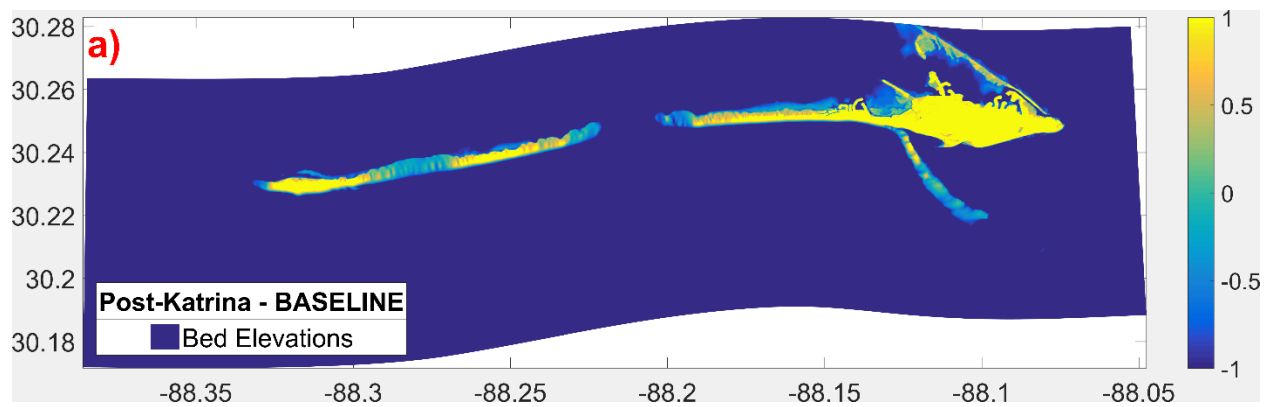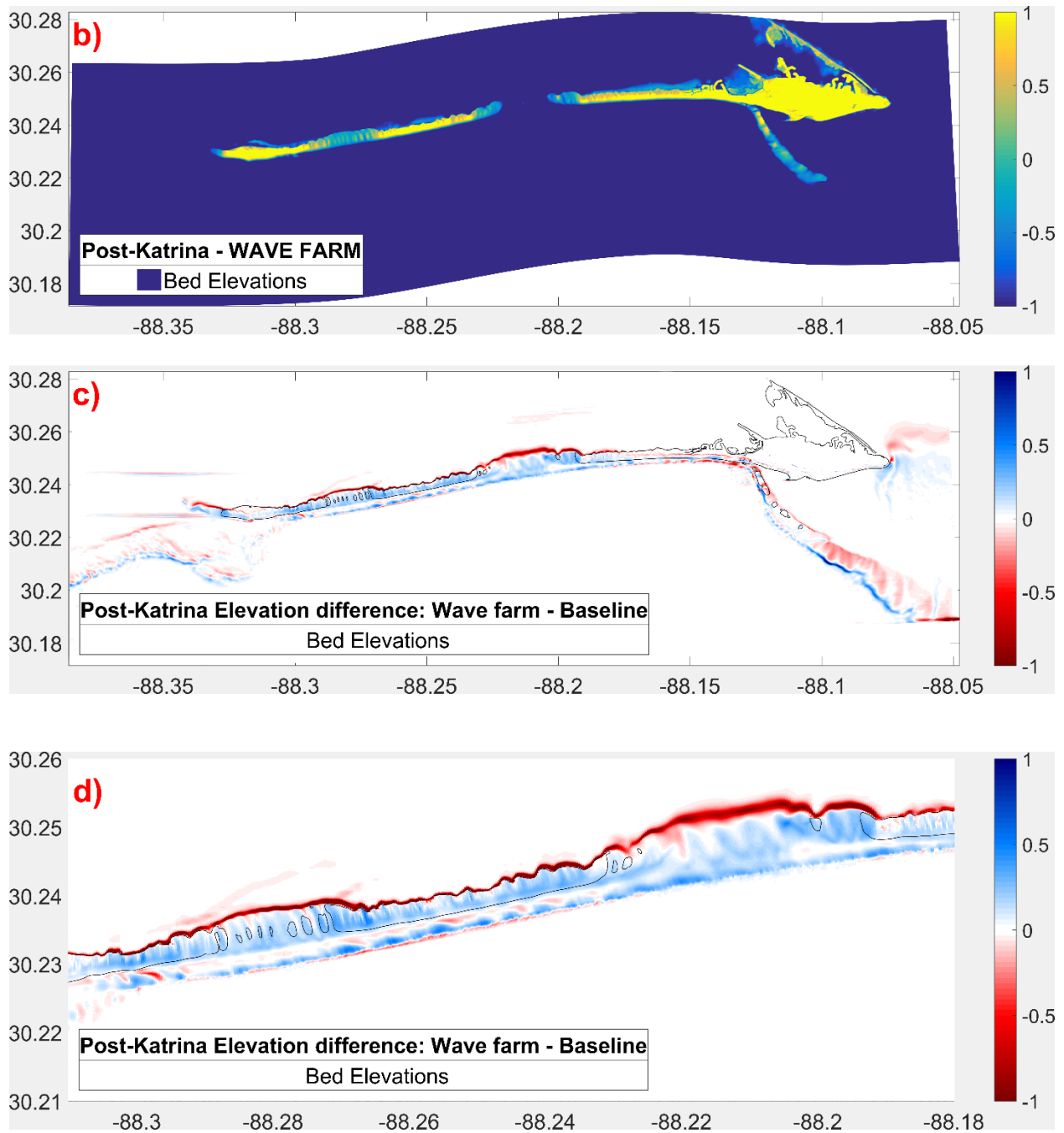
Figure 3-14: Hurricane Katrina - Final bed elevations for baseline (a) and wave farm (b) scenarios (c) Difference between the two scenarios (d) Magnified version of (c) showing the channels in the western portion – Positive (blue) values show the locations where the final elevations are higher in the wave farm scenario. Black lines are the post-storm zero-meter contours of the island.

Impacts of WECs on the inundated area and volume loss are found to be similar to those seen in Hurricane Ivan, i.e., more dry areas and less sand volume loss are seen with the presence of WECs (Table 3-2). In the wave farm scenario, the island experiences less inundated area and an 11% reduction in net loss of sediment volume compared to the baseline scenario. Compared to the Ivan case, the difference between the two scenarios is less substantial in the Katrina case.

Finally, results show that the bed shear stress values are reduced from 313.76 to 245.37 N/m^2 in the presence of a wave farm, indicating a smaller likelihood of the mobilization and erosion of bottom sediment (Table 3-2). This ties into why we see less cross-barrier sediment transport in the bed level difference figures (Figure 3-14 c&d).

Table 3-2: Inundated and dry areas, initial and final sand volume, net loss in sand volume, and max bed shear stress values in x- and y- directions [N/m2] averaged over time in the mid-domain nearshore area for Hurricane Katrina under baseline and wave farm scenarios

KATRINA	Baseline	Wave farm	Difference	Impacts of WECs
Initial island area (millions of m^2)	14.19	14.19	-	-
Total dry area (millions of m^2)	1.88	1.92	0.04	More dry area w/ WECs
Total inundated area (millions of m^2)	12.31	12.27	0.04	Less inundation w/ WECs
Initial sand volume (millions of m^3)	19.73	19.73	-	-

Final sand volume (millions of m³)	17.86	18.07	0.21	More sand volume w/ WECs
Net loss in sand volume (millions of m³)	1.87	1.66	0.21 (11%)	Less sand loss w/ WECs
Max τ_{bx}	295.03	224.38	-24%	Less τ_{bx} w/ WECs, less sediment mobilization
Max τ_{by}	106.77	99.30	-7%	Less τ_{by} w/ WECs, less sediment mobilization
Max $\tau_b = \sqrt{\tau_{bx}^2 + \tau_{by}^2}$	313.76	245.37	-22%	Less τ_b w/ WECs, less sediment mobilization

Finally, results show that the bed shear stress values are reduced from 313.76 to 245.37 N/m² in the presence of a wave farm, indicating a smaller likelihood of the mobilization and erosion of bottom sediment. This is also connected to lower cross-barrier (towards mainland Alabama) sediment transport and deposition in the back-barrier in the wave farm scenario (Sections 3.4.1.2 & 3.4.2.2)

3.5   Discussion

Simulations to investigate the impacts of a wave farm on coastal morphology under storm conditions show that there is overall lower TWL and max Hs, less overwash, less inundated area, less sand volume loss, and lower bed shear stress magnitudes in the wave farm scenario, compared to the baseline scenario. However, the reduction of storm impacts from the wave farm on coastal morphology and the ensuing ocean climate vary spatially. While wave farms mitigate erosion in most parts of the domain, adverse effects or no effects are also seen in some locations. For instance,

WECs have the potential to preserve the integrity of dunes in the western region of the island, where erosion is higher in the baseline scenario, but there are some locations where the wave farm does not make any impact, such as the white areas in Figure 3-7c indicating the same Hs for both scenarios. Also, it is observed that the presence of the wave farm does not change the regimes on the east side of the island, where the collision regime is prevalent. This is in contrast to the western side of the island, which has lower elevations and does experience overwash and inundation during peak water levels. For both the baseline and wave farm scenarios, the bed elevations are unchanged from the initial (pre-storm) profile in both the seaward and landward ends of the transects. This indicates that the storm does not impact the profile in the deep water (i.e., greater than ~6 meters below sea level). However, it does impact the dunes as well as the subaerial beach and surf zone, i.e., regions of shallow water, and this is also where we see the impacts of WECs. Beach profile figures of the transects show that in the baseline scenario, the sediment is transported 5 to 50 m further inland than in the wave farm scenario for all three transects under both storm conditions. This shows that wave farms can reduce the magnitude of the physical forces involved in sediment transport (e.g., wave action) and shorten the distance in which sediment is transported. This discussion also explains why we see less cross-barrier (towards mainland Alabama) sediment transport and deposition in the back-barrier in the wave farm scenario in the bed level difference figures.

Wave farms predominantly mitigate erosion in the western portion of the island. Although this area is uninhabited by humans, it is an important area for wildlife, especially critical for the bird habitat and sea turtle nests (Ingram et al., 2014). It also plays an essential role in protecting mainland Alabama by providing a first line of defense during storm events. Therefore, efforts to

protect this portion of the island from coastal erosion and breaching are valuable. Furthermore, the spatial variability seen with this methodology demonstrates the capacity for analyses of this sort to inform ideal configurations of wave farms for optimal mitigation.

The comparison of the results of Ivan and Katrina simulations shows that the wave farms are less effective in changing the regime and protecting the integrity of dune structures during intense storms. Because of the low dune elevations on Dauphin Island, erosion and overwash events are observed even during weak storms like Hurricane Nate, which was a tropical depression when it made landfall in Alabama in 2017 (Coogan et al., 2019). While a wave farm may not be an effective erosion mitigation strategy for intense storms like Hurricane Katrina, it can reduce erosion and overwash during weaker storm events and reduce the need for subsequent beach nourishment projects. Impacts of WECs on coastal morphology are more pronounced for Hurricane Ivan simulations compared to Katrina, meaning storm intensity plays a dynamic role in how effective the WECs are on reducing coastal erosion.

Hydrodynamic changes due to WECs impact the coastal morphodynamics as expected; however, this study also shows the instances where the opposite is also true. We can see how local bathymetry and island configuration influence how WECs modify the wave climate in their lee. In fact, impacts of WECs are reversed in the sheltered areas and at the locations of breaches. This tells us that when analyzing the hydrodynamic impacts of WECs in the lee of the wave farm, consideration of bathymetry and erosion patterns is also essential for an accurate analysis. Earlier studies on this area generally lack this consideration.

The amount of sand volume protected from inundation and loss by the wave farm in this case study is comparable to the amount of sand added to beaches during nourishment projects. For example,

250,000 m^3 of sand was added to Dauphin Island for nourishment in 2016 at the cost of $7 million (Buhring, 2017), and here we show that WECs can protect 210,000 m^3 of sand volume during Katrina and 110,000 m^3 during Ivan from inundation. Considering that beach nourishment is a temporary solution that needs to be repeated each decade, wave farms can be a long-term, cost-effective, and adaptable alternative to current coastal protection methods. The initial cost of wave farms can be high; however, they not only protect the coasts against erosion but also provide renewable energy to the coastal communities. Moreover, their payback time associated with the value of the renewable energy they provide is as short as one year (Thomson et al., 2011).

Here we have explored only the lower limits of the potential for wave energy conversion to mitigate coastal erosion, as we have not accounted for the physical wave to WEC or WEC to WEC interactions. We have also focused on short-term impacts and expect that even greater potential for protection may be found with longer-term analyses, particularly with consideration of the changing climate. This work and subsequent studies can be used to explore multi-component coastal protection strategies combining wave farms, nature-based solutions, and living shorelines, such as coral reefs and salt marshes, to increase coastal adaptability to climate change. Additionally, while we have shown that wave farms can reduce the impacts of coastal processes that are generally favorable to coastal erosion, it is known that overwash and sand deposition on the back-barrier during storms is necessary for rollover to occur and to maintain island resilience over time (Lorenzo-Trueba and Ashton, 2014; Masselink, Gerd; Hughes, Michael; Knight, 2014). This showcases an interesting trade-off between protection to existing environments and infrastructure versus future island resilience.

3.6   <u>Conclusions</u>

This study explores the potential for wave energy conversion, conventionally used to generate renewable energy, to mitigate coastal erosion simultaneously. XBeach simulations of baseline (no WECs present) and wave farm scenarios (WECs represented as reduced Hs) under tropical storm conditions at Dauphin Island, AL, demonstrate that wave farms can alleviate the factors that cause coastal erosion, such as wave attack, bed shear stress, and overwash and inundation. We also observe that the consideration of erosion patterns is essential for an accurate analysis when investigating the hydrodynamic impacts of WECs in the lee of the wave farm, which was generally not considered in earlier studies.

Simulations for both Hurricanes Katrina and Ivan yield similar results, supporting the idea that wave farms can be effective in mitigating erosion. A comparison of the results of the storm simulations shows that wave farms are less effective in changing the regime and protecting the integrity of dunes during intense, stronger storms. A wave farm is a promising approach to mitigating coastal erosion; however, its capacity to influence intense morphodynamics is limited. Coastal erosion caused by the strongest hurricanes may be assuaged by more resilient and efficient WEC technologies. Moreover, the varying impact of the wave farm across the domain emphasizes the need for a thorough analysis when implementing WECs for coastal protection of specific locations. Additional study is needed to understand the long-term impacts of WECs on coastal morphology more comprehensively, though this study serves as a foundational step forward.

3.7   Acknowledgments

CHAPTER 4: THE IMPACT OF WAVE ENERGY CONVERSION ON COASTAL MORPHODYNAMICS UNDER SEA LEVEL RISE

4.1 Introduction

Coastal erosion is a major issue for coastal areas due to the changing climate and increasing coastal population (Neumann et al., 2015). Sea level rise, storm intensity and frequency, tides and currents, and wave attack are some of the leading causes of coastal erosion (Bird and Lewis, 2015), most of which are expected to intensify with the changing climate (Masselink et al., 2020; Reguero et al., 2019). Global mean sea level has risen over 0.2 m in the past 100 years (Church and White, 2011) and is projected to rise 0.3 to 2.0 m more by 2100 (Kopp et al., 2014; Parris et al., 2012). Masselink et al. (2020) expect an increase in the coastal erosion rates in the future as a result of rising sea levels, potentially causing even the currently stable or accreting coasts to enter an erosion phase. Coastal regions are often densely populated, comprising nearly 40% of the U.S. population (NOAA, 2016), and heavily urbanized with valuable real estate and infrastructure (e.g., as shown in Layne (2019)). Beaches, dunes, and cliffs constitute the first line of defense against the impacts of storms and extreme events, therefore the efforts to mitigate coastal erosion are critical to saving lives and properties in the coastal areas.

As the climate continues to change, the conventional methods to mitigate coastal erosion have been significantly challenged. Coastal management methods involving structural measures such as seawalls usually result in 'coastal squeeze', which causes a steepening of the intertidal profile (Pontee, 2013), and cannot adapt well to the changing climate (Seddon et al., 2020). Thus, researchers have begun searching for alternative solutions to protect the coasts from eroding that

are more adaptable to climate change (e.g., changing sea levels) and less invasive on the area of application (Kibler et al., 2019; Temmerman et al., 2013).

Reducing the overall carbon dioxide emissions produced from burning fossil fuels when generating electricity and moving towards renewable energy options have been more common after the Paris Agreement (UNFCCC, 2015). Along with solar, wind, and hydropower, ocean wave energy has been increasingly recognized as another promising renewable energy source since ocean waves contain about 2 TW of power globally (Gunn and Stock-Williams, 2012). Wave energy converters (WECs) generate renewable energy and potentially reduce the coastal erosion rates, as illustrated in Ozkan et al. (2020) and Ozkan and Mayo (2019), and here in Chapter 3. They are also highly adaptable to changing climate, e.g., floating type WECs can simply rise with the rising sea levels. Considering that the global wave power is predicted to increase in the future (Reguero et al., 2019), utilization of WECs to generate renewable energy and protect the coastal areas under rising sea levels appears to be promising. This chapter investigates the potential of this idea.

Coastal erosion is dominantly determined by local site properties, and predictions of the impacts of climate change on the global coastal morphodynamics will have a low confidence (Masselink and Russell, 2013). Thus, local coastal response analysis is essential. This study uses Dauphin Island, AL as a test case (study area description is provided in Section 3.2.1). The effectiveness of WECs on mitigating coastal erosion under sea level rise (SLR) projection scenarios is investigated and compared to the present-day conditions (no SLR). SLR scenarios are Intermediate Low (0.5m SLR) and Low (0.3m SLR) (Parris et al., 2012). These scenarios are selected to observe the morphologic response of coastal areas to probable increases in sea level in the next 100 years.

XBeach morphodynamics model is used to simulate the morphodynamic response to SLR scenarios and the presence of a wave farm. XBeach is forced with storm data from Hurricane Ivan and Hurricane Katrina (Section 3.2.2), and output is produced for baseline (i.e., no wave farm) and wave farm scenarios under varying SLR scenarios. Results are presented for the whole domain, as well as at the west and east transects shown in Figure 3-4.

4.2   Model Description, Setup, and Assumptions

In this study, XBeach morphodynamic model (described in detail in Section 3.3) is used to simulate the morphodynamic response to SLR scenarios and the presence of a wave farm. WECs are represented in the XBeach model through adjustments to the offshore boundary conditions, which are extracted from a coupled Advanced Circulation (ADCIRC)+SWAN model called NGOM3 (Bilskie et al., 2016). NGOM3 is forced with astronomic tides and meteorological wind and pressure data from Hurricane Ivan and Hurricane Katrina (Passeri et al., 2018a). Hourly water levels are extracted from NGOM3 in the middle of onshore and offshore boundaries of the XBeach grid for Hurricane Ivan. For Hurricane Katrina, however, water levels are extracted from NGOM3 at the four corners of the grid to consider alongshore gradients in surge northwest of the Dauphin Island, as presented in (Passeri et al., 2018b). Time series of JONSWAP (Joint North Sea Wave Project) spectra describing the wave climate (i.e., significant wave heights, peak frequencies, directional spreads, and main wave angles) is extracted from NGOM3, at the middle of the seaward boundary for both Ivan and Katrina; and applied uniformly to the offshore boundary (Passeri et al., 2018b).

82

Simulations are carried out under present-day (no SLR) conditions (Chapter 3) and projections of low and intermediate-low SLR (0.20 and 0.50 m, respectively) scenarios that are obtained from Parris et al. (2012). To account for SLR, the initial mean sea level of NGOM3 is offset by the amount of SLR (Bilskie et al., 2016).

The XBeach model is run in surfbeat (instationary) mode to develop the baseline case (i.e., the case without WECs) under low SLR and intermediate-low SLR scenarios. Next, the significant wave heights are reduced by 30% to represent the hydrodynamic effects of WECs based on recent estimates of WEC efficiency (Abanades et al., 2014a; Rijnsdorp et al., 2020). A hypothetical wave farm is assumed to be located along the offshore boundary since the adjustments to boundary conditions are made there. The rest of the wave parameters remain unchanged. The XBeach model is then run for the wave farm case under the two SLR scenarios, and differences between the cases are investigated.

With this approach, physical wave to WEC or WEC to WEC interactions are not captured, i.e., we only represent the energetic effects of wave farms. This serves as a fundamental step in understanding the minimum potential of WECs to reduce coastal erosion under changing climate, as including physical effects would likely cause an additional reduction.

4.3   Results and Discussion

Here the output of the baseline and wave farm simulations that are forced with Hurricane Ivan and Hurricane Katrina storm data is presented to assess the impacts of WECs under Low SLR (0.2 m) scenario. Results of the low SLR simulations are compared to the intermediate-low SLR (0.5 m) simulations. The higher SLR scenarios (1.2 m and 2.0 m) were also analyzed; however, due to the

low elevations of Dauphin Island, complete inundation is observed under higher SLR scenarios, and the results are not as meaningful as the lower SLR cases; therefore, they are not included here. Relevant figures are provided in Appendix A.

4.3.1   *Hurricane Ivan*

4.3.1.1 Response of Water Levels and Nearshore Wave Climate to Simulated Wave Farms Under SLR Scenarios

Time series of total water levels, wave heights, and water velocities in the cross-shore and alongshore directions are obtained as output from the XBeach simulations. Peak water levels during Hurricane Ivan, and the pre- and post-storm bed levels for the baseline (i.e., significant wave heights unchanged) and wave farm (significant wave heights reduced by 30%) cases under Low SLR (i.e., where the mean water level is 0.2 m) are presented in Figure 4-1.

A significant portion of the island is inundated in both the baseline and wave farm cases in Low SLR scenario during the peak of the storm. Peak water levels measured at the beach face during Hurricane Ivan for the baseline case are higher than those observed in the wave farm case by 0.12m in the west transect and by 0.1m in the east transect (Figure 4-1). This tells us that WECs have the potential to reduce the TWL under both no-SLR (section 3.4.1.1) and Low-SLR scenarios. The reduction in wave heights due to WECs on TWL varies in the north-south direction, as the hydrodynamics are also influenced by the bottom surface (i.e., friction and topography) and geometry of the island.

The maximum water levels reached at each grid cell during the simulation for the baseline and wave farm cases, as well as the difference between the two cases, are illustrated in Figure 4-2. The

84

dominant red color in the middle to west portion of the domain shown in Figure 4-2c illustrates the higher TWL in the wave farm scenario compared to the baseline scenario, whereas the blue color representing the lower TWL with the presence of WECs is dominant in the eastern part of the island. Thus, it should not be assumed that reduced wave heights offshore will result in uniformly lower total water levels across the whole domain. For this storm, the wave farm is more effective in reducing the TWL in the eastern part of the island, where the maximum TWL is the highest.
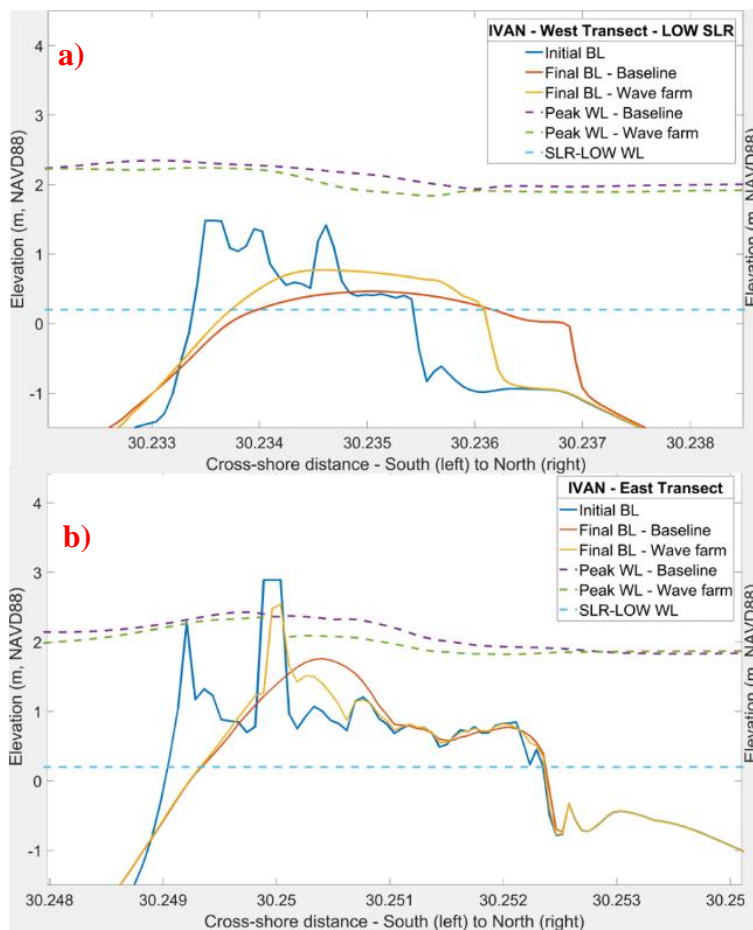
Figure 4-1: Bed levels (BL) and water levels (WL) before and during Hurricane Ivan, at the west transect (a) and the east transect (b) under Low SLR scenario. Blue dashed line indicates the mean sea level (0.2 m)
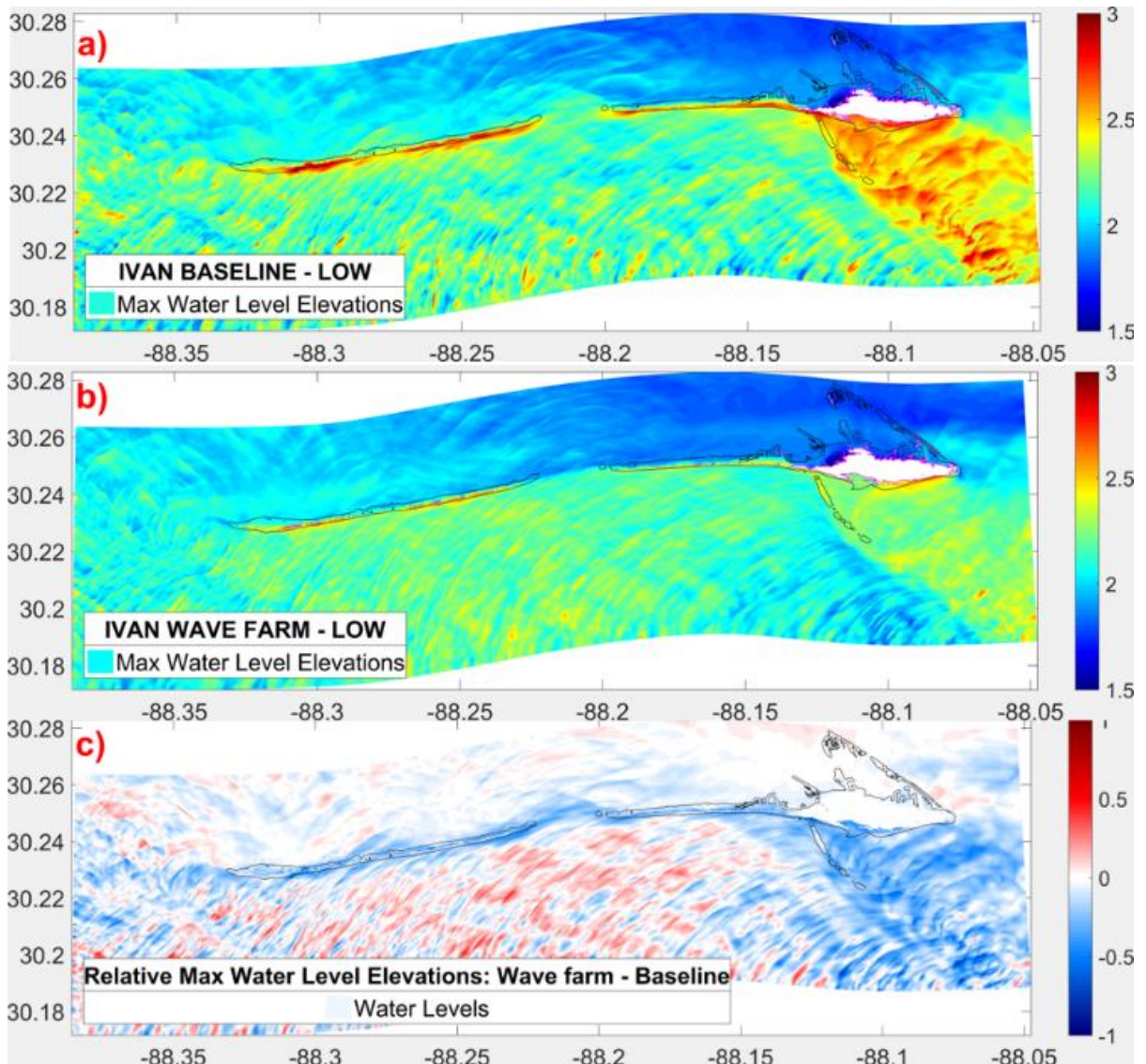
Figure 4-2: Low SLR scenario: Max Water Levels observed at each grid cell throughout the storm for baseline (a) and wave farm (b) cases (c) Difference between the two cases: b subtracted from a. (Blue color represents the areas where maximum TWLs are lower in the wave farm scenario compared to the baseline scenario, and the red color represents the areas where the TWLs are higher with the presence of a wave farm) The black line is the post-storm zero-meter contour of the island.

It is known that high significant wave heights (Hs) nearshore can cause substantial coastal erosion (Bird and Lewis, 2015). Thus, the impacts of WECs on wave-induced erosion are analyzed through the study of the maximum Hs across the domain in wave farm and baseline cases under the Low

SLR scenario. Figure 4-3a & b show overall lower Hs in the wave farm scenario compared to the baseline scenario as expected due to the reduction in Hs on the offshore boundary conditions for the representation of the wave farm. It is observed that wave heights dissipate as the waves propagate towards the shore (Figure 4-3 a&b). On average, at a reference mid-domain nearshore alongshore transect (~latitude 30.2343°N), the wave heights in the wave farm case are found to be 0.71 m lower than the baseline case. Lower Hs results in lower potential beach face and dune erodibility due to wave action. Figure 4-3c shows the difference between the two cases and illustrates that the impacts of WECs on Hs are not uniform due to the complex hydrodynamics. No changes in Hs are observed behind the island due to the presence of WECs except for the Katrina Cut, where slightly higher wave heights are seen in the wave farm scenario at the western end of the breach, likely due to the channeling that is discussed in the next section.
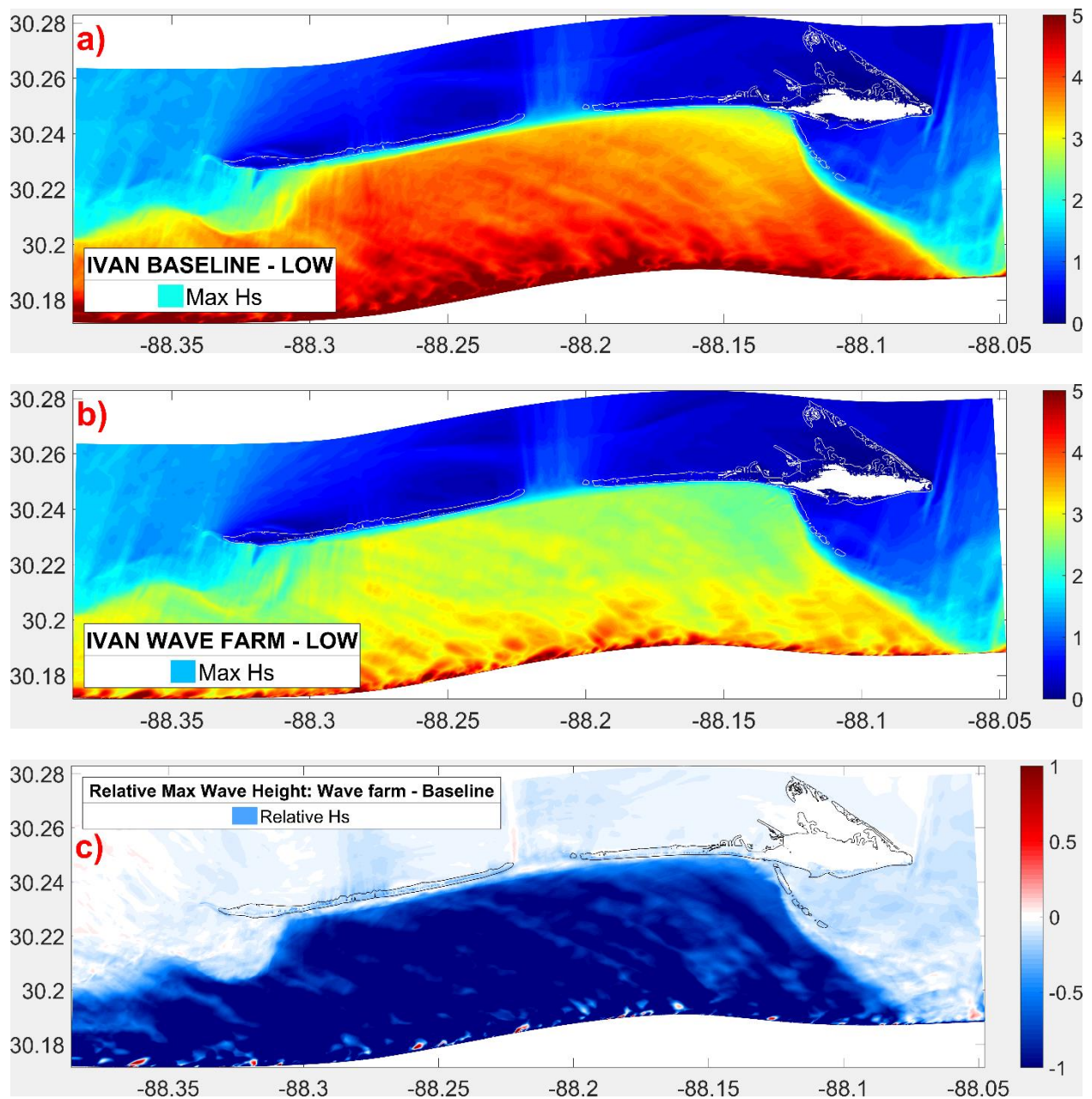
Figure 4-3: Hurricane Ivan - Low SLR: Maximum wave heights (Hs) across the domain: (a) baseline scenario, (b) wave farm scenario (c) Hs difference between the two scenarios in [m] Baseline values are subtracted from wave farm values. The blue color represents the reduction in Hs due to WECs, and the red color represents the increase in Hs due to WECs. White and black lines are the post-storm zero-meter contours of the island

The analysis is repeated for the *intermediate-low SLR* scenario where the mean water level is 0.5 m to observe the changes in the results under the rising sea levels (the relevant figures and tables are included in Appendix A). The island experiences almost complete inundation except for some high dune crests in the eastern portion under this scenario. TWL trends in the west and east transects for the Int-Low SLR scenario follows a similar pattern as Low SLR scenario (as seen in Figure 4-1), i.e., peak water levels measured at the beach face during Hurricane Ivan for the baseline case are higher than those observed in the wave farm case by 0.15m in the west transect and by 0.11m in the east transect under Int-Low SLR (Figure A- 1). Like in the Low-SLR scenario, the wave farm is most effective in reducing the TWL in the eastern part of the island where the highest max water levels are observed in the Int-Low scenario. It is consistent between the three SLR conditions (including the no SLR case presented in section 3.4.1.1) that the WECs are most effective in reducing the *offshore* TWL at the location of the highest maximum water levels (Figure 3-6c, Figure 4-2c, Figure A- 2c).

The maximum Hs difference figures (Figure 3-7c, Figure 4-3c, and Figure A- 3c) indicate an increasing *offshore* Hs reduction potential of WECs as the mean sea level rises. While we observe some white areas (i.e., locations of no difference between the Hs in wave farm and baseline scenarios) and red areas (i.e., locations of higher Hs in the presence of WECs) in Figure 3-11c under no-SLR conditions, these occurrences decline as the mean sea level increases in the Low and Int-Low SLR cases. Lower relative max Hs values (i.e., darker blue areas) are predominantly seen in Figure 4-3c and Figure A- 3c. On the other hand, it is observed that WECs are more efficient in reducing the *nearshore* wave heights under lower mean sea level conditions. On average, at a reference nearshore alongshore transect, WECs reduce the wave heights by 0.67 m

under the Int-Low SLR scenario, as opposed to a 0.71 m reduction under the Low-SLR scenario. This tells us that the effectiveness of WECs to reduce nearshore Hs declines under rising sea level conditions.

4.3.1.2 Response of Morphology to Simulated Wave Farms Under SLR Scenarios

To relate the impacts of water levels to coastal morphology, the dune heights, bed elevations, inundated area, and bed shear stress are observed across the island under the Low-SLR scenario. Initial and final beach profiles are extracted from transects located on the east and west regions of the island. Changes in dune heights, beach profiles (i.e., overall shapes of the transects), and areas of the dune face are used as proxies for coastal erosion and bed level change. These proxies are compared between the baseline and wave farm scenarios to assess the impact of WECs. For example, higher dune heights at the end of the wave farm simulation relative to the baseline simulation are considered indicative of effective erosion mitigation by WECs.

The TWL exceeds the dune heights and completely inundates the western portion of the island during the peak of the storm under Low-SLR scenario (Figure 4-1a). Despite the complete inundation, final dune height in the west transect is 0.35 m higher when the wave farm is present. Due to the higher elevations in the eastern portion, the secondary (landward) dune stays intact during the peak water levels in the wave farm case, while it loses its integrity in the baseline case (Figure 4-1b). The final dune height in the wave farm case is 1.1 m higher than the baseline case. To see the impacts of WECs on dune heights across the island, average post-storm dune heights under Low-SLR scenario are calculated and found to be 2.86 m and 3.12 m in the baseline and wave farm cases, respectively. In other words, the dune erosion across the island is mitigated by

8% when the hydrodynamic impacts of wave farms are represented. Since high dunes better protect the coastal communities behind them from being inundated, it can be concluded that wave farms can help diminish the damage due to inundation and overtopping by preserving the height of the dunes under the Low-SLR scenario.

Changes in the dune structure and full beach profile are also investigated for west and east transects to better understand the spatial variation of morphological response. At the west transect, the inundation caused by the storm mobilizes the sediment at the dune face and deposits behind the dune in the baseline case. The east transect is prevented from complete inundation by the high double-dune structure (Figure 4-1b) in the wave farm case. The primary dune takes on the impacts of the storm (i.e., wave action and surge) and is eroded, while the secondary dune stays intact in both scenarios. The bed elevations remain unchanged post-storm in both the seaward and landward ends of the transects under both baseline and wave farm cases (Figure 4-1a&b). This indicates that the storm does not impact the beach profile in water levels greater than ~3 meters below mean sea level. However, it does impact the dunes as well as the subaerial beach and surf zone, i.e., regions of shallow water, and this is also where we see the impacts of WECs. At the east and west transects and for both cases, the sediment in the beach face is transported and deposited behind the pre-storm dunes, creating irregular and shallow sand dunes. It is noted that in the baseline scenario, the sediment is transported ~110 m further inland than in the wave farm scenario at the west transect. This shows that wave farms can reduce the magnitude of the physical forces involved in sediment transport (e.g., wave action) and shorten the distance in which sediment is transported.

The differences in the final bed elevations across Dauphin Island post-Ivan for the baseline and wave farm conditions under Low-SLR scenario are shown in Figure 4-4. Higher accretion in the

west most point and lower cross-barrier sediment transport are observed on the western portion of the island when the wave farm is present compared to its absence (i.e., the baseline case). Also, fewer channel cut-throughs are observed here in the wave farm case (Figure 4-4d). This considerably decreases the breaching predispositions in the area where the island is the narrowest. Similar to the western channels, lower cross-barrier sediment transport is seen in the middle breach in the presence of WECs. In Pelican Island, however, slightly lower bed elevations (i.e., more erosion) are observed in the wave farm case. As discussed in 3.4.1.2, this can be attributed to the dominant swell wave angle coming from the southeast (SE 144.05°), which causes the sediment to be transported to the west (Buhring, 2017).
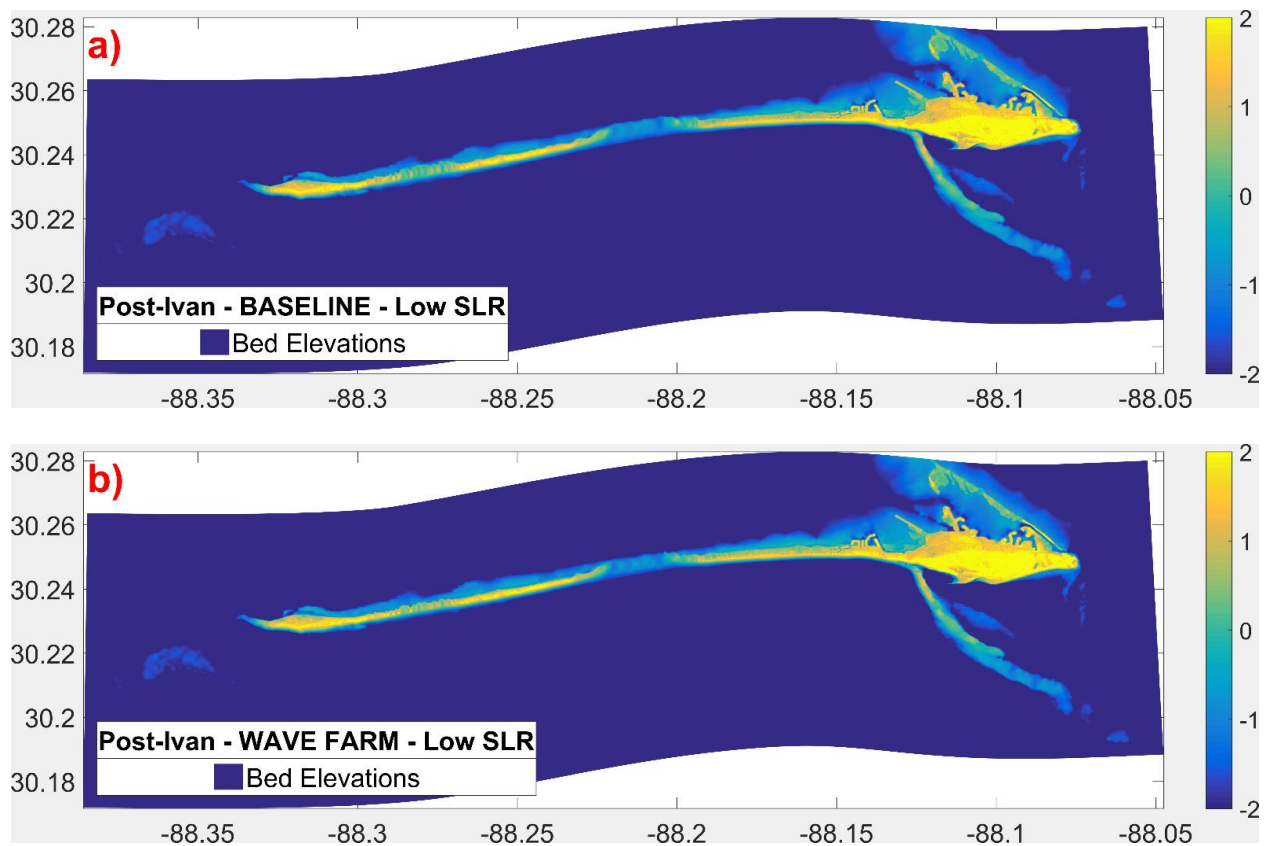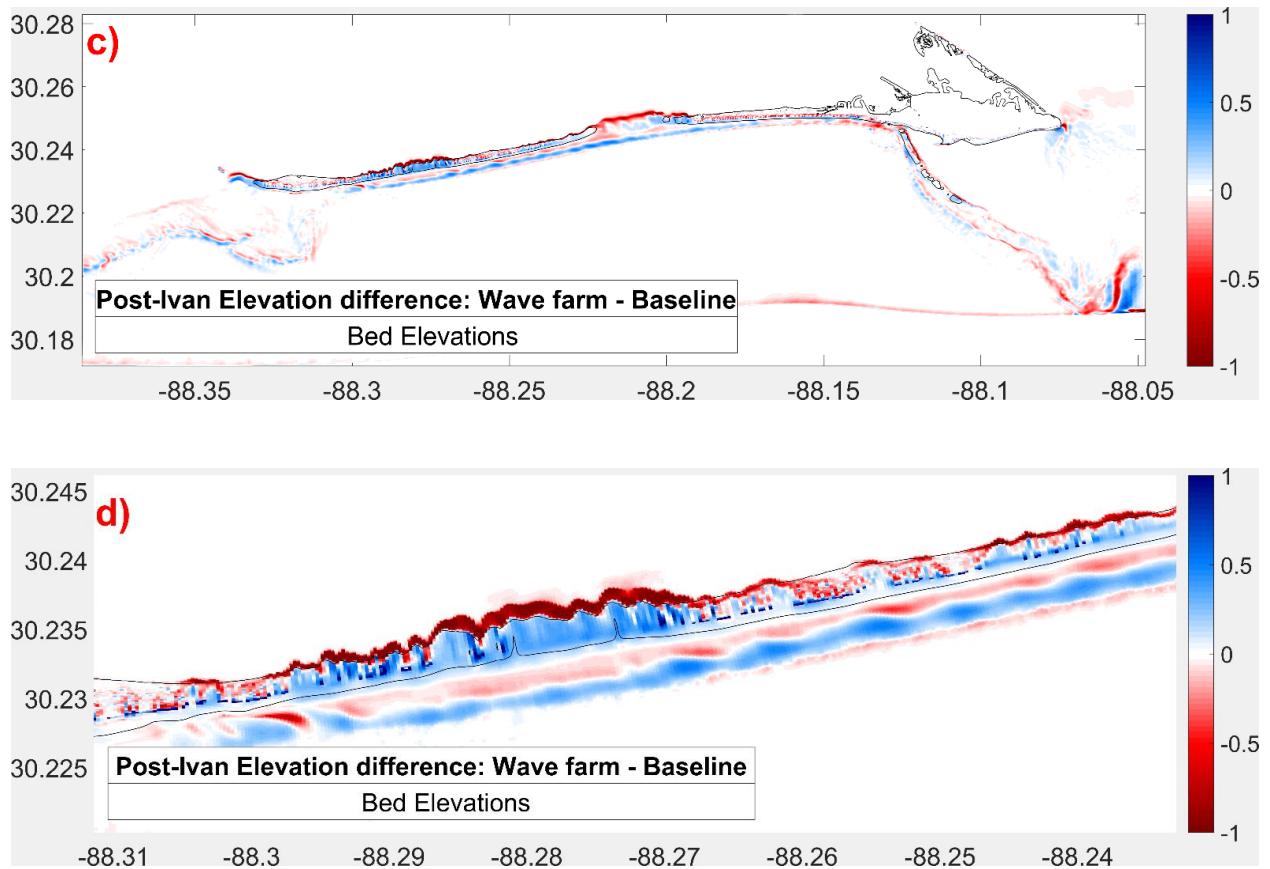
Figure 4-4: Final bed elevations [m] for baseline (a) and wave farm (b) cases under Low-SLR scenario (c) Difference between the two scenarios (d) Magnified version of (c) showing the channels in the western portion – Positive (blue) values show the locations where the final elevations are higher in the wave farm scenario. The black line is the post-storm zero-meter contour of the island.

To better quantify the impacts of the wave farm on coastal sediments, the results of the inundated area, volume loss, and bed shear stress calculations for both cases under Low-SLR are presented in Table 4-1.

It is observed that the post-storm subaerial island area and subaerial sand volume are higher, and the total inundated area and net loss in the sand volume are lower in the wave farm case compared to the baseline case. Results indicate a 13% less net loss in sand volume due to the wave farm, which illustrates the potential benefits of WECs as a coastal defense mechanism.

Bed shear stress is used as another indicator of erosion at the bed level, as the likelihood of ocean bottom sediment to be mobilized is directly correlated to the intensity of bed shear stress (Jones et al., 2018; Wang et al., 2011). XBeach calculates the bed shear stress, as described in section 4.3.1.2. The maximum shear stress in the wave farm and baseline cases are listed in Table 4-1. The maximum averaged bed shear stress values are reduced from 277.94 to 235.76 N/m^2 for the baseline and wave farm scenarios, respectively (15% reduction). This exemplifies that the presence of wave farms can reduce sediment transport on the ocean floor by weakening the bed shear stress. It is observed that the reduction in the y-direction (alongshore) (10%) is lower than the reduction in the x-direction (cross-shore) (23%), demonstrating that the wave farms have a higher impact on the bottom sediment transport in cross-shore direction than in alongshore direction. The uniform application of wave conditions at the offshore boundary (in the alongshore direction) may have also caused this result.

Table 4-1: Inundated and dry areas, initial and final sand volume, net loss in sand volume, and max bed shear stress values in x- and y- directions [N/m2] averaged over time in the mid-domain nearshore area for Hurricane Ivan for baseline and wave farm cases under Low SLR scenario.

Ivan Low-SLR	Baseline	Wave farm	Difference $(m^2/m^3/\%)$	Impacts of WECs
Initial island area (millions of m^2)	13.70	13.70	0	-
Total dry area (millions of m^2)	3.22	3.54	0.32	More dry area w/ WECs
Total inundated area (millions of m^2)	10.48	10.16	-0.32	Less inundation w/ WECs
Initial sand volume (millions of m3)	19.73	19.73	0	-
Final sand volume (millions of m^3)	18.63	18.77	0.14	More sand volume w/ WECs
Net loss in sand volume (millions of m^3)	1.07	0.93	-0.14 (-13%)	Less sand loss w/ WECs
Max τ_{bx}	179.07	137.79	-23%	Less τ_{bx} w/ WECs, less sediment mobilization
Max τ_{by}	212.56	191.30	-10%	Less τ_{by} w/ WECs, less sediment mobilization
Max $\tau_b = \sqrt{\tau_{bx}^2 + \tau_{by}^2}$	277.94	235.76	-15%	Less τ_b w/ WECs, less sediment mobilization

The analysis is repeated for the *Intermediate-Low SLR* scenario where the mean water level is 0.5 m to observe the changes under the rising sea levels (the relevant figures and tables are included in Appendix A). In the west transect, the final dune height is observed to be 0.50 m higher in the wave farm case compared to the baseline case in the Int-Low SLR scenario (Figure A- 1). This number is 0.35 m for Low SLR case. In the east transect, however, with the increase in mean sea

level, the secondary dune gets overwashed and loses its integrity in both wave farm and baseline cases. In other words, WECs performed slightly better in mitigating the dune erosion in the west transect, whereas they were less effective in protecting the dune structure in the east transect under rising sea levels. Since these two transects were isolated cases, and they do not represent the whole island, average post-storm dune heights across the domain are calculated for the two SLR scenarios. While the dune erosion reduction percentage of WECs is 8% in the Low SLR scenario, this percentage reduces to 6% in the Int-Low SLR scenario (Table 4-2). Therefore, the overall conclusion from the dune erosion patterns under rising sea levels is that the WECs are slightly less effective in mitigating dune erosion when the mean sea level is increasing. Despite the reduced effectiveness with rising sea levels, WECs still result in overall higher dunes (compared to the baseline case) in the int-low SLR.

Analysis of the final bed level figures of both SLR scenarios (Figure 4-4 and Figure A- 4) indicates less accretion in the west most point of the island and more channel cut-throughs in the western portion of the island under the Int-Low SLR conditions. To quantify this, total dry and wet area, and net loss in sand volume are calculated under both SLR conditions for both cases (Table 4-1 and Table A- 1). Percent reduction in net sand volume loss w/ WECs is found as 13% and 8% for Low SLR and Int-Low SLR scenarios, respectively. Similarly, the percent reduction in total max shear stress w/ WECs are found to be 15% and 8% for Low SLR and Int-Low SLR scenarios, respectively. Table 4-2 summarizes the qualitative comparison between the three SLR scenarios. It is observed that the effectiveness of WECs on mitigating coastal erosion decreases as the mean sea level increases, except for the Low SLR scenario. Lower percent reduction in dune erosion in the Low SLR scenario can be attributed to the sand deposition nearshore and presence of higher

water level gradients compared to higher SLR scenarios(Passeri et al., 2018a). Percent reduction

in dune erosion due to WECs in Low SLR (8%) is higher than that of no SLR conditions (3%).

However, wave farm case still results in an overall higher post-storm bed level elevation, higher

dunes, more dry area, and less shear stress compared to the baseline case.

Table 4-2: Comparison of the qualitative results under present-day (no SLR), Low and Int-Low
SLR cases

	Ivan No SLR	Ivan Low	Ivan Int-Low
Dune erosion reduction due to WECs	3%	8%	6%
Reduction in net sand volume loss due to WECs	13%	13%	8%
Reduction in total max shear stress due to WECs	30%	15%	8%

4.3.2   Hurricane Katrina

In order to investigate the applicability of our results to other storms, the methodology described

in the previous section is repeated with storm data from Hurricane Katrina.

4.3.2.1 Response of Water Levels and Nearshore Wave Climate to Simulated Wave Farms Under
SLR Scenarios

Results of the simulations of Hurricane Katrina showed similar patterns to those seen for Hurricane

Ivan in terms of the water levels and inundation/overwash regimes experienced along the transects.

However, Hurricane Katrina is a stronger storm than Ivan, and with the addition of higher sea

levels, peak water levels reach up to 4 m, inundating both the western and the eastern portion of

the island. Peak water levels are observed to be consistent between the baseline and wave farm

scenarios for both transects (Figure 4-5). This indicates that wave farms are not as effective in changing the regime (e.g., collision, overwash) during intense storms and under SLR conditions when TWL is higher.

The maximum water levels reached at each grid cell during the simulation for the baseline and wave farm cases, as well as the difference between the two cases, are illustrated in Figure 4-6. Overall lower max water elevations are observed in the wave farm case (Figure 4-6b) compared to the baseline case under Low SLR scenario (Figure 4-6a). In Figure 4-6c, higher TWL in the wave farm scenario is observed in the western portion of the domain, whereas middle to eastern parts experience a reduction in TWL in the wave farm case. Similar to the Ivan case, the wave farm is observed to be more effective in reducing the TWL in the eastern part of the island, where the maximum TWL is the highest. Also, this tells us that the reduced wave heights at the offshore boundary may not result in uniformly lower total water levels across the domain.

Figure 4-7a & b show overall lower Hs in the wave farm scenario compared to the baseline scenario as expected due to the reduction in Hs on the offshore boundary conditions to represent the wave farm. Also, the dissipation of the wave heights as the waves propagate towards the shore is observed. On average, at a reference mid-domain nearshore alongshore transect (~ latitude 30.2343°N), the wave heights in the wave farm case are found to be 0.72 m lower than the baseline case. This results in lower potential beach face and dune erodibility due to wave action. Figure 4-7c shows the difference between the two cases and illustrates that the impacts of WECs on Hs are not uniform due to the complex hydrodynamics. The presence of WECs does not impact the Hs behind the island except for the Katrina Cut where slightly higher (~0.05 m) wave heights are

seen in the wave farm scenario at the western end of the breach, likely due to the channeling that

is discussed in the next section.
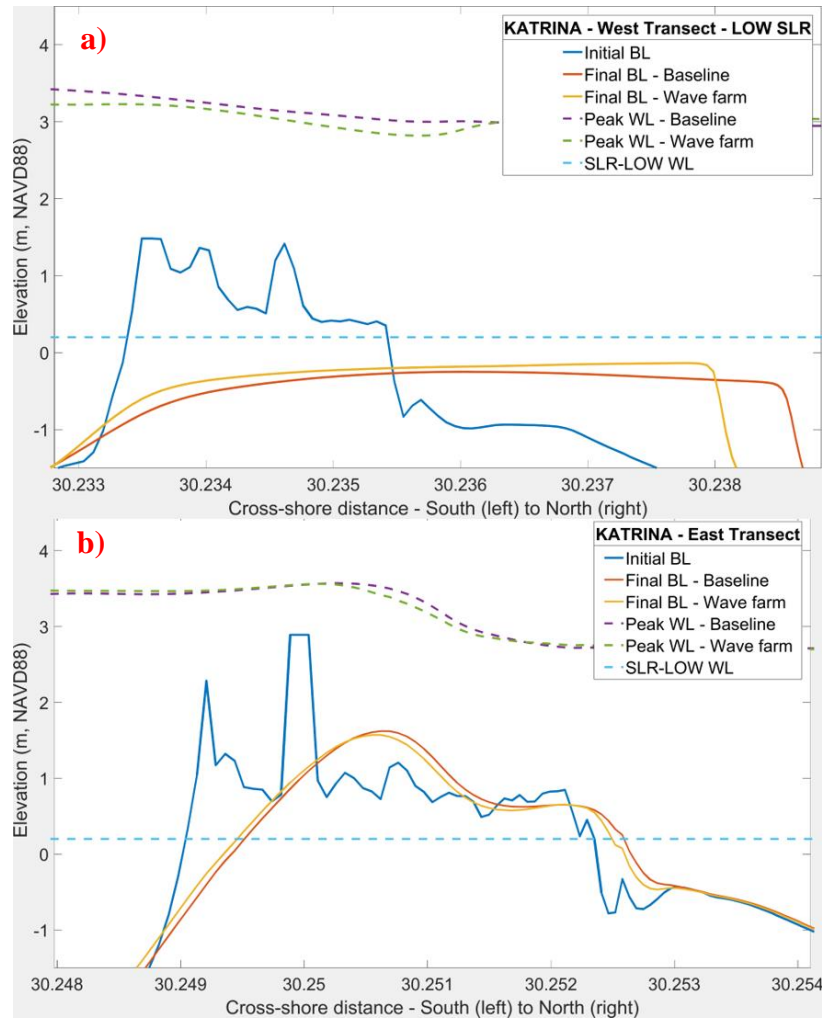
Figure 4-5: Bed levels (BL) and water levels (WL) before and during Hurricane Katrina, at the west transect (a), and the east transect (b) under Low SLR scenario. Blue dashed line indicates the mean sea level (0.2 m)
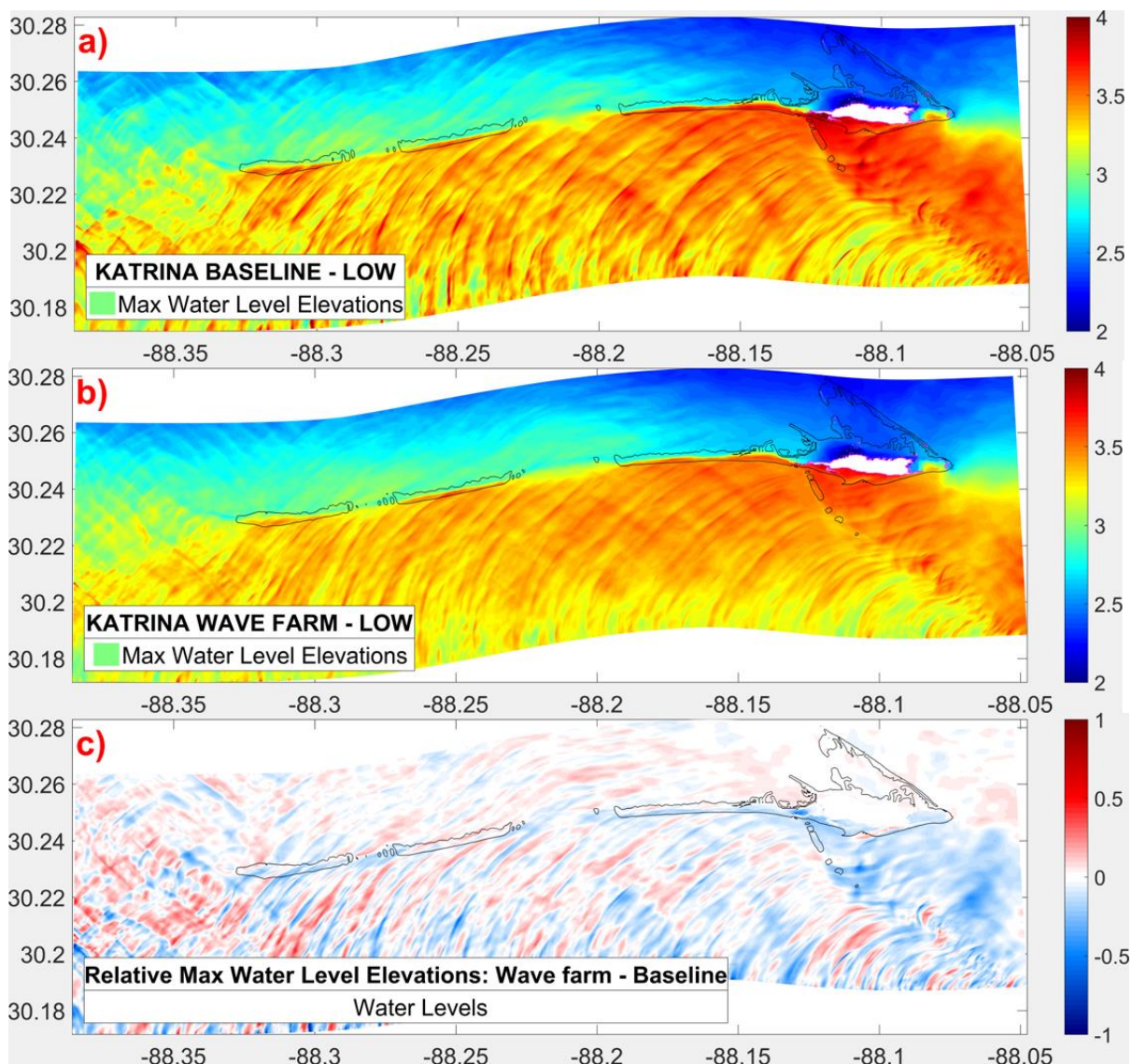
Figure 4-6: Hurricane Katrina - Low SLR scenario: Max Water Levels for baseline (a) and wave farm (b) cases (c) Difference between the two cases: b subtracted from a. (Blue color represents the areas where maximum TWLs are lower in the wave farm scenario compared to the baseline scenario, and the red color represents the areas where the TWLs are higher with the presence of a wave farm) The black line is the post-storm zero-meter contour of the island.
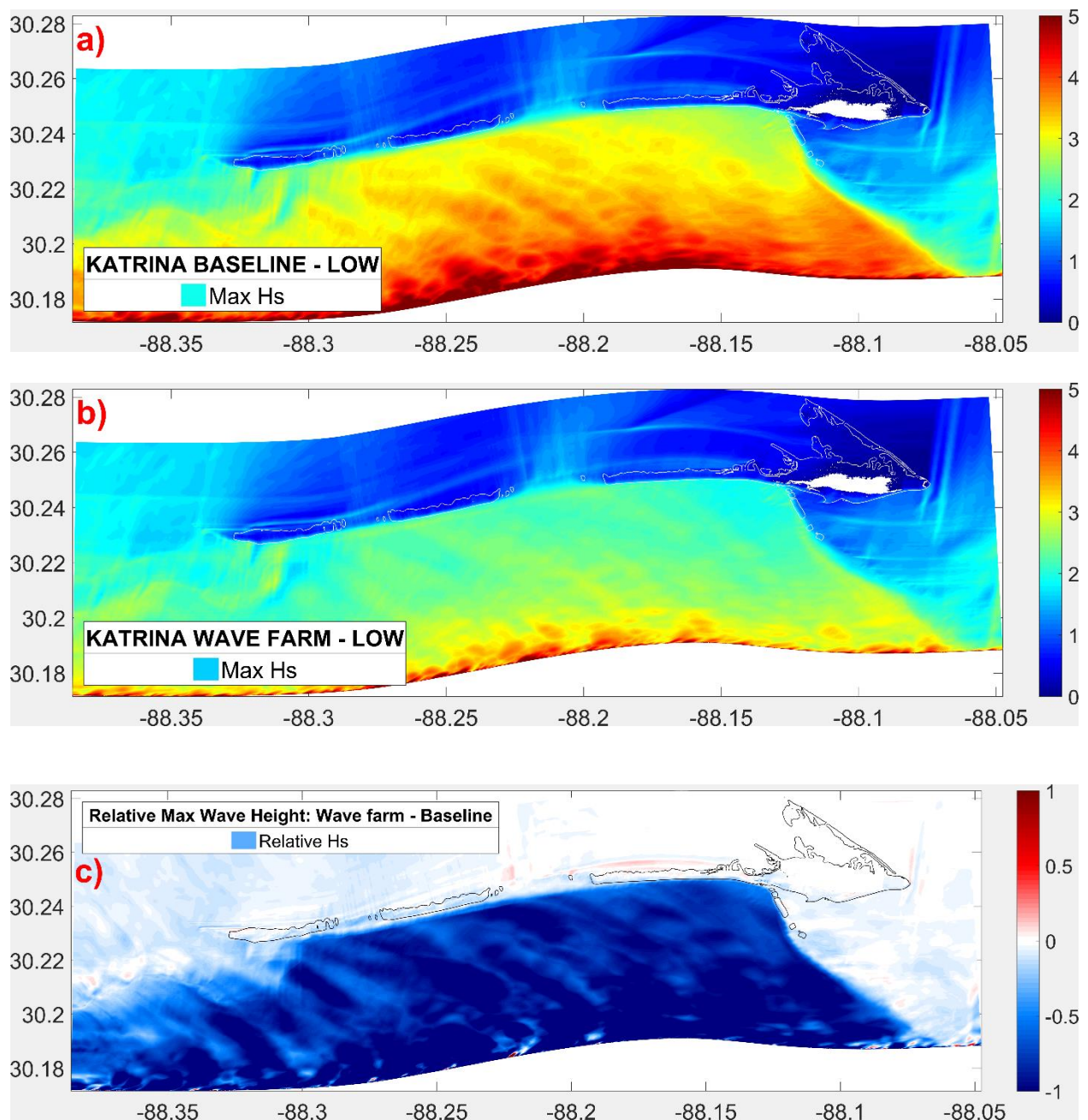
Figure 4-7: Hurricane Katrina - Low SLR: Maximum wave heights (Hs) across the domain: (a) baseline scenario, (b) wave farm scenario (c) Hs difference between the two scenarios in [m] Baseline values are subtracted from wave farm values. The blue color represents the reduction in Hs due to WECs, and the red color represents the increase in Hs due to WECs. White and black lines are the post-storm zero-meter contours of the island

The analysis is repeated for the *intermediate-low SLR* scenario where the mean water level is 0.5

m to observe the changes in the results under the rising sea levels (the relevant figures and tables

101

are included in Appendix A). The island gets completely inundated under both Low and Int-Low SLR scenarios. Therefore, the impacts of WECs on the hydrodynamics remain unchanged as the mean sea level increases by 0.3 m. This indicates that the effectiveness of WECs to impact the hydrodynamics decreases as the SLR and TWL increases.

Unlike the Hurricane Ivan simulations, the maximum Hs difference figures (Figure 3-11c, Figure 4-7c, and Figure A- 7) do not show an increasing *offshore* Hs reduction potential of WECs as the mean sea level rises. This tells us that the Hs reduction potential of WECs in the offshore wave climate depends on the storm conditions, i.e., an increase in mean sea level improves the efficiency of WECs to reduce offshore Hs; however, higher TWL due to the intense storm conditions (as in Hurricane Katrina) may dampen this efficiency. On the other hand, it is observed that WECs are most efficient in reducing the *nearshore* wave heights under lower mean sea level conditions, like in the case of Ivan. On average, at a reference mid-domain nearshore alongshore transect (~latitude 30.2343°N), WECs reduce the wave heights by 0.66 m under Int-Low SLR scenario, as opposed to a 0.72 m reduction under Low-SLR scenario. This suggests that the effectiveness of WECs to reduce nearshore Hs declines under rising sea level conditions.

4.3.2.2 Response of Morphology to Simulated Wave Farms Under SLR Scenarios

To relate the impacts of water levels to coastal morphology, the dune heights, bed elevations, inundated area, and bed shear stress are observed across the island under Low-SLR scenario.

The TWL exceeds the dune heights and completely inundates the whole island during the peak of the storm under Low-SLR scenario (Figure 4-5a). Despite the complete inundation, final dune heights in both transects are slightly (~0.1m) higher when the wave farm is present. Average post-

storm dune heights across the island under Low-SLR scenario are found to be 2.43 m and 2.50 m in the baseline and wave farm cases, respectively. In other words, the dune erosion across the island is mitigated by 3% when the hydrodynamic impacts of wave farms are present.

It is noted that in the baseline scenario, the sediment is transported ~60 m further inland compared to the wave farm cases at the west transect (Figure 4-5a), while sediment transport follows a similar pattern for both cases at the east transect (Figure 4-5b). Differences in the final bed elevations across Dauphin Island post-Katrina for the baseline and wave farm conditions under Low-SLR scenario are shown in Figure 4-8. A large breach occurs in the western portion of the island under the intense storm and Low-SLR conditions in both baseline and wave farm cases. Although the presence of WECs does not prevent breaching, less cross-barrier sediment transport is observed in the wave farm scenario in the west and middle breach locations.
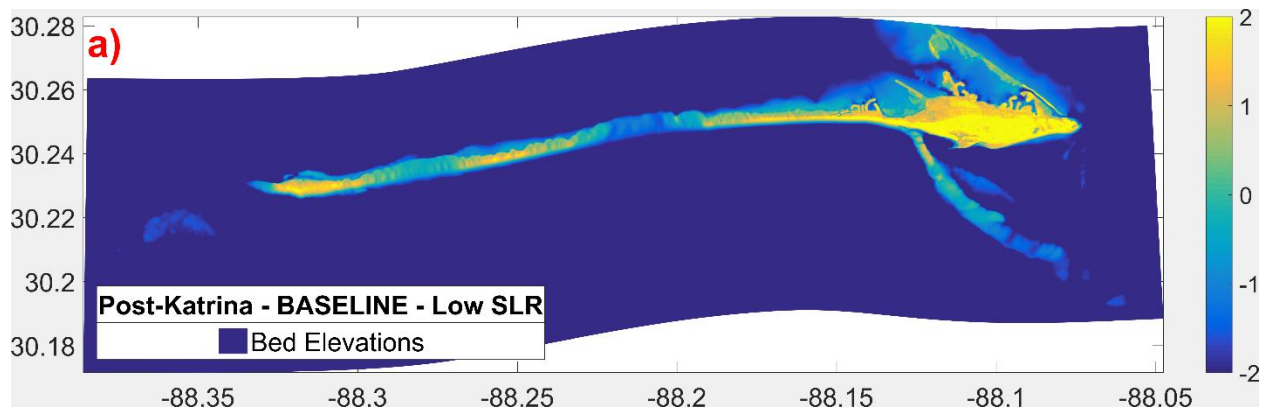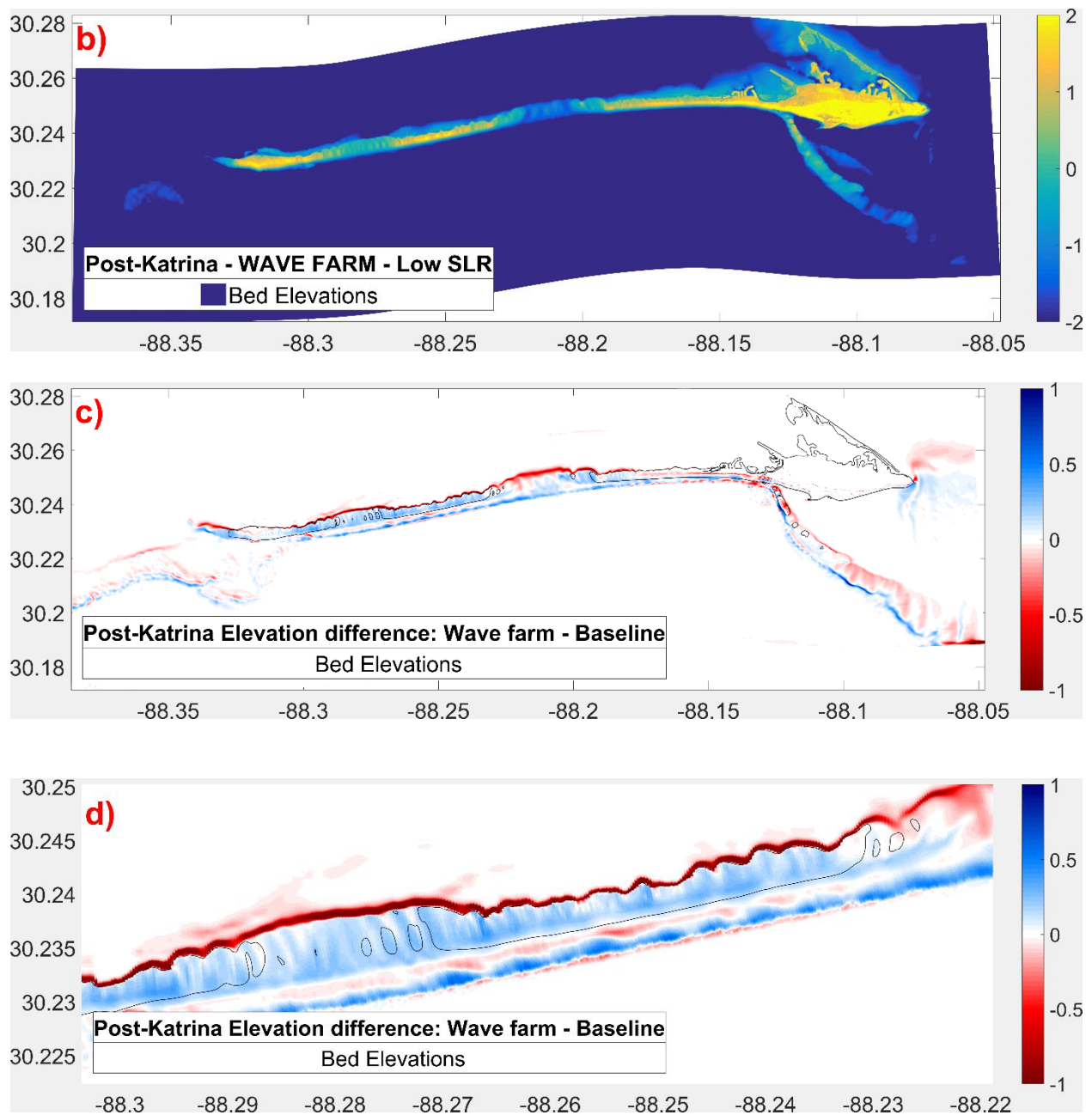
Figure 4-8: Final bed elevations [m] for baseline (a) and wave farm (b) cases under Low-SLR scenario (c) Difference between the two scenarios (d) Magnified version of (c) showing the channels in the western portion – Positive (blue) values show the locations where the final elevations are higher in the wave farm scenario. The black line is the post-storm zero-meter contour of the island.

The results of the inundated area, volume loss, and bed shear stress calculations for both cases under Low-SLR are presented in Table 4-3. It is observed that the post-storm subaerial island area

and subaerial sand volume are higher, and the total inundated area and net loss in the sand volume are lower in the wave farm case compared to the baseline case. Results indicate a 10% less net loss in sand volume due to the wave farm, which illustrates the potential benefits of WECs as a coastal defense mechanism, despite being less substantial compared to Hurricane Ivan cases.

The maximum shear stress in the wave farm and baseline cases are listed in Table 4-3. The maximum averaged bed shear stress values are reduced from 104.65 to 100.45 N/m^2 for the baseline and wave farm scenarios, respectively (11% reduction). This exemplifies that the presence of wave farms can reduce sediment transport on the ocean floor by weakening the bed shear stress. Again, the reduction in the y-direction (alongshore) (4%) is found to be lower than the reduction in the x-direction (cross-shore) (12%), demonstrating that the wave farms have a higher impact on the bottom sediment transport in cross-shore direction than in alongshore direction.

Table 4-3: Inundated and dry areas, initial and final sand volume, net loss in sand volume, and max bed shear stress values in x- and y- directions [N/m2] averaged over time in the mid-domain nearshore area for Hurricane Katrina for baseline and wave farm cases under Low SLR scenario.

Katrina Low-SLR	Baseline	Wave farm	Difference (m^2/m^3/%)	Impacts of WECs
Initial island area (millions of m^2)	13.70	13.70	0	-
Total dry area (millions of m^2)	1.69	1.79	0.1	More dry area w/ WECs
Total inundated area (millions of m^2)	12.01	11.91	-0.1	Less inundation w/ WECs
Initial sand volume (millions of m3)	19.7	19.7	0	-
Final sand volume (millions of m^3)	17.69	17.89	0.2	More sand volume w/ WECs

Net loss in sand volume (millions of m^3)	2.01	1.81	-0.2 (10%)	Less sand loss w/ WECs
Max τ_{bx}	292.4	258.06	-12%	Less τ_{bx} w/ WECs, less sediment mobilization
Max τ_{by}	104.65	100.45	-4%	Less τ_{by} w/ WECs, less sediment mobilization
Max $\tau_b = \sqrt{\tau_{bx}^2 + \tau_{by}^2}$	310.56	276.92	-11%	Less τ_b w/ WECs, less sediment mobilization

The analysis is repeated for the *Intermediate-Low SLR* scenario to observe the changes under the rising sea levels (the relevant figures and tables are included in Appendix A). Due to high TWL (up to 4 m) and intense storm conditions, no substantial difference between the Low and Int-Low SLR scenarios are observed during Hurricane Katrina. Table 4-4 summarizes the reduction percentages of some proxies that do change with the rising sea levels. Table 4-4 supports that the effectiveness of WECs on mitigating coastal erosion decreases as the mean sea level increases; however, wave farm case still results in overall higher post-storm bed level elevations, higher dunes, more dry area, and less shear stress compared to the baseline case. Also, the percent reductions in the dune erosion, net sand volume loss, and total max shear stress due to WECs appear to reduce as the sea levels increases. This again shows that WECs are more effective in protecting the coast under lower SLR scenarios.

Table 4-4: Comparison of the qualitative results under present-day (no SLR), Low and Int-Low SLR scenarios

	Katrina No SLR	Katrina Low	Katrina Int-Low
Dune erosion reduction due to WECs	4%	3%	2%
Reduction in net sand volume loss due to WECs	11%	10%	6%
Reduction in total max shear stress due to WECs	22%	11%	8%

4.4   Discussion

Simulations to investigate the impacts of a wave farm on coastal morphology during storm conditions and SLR scenarios show that there is overall lower TWL and max Hs, less overwash, less inundated area, less sand volume loss, lower cross-barrier sediment transport, and lower bed shear stress magnitudes in the wave farm scenario, compared to the baseline scenario under both Low and Int-Low SLR scenarios. However, the reduction of storm impacts from the wave farm on coastal morphology and the ensuing ocean climate vary spatially. Despite having some areas that are negatively impacted by the WECs (i.e., due to increased Hs, TWL, and bed erosion due to WECs), or not impacted at all, most of the domain experiences the erosion mitigation impacts of the wave farm under both SLR scenarios. This shows that wave farms have the potential to be used as a coastal defense mechanism.

It is observed that the WECs are most effective in reducing the offshore TWL at the location of the highest maximum water levels under both SLR scenario and the present-day (no SLR) scenario

(Figure 3-6c, Figure 4-2c, Figure A- 2c). The figures illustrating the difference between maximum Hs in wave farm and baseline cases (Figure 3-7c, Figure 4-3c, and Figure A- 3c) show an increasing offshore Hs reduction potential of WECs as the mean sea level rises from 0 to 0.5m. This can be attributed to the lowered ocean bottom friction felt at the sea level due to increased TWLs; therefore, the impacts of WECs on TWL can be more pronounced. On the other hand, it is observed that WECs are most efficient in reducing the nearshore wave heights under lower mean sea level conditions. This is likely due to the representation of wave farms at the offshore boundary and that the impacts of WECs diminish as waves propagate to shore. When the mean sea level is lower nearshore, it is less likely to have overwash and inundation. Therefore, the impacts of WECs on Hs reduction nearshore can be more distinct. This could be useful when deciding on the location of a potential wave farm, although the varying impact of the wave farm across the domain emphasizes the need for a thorough analysis when implementing WECs for coastal protection of specific locations.

Table 4-2 and Table 4-4 illustrate the gradually reduced impact of WECs on mitigating coastal erosion as the sea levels rise from 0 to 0.5 m. Also, the reductions in dune erosion, net sand volume loss, and max shear stress percentages with the presence of WECs are lower under Hurricane Katrina compared to Hurricane Ivan. This tells us that the effectiveness of WECs in preventing coastal erosion depends on the mean sea level and peak stormwater levels, i.e., WECs are more effective in mitigating coastal erosion when the mean sea level is lower than 0.5 m. The same analysis is repeated for Intermediate-High (1.2 m) and High (2 m) SLR scenarios to determine the threshold mean sea level where the WECs are still effective in altering the hydrodynamics and morphodynamics in their lee. Simulations show minimal difference between the baseline and wave

farm scenarios under Int-High and High SLR conditions (Appendix A). Therefore, it can be concluded that the wave farms can be effective in mitigating the coastal erosion for a mean sea level of 0.5 m and lower under mild storm conditions.

4.5 Conclusions

This study investigates the potential for wave farms, conventionally used to generate renewable energy, to mitigate coastal erosion during storm conditions and rising sea levels. XBeach simulations of baseline and wave farm cases demonstrate that wave farms can alleviate the factors that cause coastal erosion, such as wave attack, bed shear stress, and overwash and inundation even under Low and Int-Low SLR scenarios. It has shown that the dune erosion across the island is mitigated up to 8% during Ivan, and up to 3% during Katrina when the hydrodynamic impacts of wave farms are represented under SLR conditions. Similarly, reduction in net sand volume loss due to WECs reaches 13% and 10% during Ivan and Katrina, respectively. These percent reductions in the dune erosion, net sand volume loss, and total max shear stress due to WECs appear to reduce as the sea levels increases in Katrina simulations. This shows that WECs are more effective in protecting the coast under lower SLR scenarios.

Simulations for both Katrina and Ivan yield similar results, supporting the idea that wave farms can be effective in mitigating erosion under SLR conditions for storms of varying intensity, at varying effectiveness levels. A comparison of the results of Ivan and Katrina simulations shows that wave farms are shown to be less effective in changing the regime and protecting the integrity of dunes during intense, stronger storms combined with a 0.5m and higher mean sea level. Moreover, WECs are most effective in reducing the nearshore Hs under lower mean sea level. On

the other hand, Ivan simulations show an increasing offshore Hs reduction under higher mean sea level while this has not been observed in the Katrina simulations. This indicates that Hs reduction potential of WECs in the offshore wave climate depends on the storm conditions. In other words, an increase in mean sea level improves the efficiency of WECs to reduce *offshore* Hs; however, higher TWL due to the intense storm conditions (as in Hurricane Katrina) may dampen this efficiency. This observation can be useful when deciding on the location of a potential wave farm, although the varying impacts of the wave farm across the domain highlights the need for an exhaustive analysis when implementing WECs for coastal protection of specific locations.

Intermediate-High (1.2 m) and High (2 m) SLR scenarios are also analyzed to determine the threshold mean sea level where the WECs are still effective in altering the hydrodynamics and morphodynamics. Although these higher SLR scenarios are too extreme to mitigate with this measure, WECs have been demonstrated to modulate coastal erosion under lower SLR scenarios. This tells us that the effectiveness of WECs in preventing coastal erosion depends on the mean sea level and peak stormwater levels, i.e., WECs are more effective in mitigating coastal erosion when the mean sea level is lower than 0.5 m.

A wave farm is a promising approach to mitigating coastal erosion; however, its capacity to influence intense morphodynamics is limited; it cannot reckon with the most severe storms. More resilient and efficient WEC technologies may be able to reduce coastal erosion caused by the strongest hurricanes, especially considering that the WECs are highly adaptable to the changing climate (e.g., floating point-absorber WEC types can simply rise with rising sea levels). It is seen that the effectiveness of WECs to alter hydrodynamics and morphodynamics in their lee generally reduces with the increasing mean sea level and storm intensity. Therefore, additional erosion

mitigation measures such as living shorelines may be used in addition to WECs in the future when

the mean water level exceeds 0.5 m.

CHAPTER 5:   ASSESSMENT OF WAVE POWER POTENTIAL

The content in this chapter is published as: Ozkan, C., & Mayo, T. (2019). The renewable wave energy resource in coastal regions of the Florida peninsula. *Renewable energy*, *139*, 530-537.

5.1   Introduction

Recently, there has been a global effort to increase the utilization of renewable energy resources (see, e.g., adaptation strategies outlined in the Paris Agreement (UNFCCC, 2015)). In 2016, 12.4% of the electricity consumed in the United States was obtained from renewable energy resources (Department of Energy, 2019), and Executive Order 13693 proposed a reduction in the nation's greenhouse gas emissions by 40% or more over the next decade while increasing the percentage of electricity obtained by renewable energy resources to 30% by 2025 (The White House, 2015). As a result, there is a growing interest in unexploited renewable energy resources, including ocean waves, which constitute one of the largest, most consistent sources of renewable energy. The Electric Power Research Institute (EPRI) estimates the available wave power along the Gulf of Mexico and east coasts of the United States as 60 TWh and 160 TWh each year, respectively (BOEM, 2009). Given that 1 TWh can power an average of 93,850 US homes annually (BOEM, 2009), it is likely that oceans can greatly contribute to overall energy production. Ocean wave energy is an especially promising resource in coastal Florida. Furthermore, the average annual electricity consumption of a typical household in Florida is nearly 14,500 kWh (United States Energy Information Administration, 2009), and ocean wave energy has the potential to significantly contribute to the supply of this demand.

One of the primary benefits of ocean wave energy is that it is highly predictable compared to more conventional energy sources. Waves are mainly generated by wind, with wind strength dictating wave heights and wave periods, primary determinants of wave energy. Wind-driven wave energy can be harnessed and converted into electricity by wave energy conversion devices (WECs). WECs are not entirely efficient, and only a fraction of the total available ocean wave energy can be harnessed; they generally operate with an efficiency of 20-40% (Previsic et al., 2004). There are various types of WECs, and for a specific location, the most suitable type should be chosen for installation based on local coastal properties including bathymetry, geography, dominant wind, wave directions. Potential impacts on human and marine life must also be considered. The implementation and operation of WECs can be both economically and environmentally costly, thus available wave energy should be carefully assessed for regions of interest prior to investment in WEC farms.

To date, both regional and global wave power assessments have been conducted. Many studies have focused on regions in Western Europe, as wave heights are considerably high there year-round (Gallagher et al., 2016; Pontes, 1998; Smith et al., 2013; Van Nieuwkoop et al., 2013). In the United States, wave power assessment studies have focused on regions in the Pacific Coast and Hawaii (Bedard and Date, 2004; Bedard and Previsic, 2004; Beyene and Wilson, 2007, 2006; Kim, 1997; Stopa et al., 2013; Wilson and Beyene, 2007). Though several early studies have described portions of the Florida coast as "low energy" (Davis and Hayes, 1984; Gorsline, 1966; Hine et al., 1988), recent studies have not quantitatively assessed available wave power. We aim to bridge this gap here. Among existing wave power assessments, both numerical models and observed data have been used to estimate wave power potential (Lenee-Bluhm et al., 2011; Stopa

et al., 2013). These methods have advantages and disadvantages. Using buoy data to calculate wave power yields the most accurate results in theory, however, this method is limited by available measurement instruments and their accuracy. Mackay et al. (Mackay et al., 2009) and Young et al. (Young et al., 2012) investigate the uncertainty in wave buoy measurements and numerical models, as well as the difference between the measured wave heights using various instruments. Mackay et al. conclude that despite the variability between wave measurement instruments, the amount of uncertainty that comes with wave buoy measurements is less than the uncertainty associated with the errors in modeled data. Numerical models enable researchers to assess the wave climate on large scales, however, they are subject to the uncertainties arising from the approximation of physics and discretization of equations, and relying solely on their results may lead to design failures. As stated in (Mackay et al., 2009), several errors including non-stationary bias, large variance in model output, and temporal offsets are likely to occur when using modeled data. In light of these findings, this study focuses on a wave resource assessment using historical buoy data in coastal regions of Florida.

Available wave power can be estimated using one of two equations. The first (hereafter referred to as the spectral wave equation) requires spectral wave data for different wave frequencies. The second equation (hereafter referred to as the standard wave equation) is a simplified version of the first and is most often used. It assumes deep water to reduce the number of parameters necessary for the calculation of available wave power to the "standard" wave parameters, wave height and wave period. We anticipate that the spectral wave equation more accurately estimates available wave power (Mackay et al., 2009; Prevosto et al., 2007); it does not require the deep water

assumption used in the standard wave equation, and it accounts for different wave frequencies in contrast to standard wave data, which only describes the wave height and wave period.

In this paper, we investigate potential WEC farm locations in coastal regions of Florida by assessing available wave power. Wave characteristics vary both temporally and spatially, so we assess wave power for several locations and time periods. Initially, we compute wave power estimates using the standard wave equation, as is commonly done in wave energy assessments (see e.g. (Defne et al., 2009b; Saglam et al., 2010; Sierra et al., 2016)). We then assess the impact of using this simplification by recomputing the estimates using the more comprehensive spectral wave equation, with the goal of understanding how standard wave data might be used to produce accurate estimates of wave power for a larger number of coastal locations, i.e., where spectral wave data is not available.

5.2   Methodology

5.2.1   *Estimation of Wave Power*

Wave power is often approximated using the following equation

$$P = \frac{\rho g^2}{4\pi} \int_0^\infty \frac{S(f)}{f}\left[\left(1 + \frac{2k_f d}{\sinh(2k_f d)}\right)\tanh(k_f d)\right] df$$

(see e.g. the 2011 technical report of the EPRI (EPRI, 2011)), where ρ is the density of water (kg/m^3), g is gravitational acceleration (m/s^2), S is the spectral energy density (m^2/Hz), f is the wave frequency (1/s), k_f is the wave number for wave frequency f (m^{-1}), and d is the water depth (m). Since the wave records and the frequency spectrum are generally represented using discrete values, the above equation can be expressed as a summation,

115

$$P = \frac{\rho g^2}{4\pi} \sum_{i=1}^{N} \frac{S_i}{f_i} \left[\left(1 + \frac{2k_{f_i}d}{\sinh(2k_{f_i}d)} \right) \tanh(k_{f_i}d) \right] \Delta f_i \qquad (5.1)$$

where S_i is the spectral energy density for the ith frequency bin (m^2/Hz), f_i is the ith wave frequency

(1/s), and k_{fi} is the corresponding wave number (m^{-1}). (The wave number, k, is determined using

the implicit formula $k = \frac{4*\pi^2*f^2}{g*tanh(kd)}$. In this work, we determine k using fixed point iterations.)

This equation computes the power (kW/m) of the wave spectrum at a given location. We average

hourly power data over one year to estimate the average annual wave power available at locations

of interest.

For large values of $k_f d$, the limit of *sinh* approaches infinity and the limit of *tanh* approaches 1,

$\lim_{k_f d \to \infty} \sinh(k_f d) = \infty$ and $\lim_{k_f d \to \infty} \tanh(k_f d) = 1$. In these cases, the term in the square brackets

of Eq (5.1) reduces to 1, and

$$P = \frac{\rho g^2}{4\pi} \sum_{i=1}^{N} \frac{S_i}{f} \Delta f$$

The summation is the -1th spectral moment, $m_{-1} = \sum_{i=1}^{N} \frac{S_i}{f} \Delta f$, which can be expressed in terms

of significant wave height, H_s, and the average wave energy period, T_e, $m_{-1} = \frac{T_e * H_s^2}{16}$. Large

values of $k_f d$ most often result from large values of d, thus in deep water Eq (5.1) can be

reduced to

$$P = \frac{\rho g^2}{4\pi} \sum_{i=1}^{N} \frac{S_i}{f} \Delta f = \frac{\rho g^2}{4\pi} \frac{T_e * H_s^2}{16} = \frac{\rho g^2}{64\pi} T_e * H_s^2$$

Approximating the density of (sea) water as $\rho = 1.025$ kg/m^3 and gravitational acceleration as g

$= 9.8067$ m/s^2, the hourly power potential can thus be approximated as

$$P = 0.49 * T_e * H_s^2 \qquad\qquad (5.2)$$

Note that this equation only requires standard wave parameters, which are more readily available than the spectral wave data required in Eq (5.1). We use both equations with existing wave data to assess the available wave power in coastal Florida and quantify the errors introduced by implementing the simplification.

5.2.2   *Availability of Wave Data*

We perform all wave power calculations using wave data retrieved from the National Data Buoy Center (NDBC). The NDBC has continuously monitored hourly standard wave data (wave height and wave period) at several buoys in close proximity to Florida for the past 10 to 30 years. The data is publicly available and is regularly updated on the NDBC website (NOAA, 2005).

The NDBC obtains wave measurements through accelerometers that are built into the buoys. Accelerometers record the heave acceleration of buoy hulls throughout the wave acquisition time, which is 20 minutes for the buoys used in this study. From the heave acceleration, vertical displacement of the buoys and sea surface elevation data is calculated (CDIP, 2019). Spectral wave density measurements can also be taken. Time-series measurements of the sea surface elevation are transformed to the wave spectrum through a Fast Fourier Transform (FFT), i.e., data is transformed from the temporal domain to the frequency domain, here with N = 47 frequency bins (NDBC, 2018). Once the non-directional wave spectrum measurements are obtained, wave parameters such as significant wave height, average wave period, and dominant wave period can also be derived.

The measured wave data is compiled and distributed to the public online, but not until the datasets undergo a tedious quality control process. Despite and perhaps due to this process, historical datasets still have considerable amounts of missing data. This is largely due to the fact that buoys cannot stay operational during extreme events or maintenance periods. Also, older measurement technologies were not of the same quality as the state of the art techniques of today.   For both standard wave data and spectral wave data sets, we have opted to exclude missing data from our calculations (as opposed to, e.g., interpolating data from nearby points). Once the gaps in data are addressed, we estimate the wave power potential at locations of interest using both wave equations, Eq (5.1) and Eq (5.2).

The NDBC buoys in coastal Florida are pictured in Figure 5-1. While the implementation of Eq (5.2) requires wave height and wave period only, the FFT needed to implement Eq (5.1) must be executed by an on-board processor. Only some buoys have processors with this capability, therefore spectral wave data can only be collected at locations with this specific type of instrumentation. The majority of the buoys in coastal Florida do not have this, and as a result, spectral wave data is much more sparse than standard wave data; spectral wave data is only available at six of the ten NDBC measuring locations near Florida (circled in red in Figure 5-1). Additionally, the data has not been available for nearly as long nor has it been collected as frequently.   This sparsity of data limits the times and locations for which Eq (5.1) can be implemented.
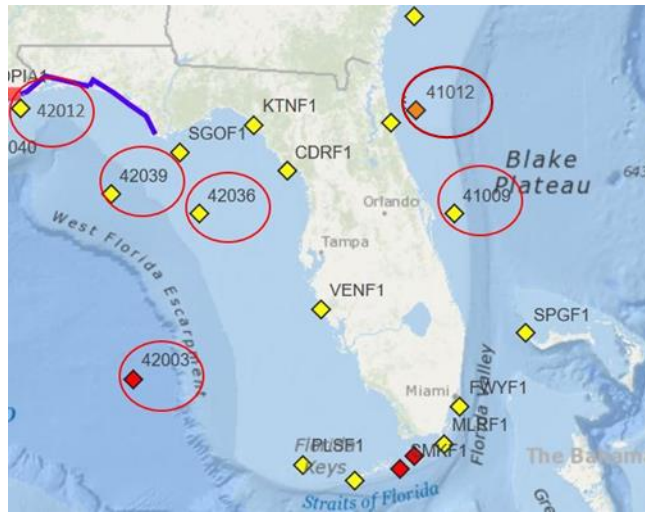
Figure 5-1: NDBC measuring locations, denoted by five character station codes. Standard wave data, wave height and wave period, are available at all locations. Locations that additionally measure spectral wave density values are circled in red

The availability of wave data for ten buoys in the Gulf of Mexico and the Atlantic Ocean is summarized in Table 5-1. For these stations, wave data is available over the past 10 to 20 years for spectral wave data and up to 30 years for standard wave data. Station 41012 was disestablished in 2014 and there are only 8 years of available spectral wave data and 10 years of standard wave data for this location. Given these constraints, we estimate available wave power in coastal Florida using both Eq (5.1) and Eq (5.2) for the five-year period 2010-2014 at the six locations corresponding to the NDBC buoys that measure spectral wave data (i.e., Stations 41012, 41009, 42003, 42036, 42039, and 42012). The specifications of these buoy stations are summarized in Table 5-1.

Table 5-1: Data availability for NDBC buoys in coastal Florida

Station Code	Standard data Available	Spectral data Available
41112	X	-
41012	X	X
41009	X	X
41113	X	-
41114	X	-
42003	X	X
42099	X	-
42036	X	X
42039	X	X
42012	X	X

Table 5-2: Buoy locations and specifications

Station	Buoy Type	Owner	Location	Payload Type	Water depth	Watch circle radius
ST41012	3-meter discus buoy	NDBC (Funded by NOAA)	30.042 N 80.534 W	AMPS payload	38.1 m	94.4 yards
ST41009	3-meter foam buoy	NDBC	28.501 N 80.184 W	SCOOP payload	40 m	115 yards

Station	Buoy Type	Owner	Location	Payload Type	Water depth	Watch circle radius
ST42003	3-meter discus buoy	NDBC	25.930 N 85.638 W	SCOOP payload	3250 m	3305 yards
ST42036	3-meter discus buoy	NDBC	28.501 N 84.516 W	ARES payload	49.7 m	129 yards
ST42039	3-meter foam buoy	NDBC	28.788 N 86.008 W	AMPS payload	270 m	477 yards
ST42012	3-meter foam buoy	NDBC	30.064 N 87.551 W	AMPS payload	25.9 m	60 yards

5.3   Results

Using the procedures discussed above, we assess the available wave power in coastal Florida. We first evaluate the errors introduced by using the more commonly implemented standard wave equation. We then discuss the estimates of available wave power in coastal Florida and the temporal and spatial variability of the results. Data analysis is carried out between 2010 and 2014 for the six locations highlighted in Figure 5-1, as both standard and spectral wave data are available at these locations at these times (Table 5-1)

5.3.1   *Impact of Using Standard Wave Data to Estimate Available Wave Energy*

We use several metrics to compare estimates of the wave power computed using Eq (5.1) to estimates computed using Eq (5.2). Quantile-quantile plots of the wave power values computed using standard and spectral wave data from 2014 are shown in Figure 5-2. Each of the Q-Q plots

shown is approximately linear, and thus it can be assumed that the shapes of the distributions underlying the available wave power values are the same. In fact, for each of the stations in the Gulf of Mexico (i.e., stations 42003, 42036, 42039, and 42012), the quantiles corresponding to the spectral wave power data and standard wave power data lie along the line $y=x$ up to the last decile; the data comes from distributions that are nearly identical. However, for the two stations in the Atlantic Ocean, stations 41012 and 41009, the quantile pairs, though linear, lie along a line beneath $y=x$, indicating the standard and spectral wave power data come from different distributions. Specifically, the tail of the distribution of the wave power obtained from the spectral wave equation decays faster than that obtained from standard wave equation. Physically, this means that larger values of wave power (defined relative to the averages) are observed less frequently when spectral wave density data is used; using standard wave data may overestimate the frequency at which large values of wave power occur. The quantile-quantile plots of data for other years yield similar results (See Appendix B.1 for QQ plots of a sample location, St42003, for all years).
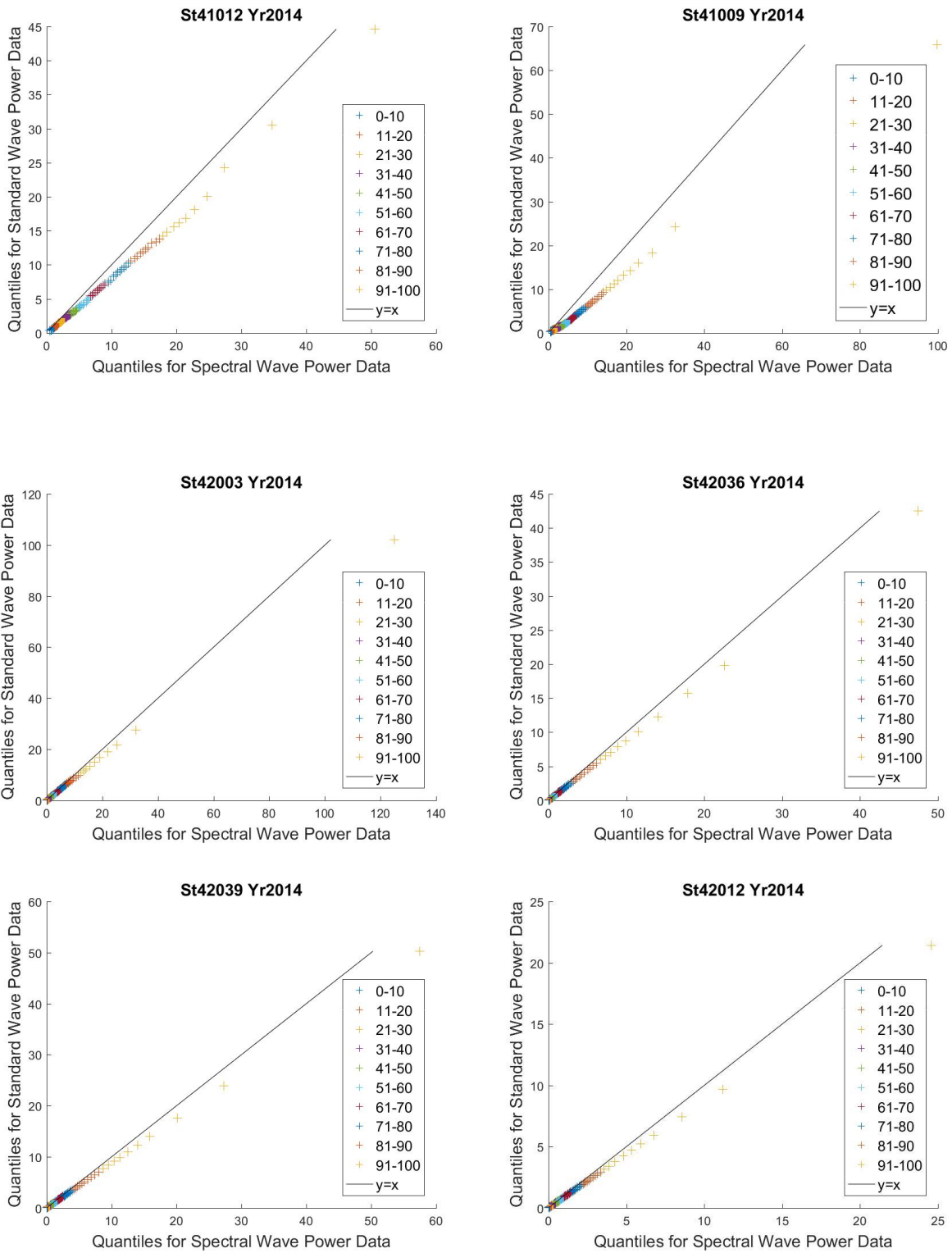
Figure 5-2: Quantile-quantile plots of available wave power estimated using standard and spectral wave data in 2014

The average annual wave power for each buoy station from 2010 to 2014 computed using standard and spectral wave data is shown in Figure 5-3. There is variation in the computed values temporally and spatially, however, the wave power estimates obtained using standard wave data are always less than those obtained using spectral wave data.
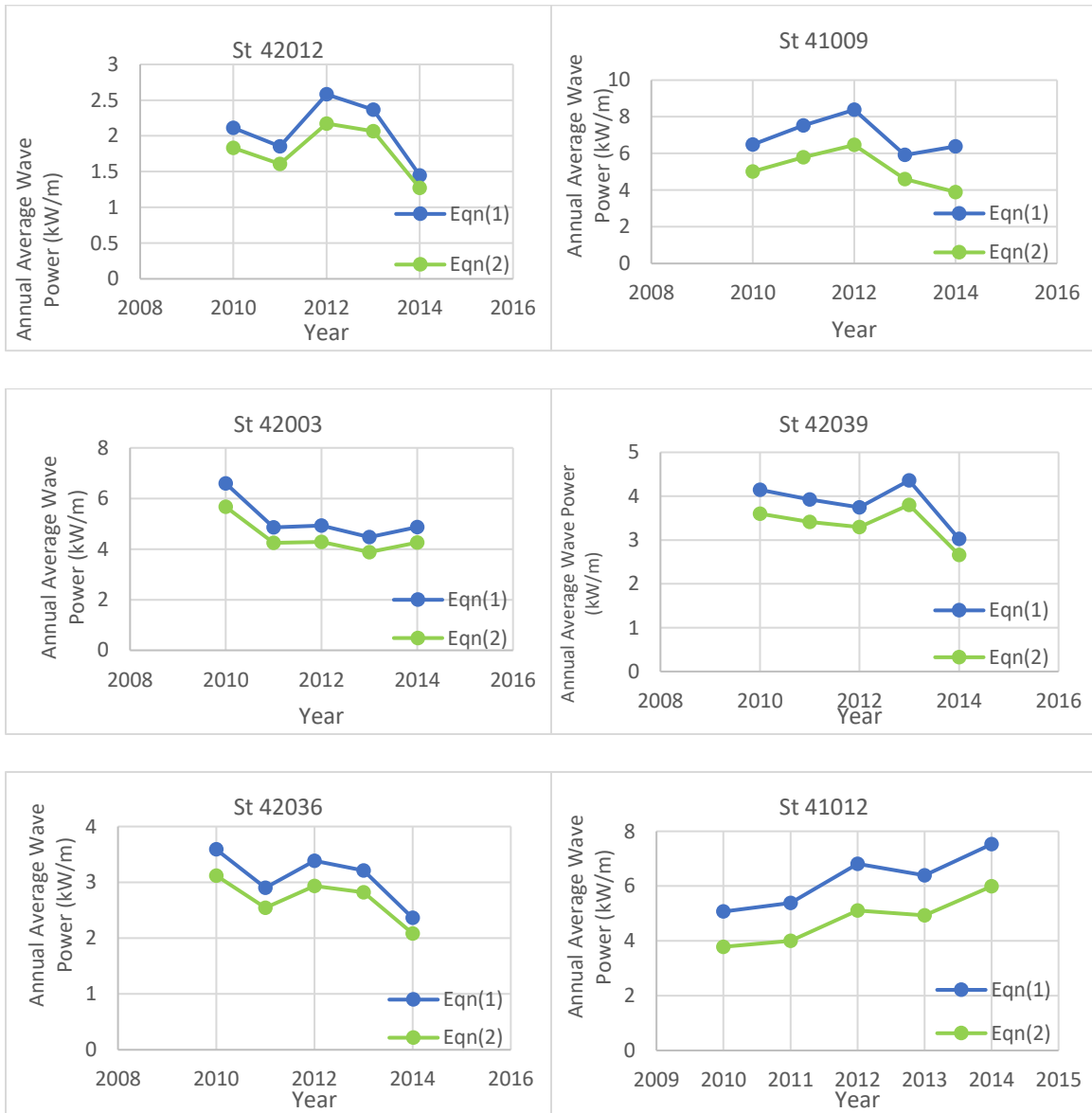

Figure 5-3: Average annual wave power estimated for the years 2010-2014

This is expressed quantitatively through the bias in hourly wave power data, or the average deviation of the standard power values from spectral power values, which has a mean value of -0.4362 kW/m across all years across all buoy stations. (For this and all other statistical values, we use the third-eight deciles of data for computation.) The root mean square difference in the power values has a mean value of 0.7335 kW/m across all years across all buoy stations. Both the bias and RMSD are considerably larger in absolute value in the Atlantic Ocean, with average values of -0.9336 and 1.300 kW/m, respectively, in contrast to the average values in the Gulf of Mexico, -0.1875 and 0.4501 kW/m. Additionally, it is worth noting that Stations 42036 and 42012 have the smallest biases, even though Stations 42003 and 42039 are at the greatest depths (Table 5-2) and are thus expected be least impacted by the deep water assumption. Hourly wave power data computed using standard and spectral wave data are highly correlated, with an average correlation coefficient of 0.9155 for data obtained between 2010 and 2014. (Linear regression plots for 2014 are shown in Figure 5-4, and linear regression plots for other years yield similar results. E.g., see Appendix B.2 for linear regression plots for 2010.) For each station, the slope of the regression line that fits the data ranges from 0.7707 to 0.9092 with the exception of Station 41009 in 2014, which has a slope of 0.5459. (It is unclear why this particular value is so low, however, the scatter index for this station is notably high. Also, there is no maintenance report for this buoy station for this year, which suggests that there is more noise in this data, as this type of low slope is not observed for the other years of study). Again, we find that trends in the data differ from the Atlantic Ocean to the Gulf of Mexico. Slopes of the regression lines are lower for every year of the study for the stations in the Atlantic Ocean. The average slope of the regression line that fits the data from the Atlantic Ocean is 0.7743 in contrast to that from the Gulf of Mexico, which has an average slope of 0.8916. The average slope overall is 0.8525, indicating that wave power estimated using

125

standard wave data should be amplified by a factor of approximately 1.173 for a more realistic assessment. However, this factor should be increased to 1.292 for regions in the Atlantic Ocean and decreased to 1.122 for regions in the Gulf of Mexico to reflect the spatial dependence of the regression analyses. This is in contrast to multiplicative factors commonly employed in the literature. For other regions, wave power estimated using standard wave data is generally reduced (e.g. in (Defne et al., 2009b) it is determined that a factor of 0.61 should be used for estimates of wave power in regions near the Atlantic coast north of Florida). This highlights the spatial dependence of the errors induced by using the simplified equation and demonstrates the need to estimate the multiplicative factor locally if spectral data is not available.
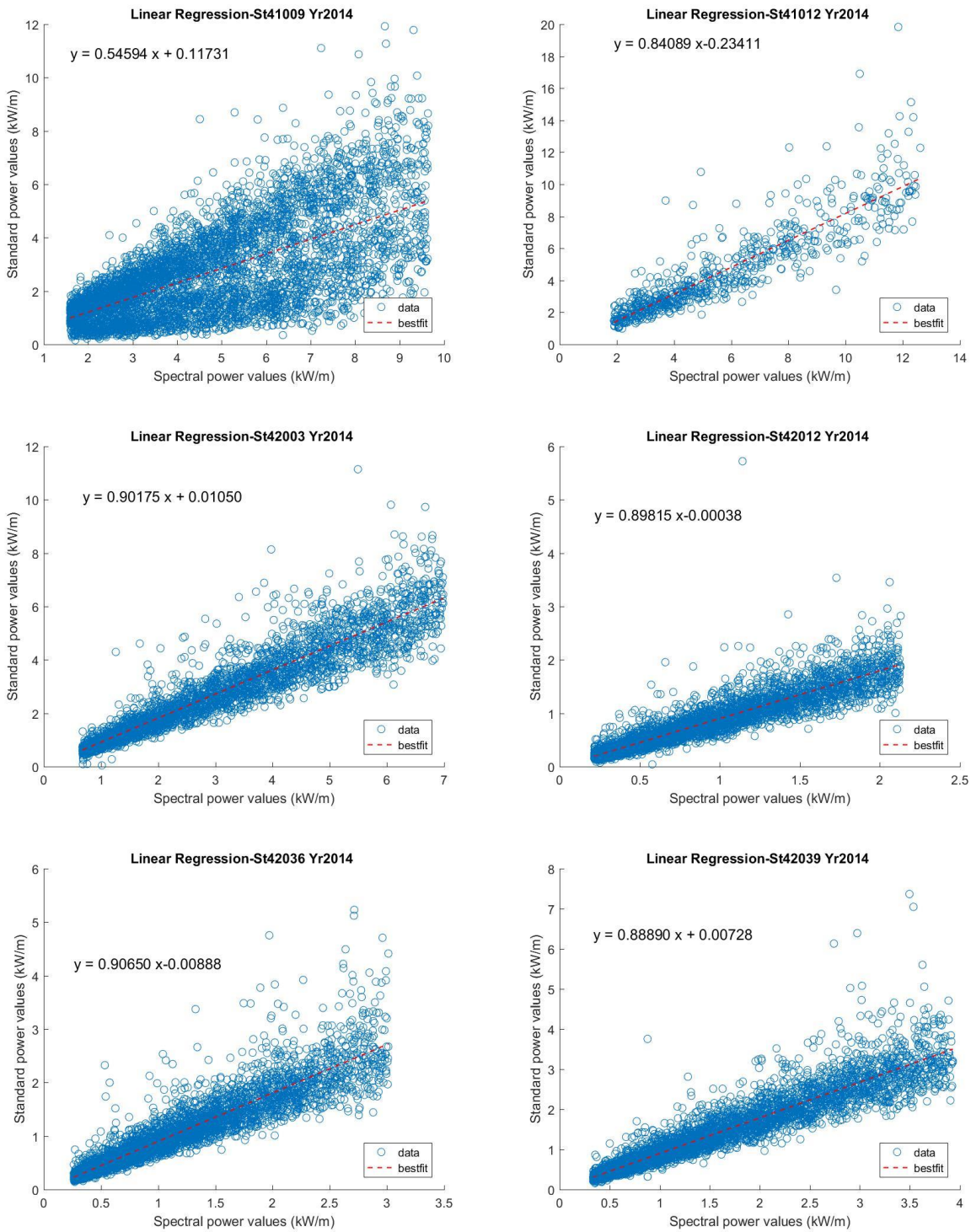
Figure 5-4: Regression analyses of available wave power computed using standard vs spectral data for 2014

5.3.2 *Available Wave Power in Coastal Florida*

The average annual wave power for each buoy station from 2010 to 2014 calculated using spectral wave data is summarized in Figure 5-5. The estimates of wave power vary spatially and approximately decrease from east to west.
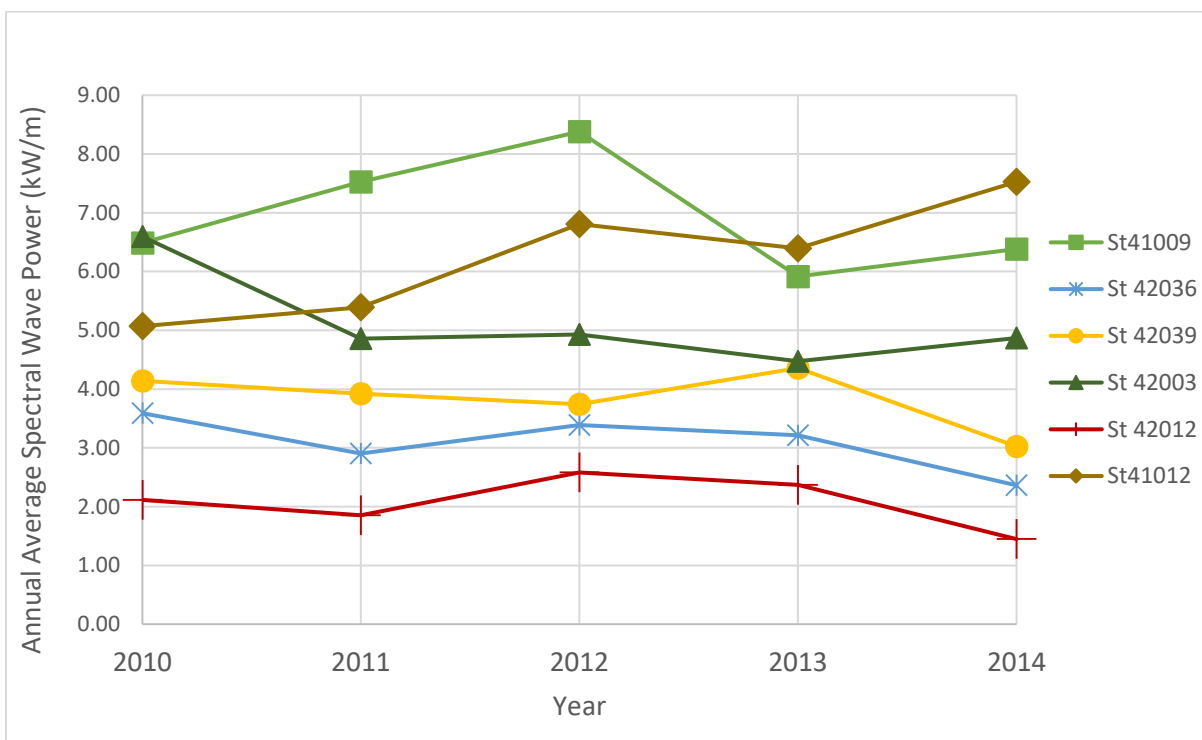

Figure 5-5: Average annual wave power for the years 2010-2014 computed from spectral data

Station 41009 has the highest estimated wave power with an average value of 6.939 kW/m over the five-year time period. Station 41012 generates an average of 6.239 kW/m. In (Stopa et al., 2013), the authors define 5 kW/m as the lower limit of operational feasibility for WEC deployment in Hawaii, and thus the results obtained at the two aforementioned stations indicate that these regions could potentially serve as sites for WEC farms. Note that these two stations are the two stations located in the Atlantic Ocean. The remaining stations (42012, 42039, 42036, and 42003)

produce lower amounts of wave power annually, with averages of 2.072, 3.838, 3.091, and 5.145 kW/m, respectively. (The average for Station 42003 is heavily influenced by the large amount of wave power estimated for 2010.)

We also calculate the annual median estimates of wave power (Figure 5-6). These values are more informative for wave power assessments since the success of WEC farms will depend on the regular generation of wave power, for example, the amount of power generated 50% of the time. Median values will also inform the selection of the type of WEC to be deployed at a given location since various WECs have different lower bounds on the wave power required to be operational. We see a similar trend in the spatial behavior of the median values as was seen in the mean values. However, the median values are much lower than the means, indicating that the means are strongly influenced by extreme values. For the Atlantic stations (41012 and 41009), the average median wave power is 3.235 and 3.625 kW/m, respectively. For the remaining stations, the wave power is even lower, ranging from 0.9025 to 2.373 kW/m. It is clear that the current state of WEC technology is not adequate for the exploitation of the wave power available in coastal Florida.
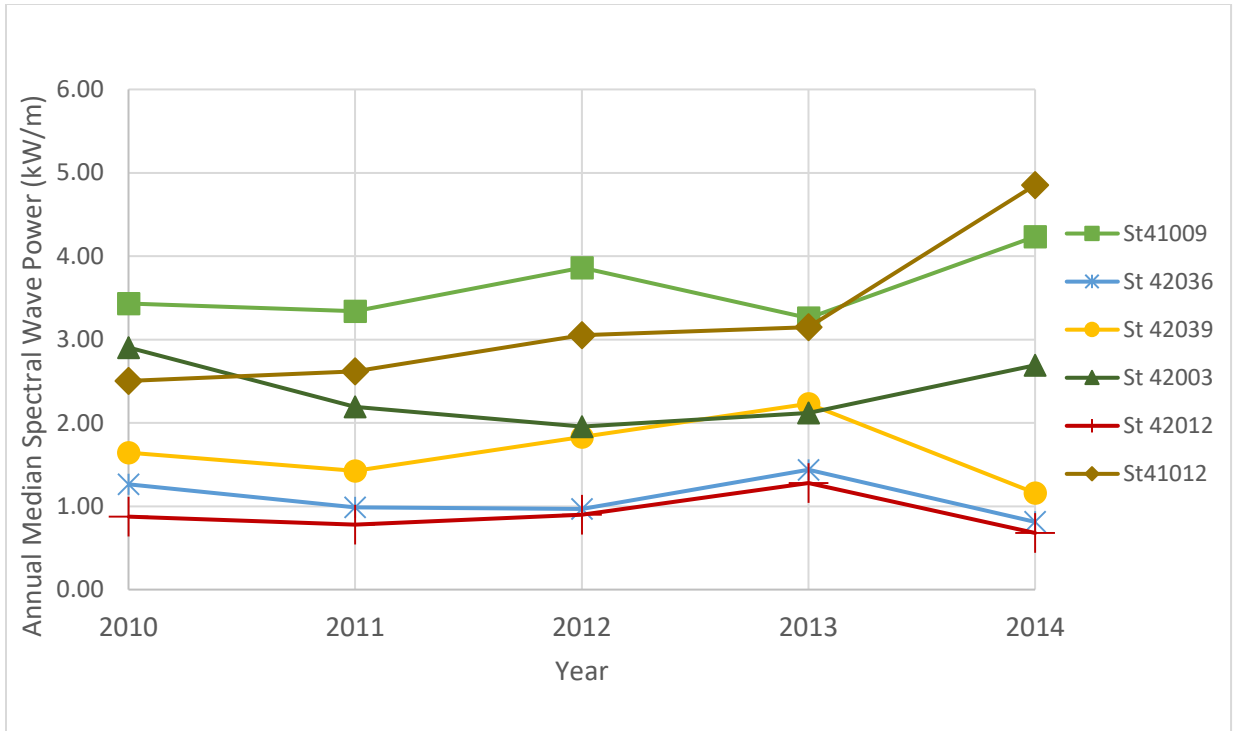
Figure 5-6: Median annual wave power for the years 2010-2014 computed from spectral data

5.3.3 *Long Term Variability in Available Wave Power*

In the analyses above we restrict the time period of consideration to the five years 2010 to 2014 due to the concurrent availability of standard and spectral wave data for the wave buoys in coastal Florida. However, we are interested in longer-term behavior of available wave energy, as there appears to be significant variability in the wave power available from year to year and we anticipate future changes in the wave climate as the globe continues to warm. The average available wave power for the 20-year period 1997-2016 at Station 41009 and Station 42039 is shown in Figure 5-7 and Figure 5-8. This allows analysis of longer-term trends and variability for stations in both the Atlantic Ocean and the Gulf of Mexico.
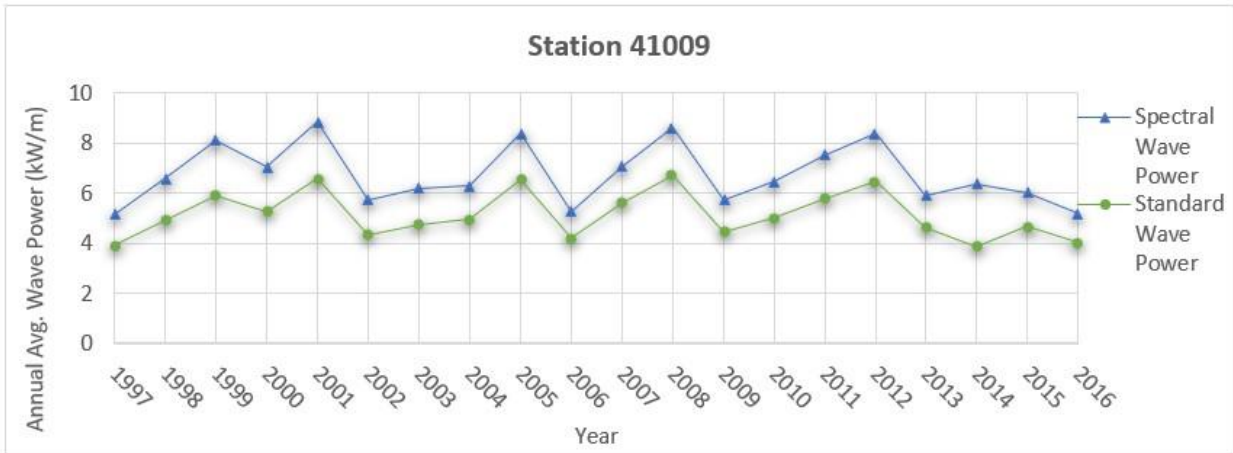
Figure 5-7: Average annual wave power from 1997-2016 in the Atlantic Ocean (St 41009)
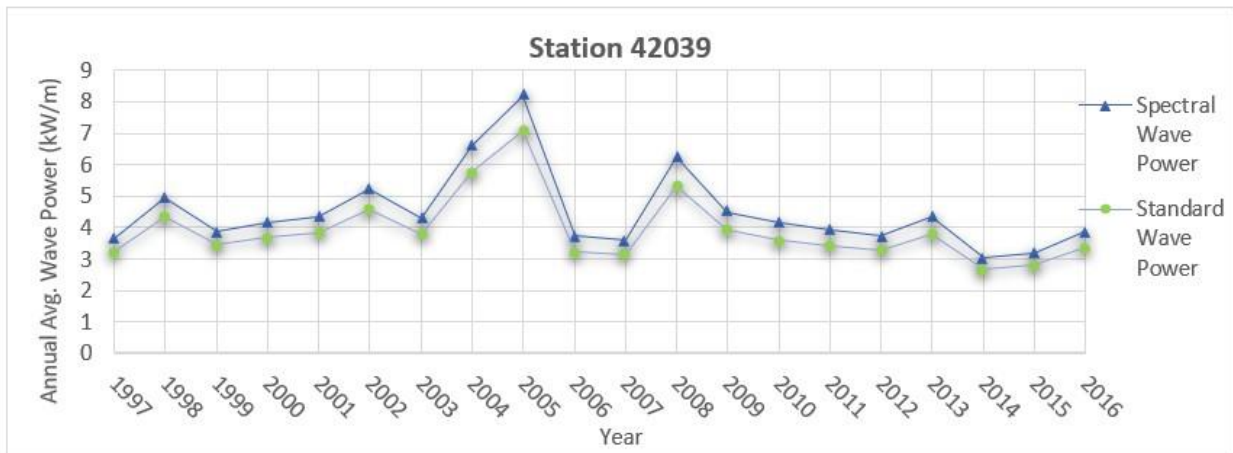

Figure 5-8: Average annual wave power from 1997-2016 in the Gulf of Mexico (St 42039)

There is notable variability in the available wave power from year to year at both stations, but particularly for Station 41009 in the Atlantic Ocean; the data is oscillatory with the sign of the gradient changing every three years at a maximum. The maximum increase between any two consecutive years is 2.077 kW/m, and the maximum decrease is 3.114 kW/m. The mean absolute difference in the available wave power between consecutive years is 1.456 kW/m. For Station 42039 in the Gulf of Mexico, the behavior of the data is more linear with several notable outliers.

Calculations of the available wave power are especially high for 2004, 2005, and 2008, three years that had particularly high tropical cyclone activity. The mean absolute difference in the available wave power between consecutive years is 1.115 kW/m. The variability from year to year at both locations indicates that we could potentially see significant changes in available wave power over the coming decades.

The overall trend of the data at both locations is relatively constant, and actually has a slightly negative slope. The slopes of linear regression lines are -0.02808 and -0.05403 for Stations 41009 and 42039, respectively. However, we expect this trend to change in the future. Available wave power quadratically depends on significant wave heights (Eq. 2), which are expected to increase near Florida by the end of the century due to increased wind speeds associated with mid-latitude storms (Mori et al., 2010). Significant wave heights are also influenced by seasonal climate variations, the most recognized of which is the phenomenon, El Nino. For the Gulf of Mexico region, there are cases where a clear relationship between El Nino indices and significant wave heights is observed (e.g. Figure 5-9), suggesting an influence of the phenomenon on wave height and wave energy. A recent study supports the idea that there is a strong correlation between El Nino and wave power (Reguero et al., 2019). Impacts of El Nino have intensified in recent years, becoming more destructive and frequent, and changes in the climate are expected to continue this trend (Reguero et al., 2013). As a result, we expect further increases in available wave power during future El Nino seasons as well. Numerical wave models implementing climate projections will be necessary for more conclusive analyses of the impacts of climate change on available wave power for coastal Florida and other regions.
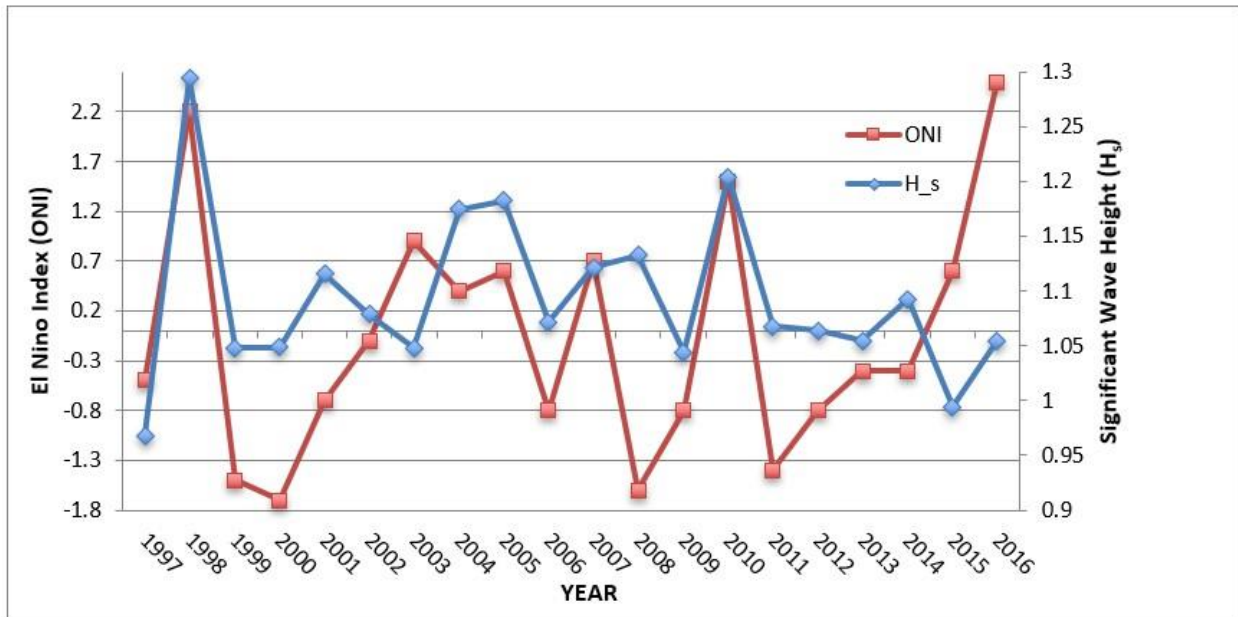
Figure 5-9: El Nino Index (ONI) and significant wave height (H$_s$) at St 42003 from 1997-2016

5.4   Conclusions

This study estimates the available wave power in coastal regions of the Florida peninsula. Wave

power is assessed with both a spectral wave power equation and a simplified equation, which uses

a deep water assumption to estimate wave power using more readily available standard wave data.

Data is analyzed at six buoy stations in coastal Florida for the years 2010 to 2014 to estimate the

average available wave power at each location and investigate the temporal and spatial variability

in these values. We find that regions of coastal Florida in the Atlantic Ocean have more available

wave power than those in the Gulf of Mexico, motivating the need for numerical wave modeling

to increase the spatial resolution of wave power estimates beyond that of the locations of buoy

stations. However, among the stations assessed, the two stations in the Atlantic Ocean, Station

41009 and Station 41012, are the most promising sites for a WEC farm, as they have an average

annual wave power of 6.939 kW/m and 6.239 kW/m, respectively. If this power were fully

harnessed, it could potentially provide energy for 205 Florida homes annually (assuming a 40 m capture width for a typical WEC farm site (Babarit and Hals, 2011)).

The effect of using the simplified wave power equation is also examined. Estimates of wave power computed from each of the two equations are compared and it is determined that in the absence of spectral wave data, standard wave data can be used to approximate available wave power, however, a factor of ~1.173 should be applied to the power estimated from standard wave data. It is also shown that this factor varies temporally; a larger factor is required for regions in the Atlantic Ocean than regions in the Gulf of Mexico. This illustrates the need to estimate the multiplicative factor locally when spectral data is not available. It also further motivates the use of numerical modeling to avoid the introduction of uncertainties surrounding the factor.

This type of assessment of available wave power is essential for the implementation of WEC farms. Specifically, such assessments should be used as part of cost-benefit analyses to determine viable WEC types for any given region. Given the current capabilities of WECs, it is not feasible or cost-effective to implement WEC farms in coastal Florida today, however, studies on increasing the efficiency of WEC devices suggest that harnessing available wave power is becoming increasingly cost-effective, and wave power may be a viable energy source over the coming decades (see e.g. (Flocard and Finnigan, 2012; Kim et al., 2015)). Additionally, it is likely that wave climatology will change with the changing climate, causing stronger wind patterns, larger wave heights, more powerful waves, and more available wave power (Hemer et al., 2013; I. R. Young, S. Zieger, 2011).

In future work, numerical wave modeling will be implemented for coastal Florida to increase the spatial resolution of spectral wave data, allowing for a more thorough assessment of the available

wave power along the peninsula. We will verify the numerical model using data obtained in this work, as in (Fairley et al., 2017; I. R. Young, S. Zieger, 2011; Smith et al., 2017). We also plan to conduct an in-depth cost-benefit analysis of harnessing wave power in order to assist in the identification of operational wave farm locations.

5.5   Acknowledgments

CHAPTER 6:   CONCLUSIONS

In the changing climate, sustainable and nature-based solutions to many coastal hazards and engineering problems has become a high priority. Two of the major issues that coastal communities currently face are coastal erosion and high power demands due to increasing population. This dissertation presents a sustainable approach to mitigating coastal erosion while generating clean and renewable energy through wave energy conversion. The aim is to impact scholarship and practice by addressing gaps in the scientific literature and enhancing the quality of the environment and human life on local and potentially global scales. By being one of the first studies on the impacts of wave farms on coastal morphodynamics in the United States, this dissertation provides foundational insights and guidance for future research.

The objective of this research was to understand coastal erosion, wave power potential estimation, wave energy extraction, impacts of wave action on coastal erosion, and the role of wave farms in shaping coastal morphology. For this purpose, extensive literature research and analysis were conducted. We have illustrated that wave farms can be an alternative method to mitigating coastal erosion while providing clean and renewable energy under present-day conditions and in future climate conditions. Although wave energy conversion has some limitations due to the storm intensity and mean sea level, the conceptual framework of using wave farms as a coastal defense mechanism offers a green solution to both energy demand and coastal protection needs.

Utilizing WECs for both coastal defense and renewable energy also provides cost-efficiency. Wave farms can be a cost-effective way of mitigating erosion compared to currently available methods, such as beach renourishment projects. Beach renourishment projects add 320,000 cubic yards of sand (250,000 m^3) to the beach every year, but they cost \$7 million and are temporary

solutions that need to be repeated every few years. Initial costs of WECs can be high, but their payback time is as short as one year. As they also provide electricity, they may become more economical than other nature-based solutions.

This work and subsequent studies can be used to explore multi-component coastal protection strategies combining wave farms, nature-based solutions, and living shorelines, such as coral reefs and salt marshes, to increase coastal adaptability to climate change. Additionally, this work can be extended by analyzing the impacts of WECs on coastal erosion in a long-term study. Erosion is a slow process that occurs gradually, not only during storm events. Current numerical modeling capabilities do not allow simulations longer than a storm duration (4-5 days); therefore, it would be valuable to observe the impacts of WECs in a longer-term simulation.

Coastal communities can benefit from the implementation of the coastal protection and power generation method presented here. It can be especially useful in critically eroding remote areas where the wave power is abundant, and conventional energy resources are not preferable or merely non-existent. Since this approach can adapt well to the changing climate (i.e., rising sea levels), it can be an economically viable solution that provides public benefits over many decades.

APPENDIX A: INTERMEDIATE LOW, INTERMEDIATE-HIGH, AND HIGH SLR SIMULATION RESULTS FOR HURRICANE IVAN AND HURRICANE KATRINA
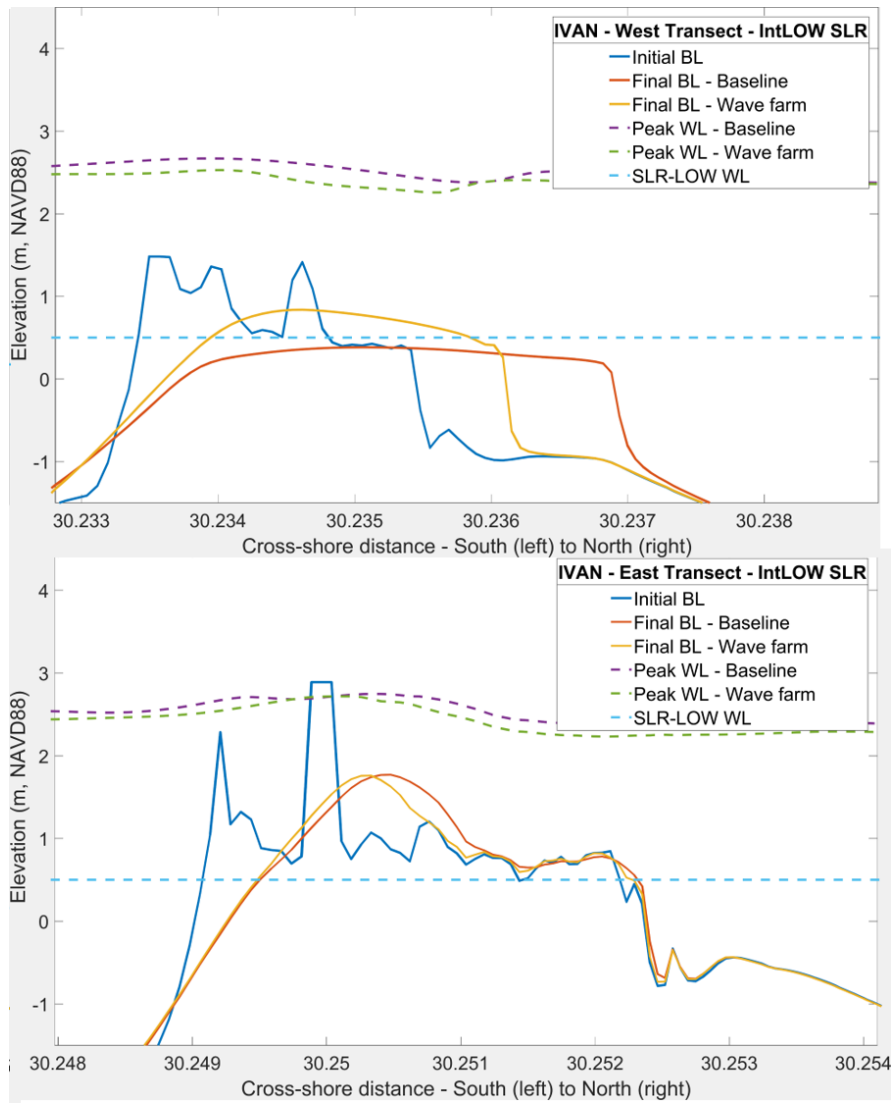
Hurricane Ivan – Int-Low SLR

Figure A- 1: Bed levels (BL) and water levels (WL) before and during Hurricane Ivan, at the west transect (a), and the east transect (b) under Int-Low SLR scenario. Blue dashed line indicates the mean sea level (0.5 m)
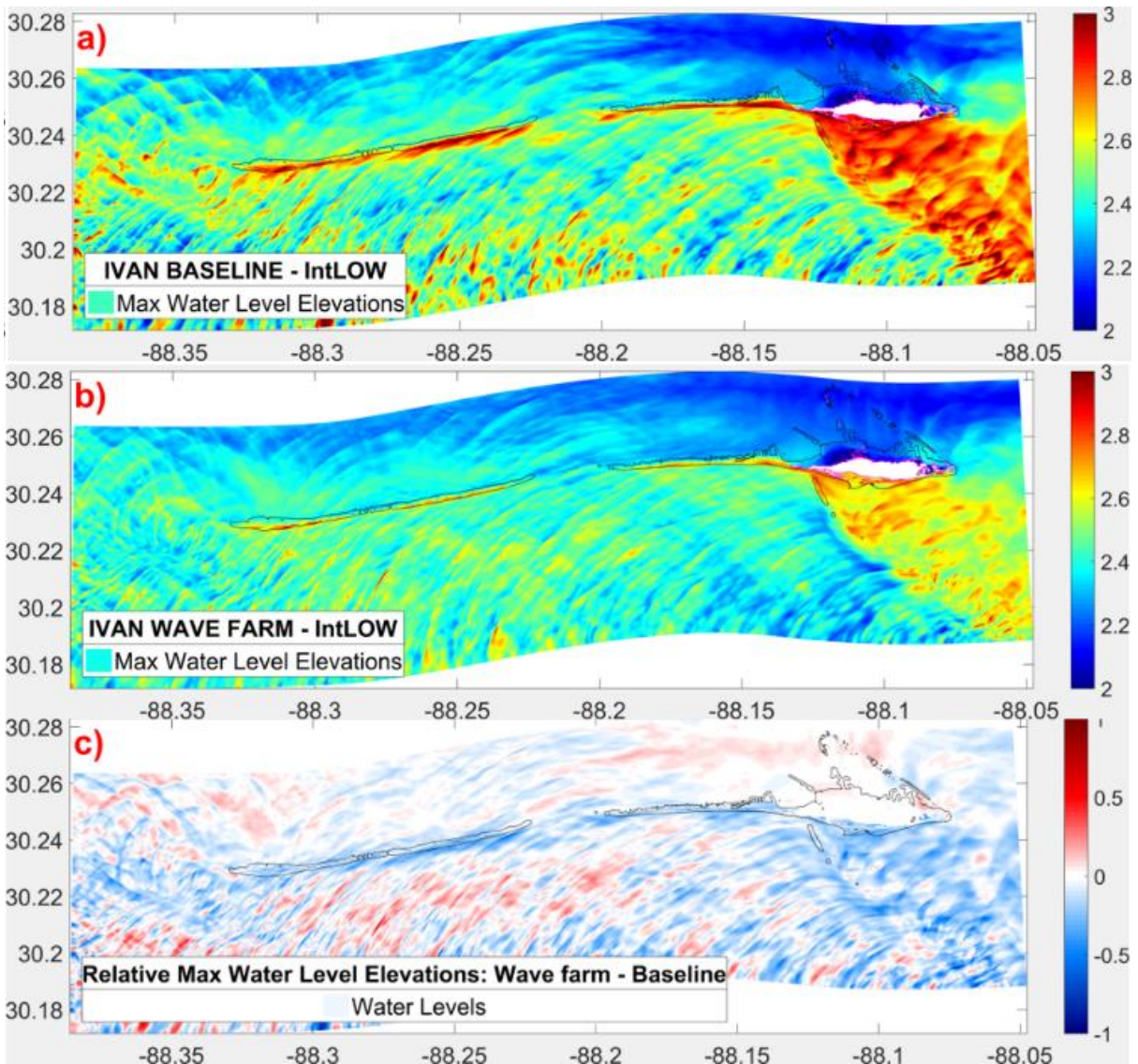
Figure A- 2: Int-Low SLR scenario: Max Water Levels for baseline (a) and wave farm (b) cases (c) Difference between the two cases: b subtracted from a. (Blue color represents the areas where maximum TWLs are lower in the wave farm scenario compared to the baseline scenario, and the red color represents the areas where the TWLs are higher with the presence of a wave farm) The black line is the post-storm zero-meter contour of the island.
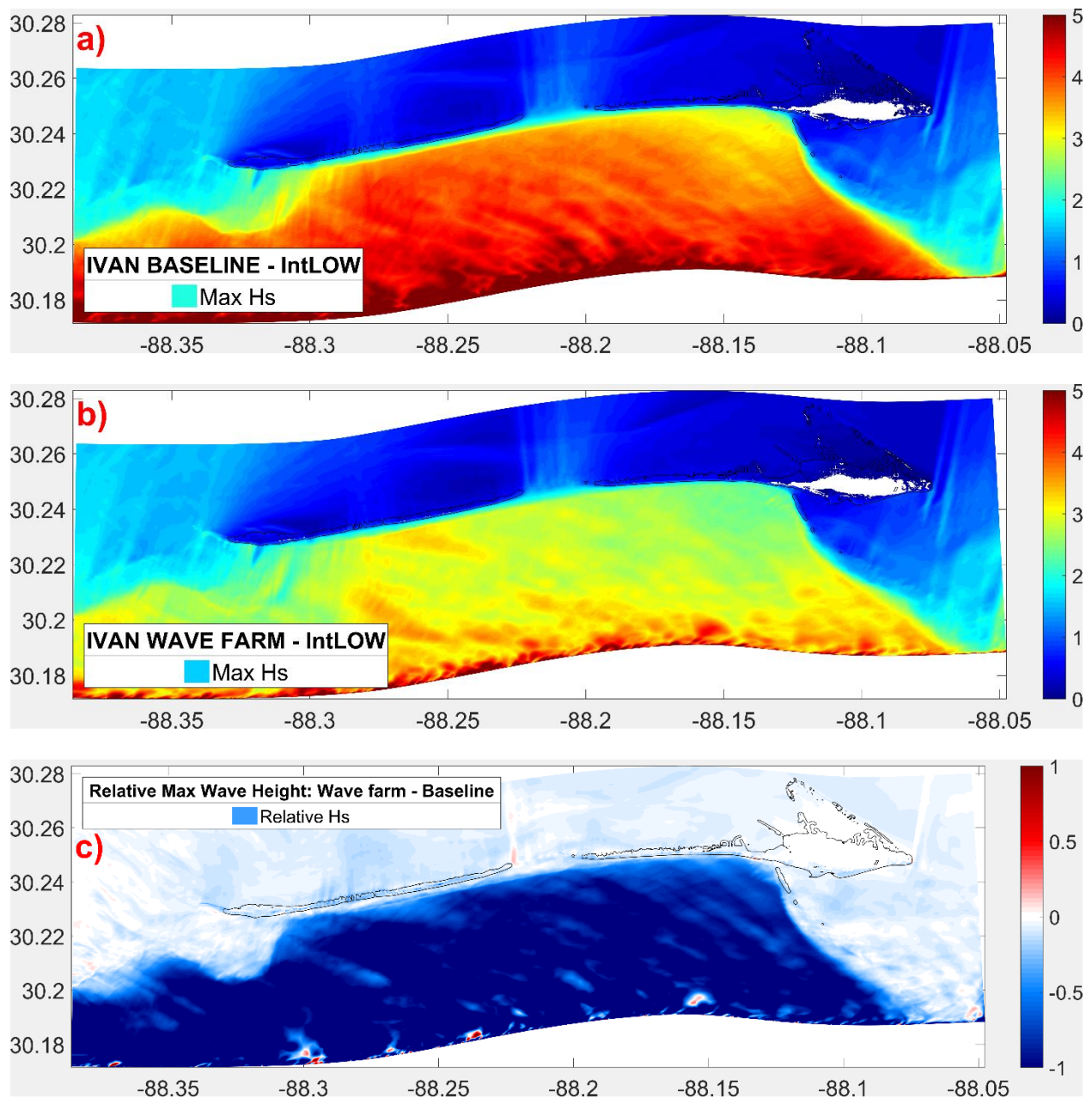
Figure A- 3: Hurricane Ivan - Int-Low SLR: Maximum wave heights (Hs) across the domain: (a) baseline scenario, (b) wave farm scenario (c) Hs difference between the two scenarios in [m] Baseline values are subtracted from wave farm values. The blue color represents the reduction in Hs due to WECs, and the red color represents the increase in Hs due to WECs. Black lines are the post-storm zero-meter contours of the island
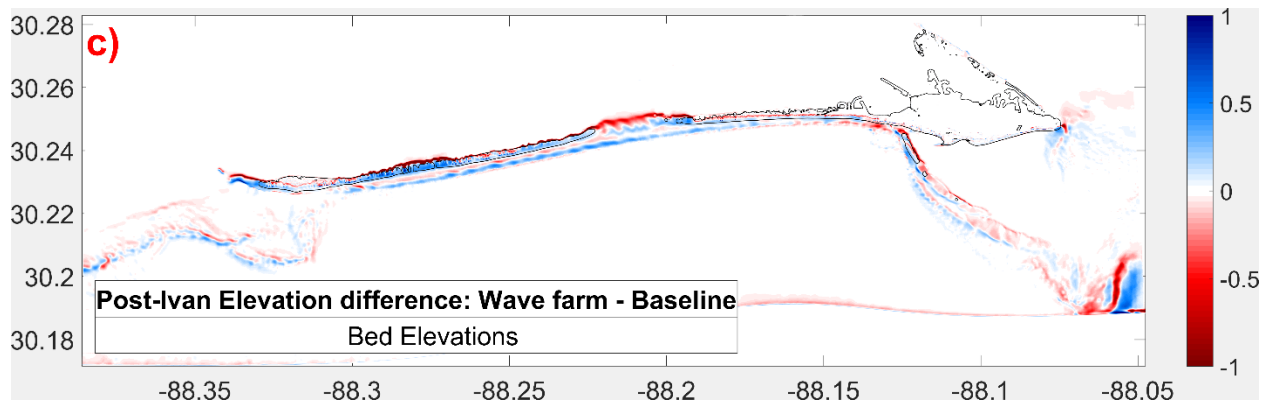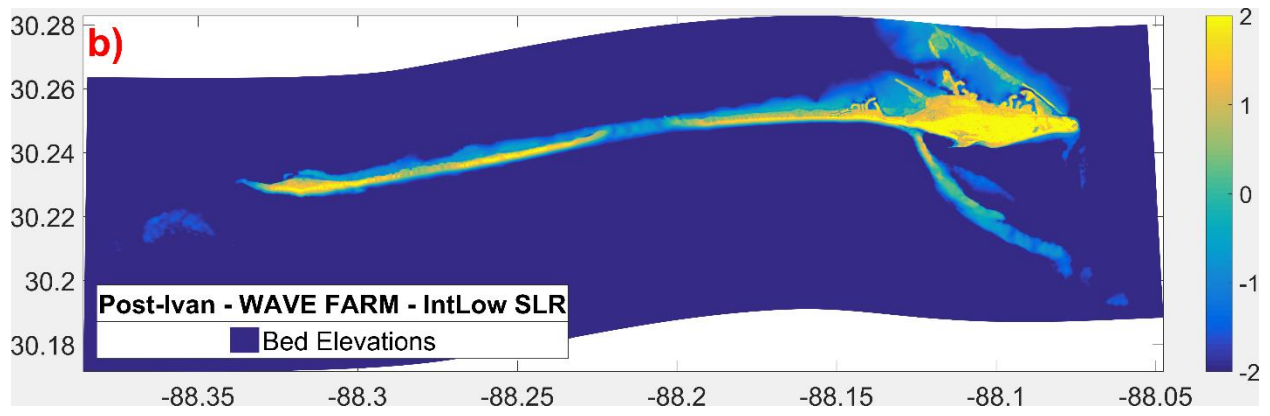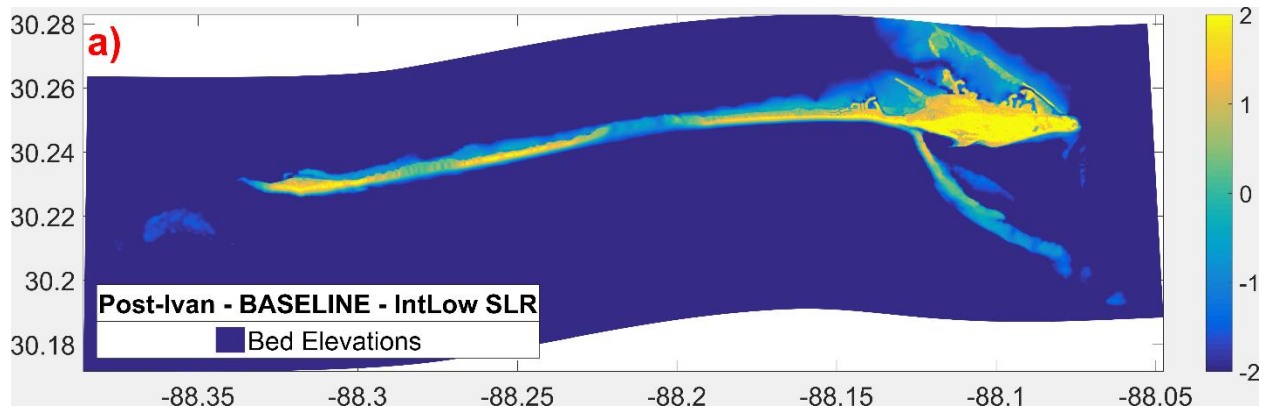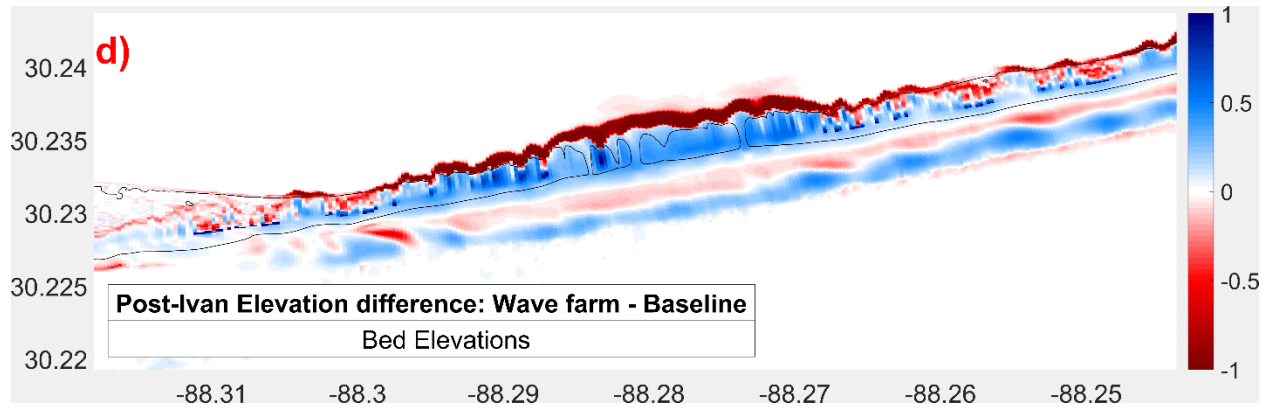
Figure A- 4: Hurricane Ivan - Final bed elevations [m] for baseline (a) and wave farm (b) cases under Int-Low SLR scenario (c) Difference between the two scenarios (d) Magnified version of (c) showing the channels in the western portion – Positive (blue) values show the locations where the final elevations are higher in the wave farm scenario. The black line is the post-storm zero-meter contour of the island.

Table A- 1: Inundated and dry areas, initial and final sand volume, net loss in sand volume, and max bed shear stress values in x- and y- directions [N/m2] averaged over time in the mid-domain nearshore area for Hurricane Ivan for baseline and wave farm cases under Int-Low SLR scenario.

Ivan Int-Low SLR	Baseline	Wave farm	Difference $(m^2/m^3/\%)$	Impacts of WECs
Initial island area (millions of m^2)	11.61	11.61	0	-
Total dry area (millions of m^2)	2.2	2.37	0.17	More dry area w/ WECs
Total inundated area (millions of m^2)	9.41	9.24	-0.17	Less inundation w/ WECs
Initial sand volume (millions of m3)	19.04	19.04	0	-
Final sand volume (millions of m^3)	18.06	18.11	0.05	More sand volume w/ WECs
Net loss in sand volume (millions of m^3)	0.98	0.9	-0.08 (-8%)	Less sand loss w/ WECs

Max τ_{bx}	151.41	134.89	-11%	Less τ_{bx} w/ WECs, less sediment mobilization
Max τ_{by}	220.21	204.8	-7%	Less τ_{by} w/ WECs, less sediment mobilization
Max $\tau_b = \sqrt{\tau_{bx}^2 + \tau_{by}^2}$	267.32	245.23	-8%	Less τ_b w/ WECs, less sediment mobilization

Int-High SLR
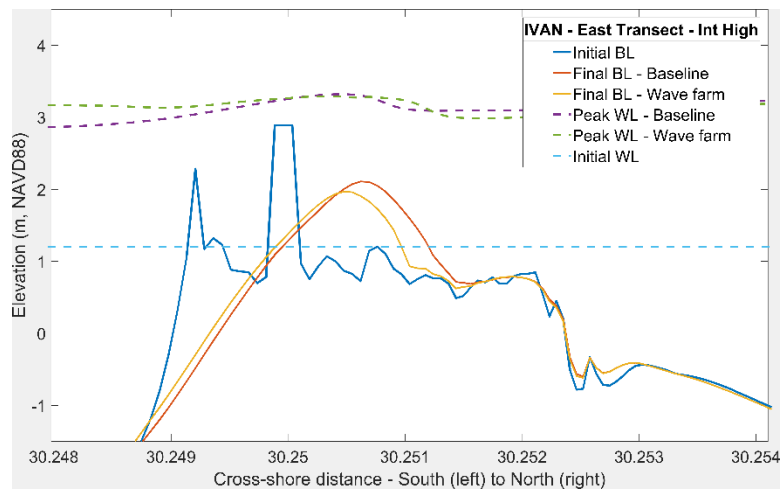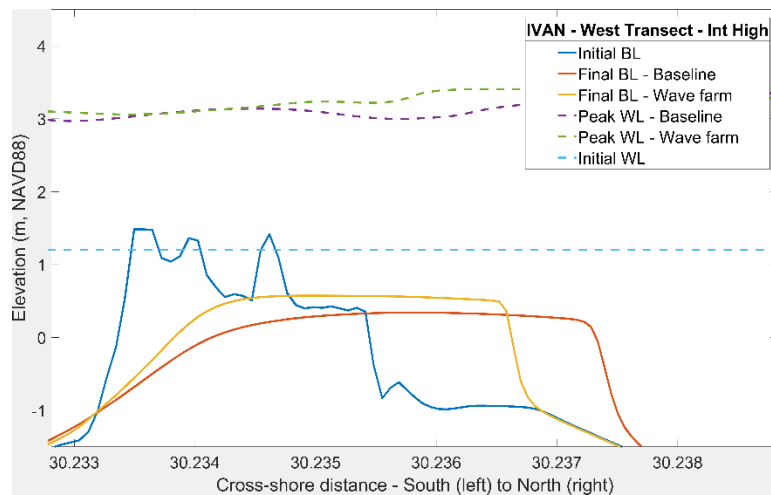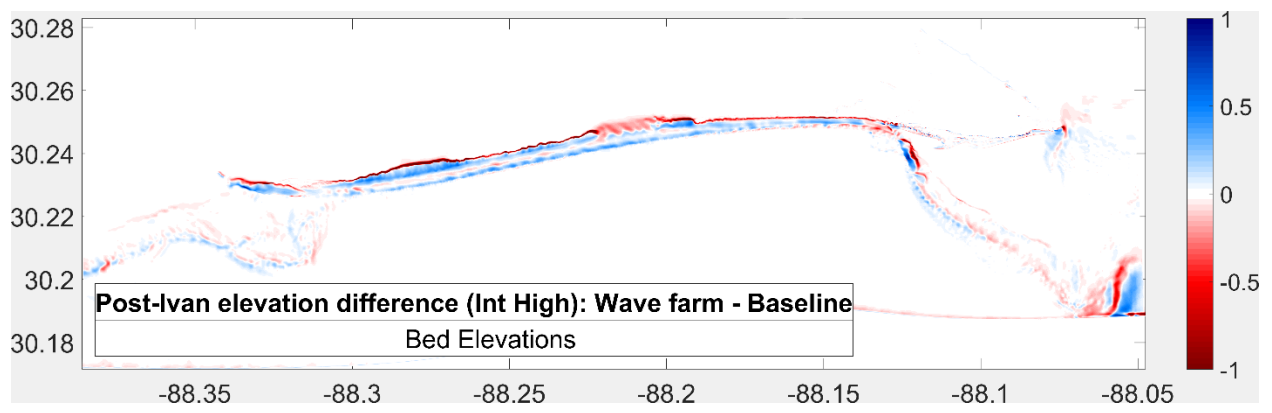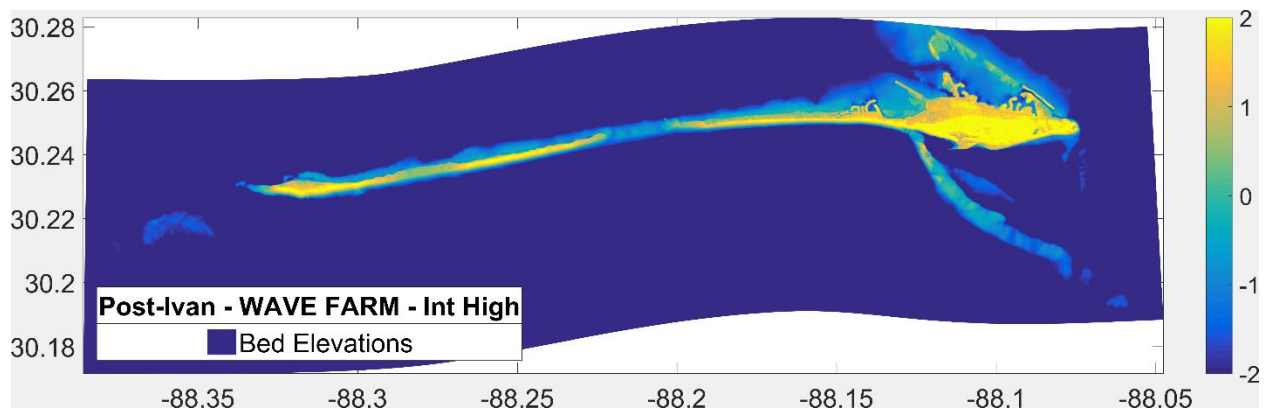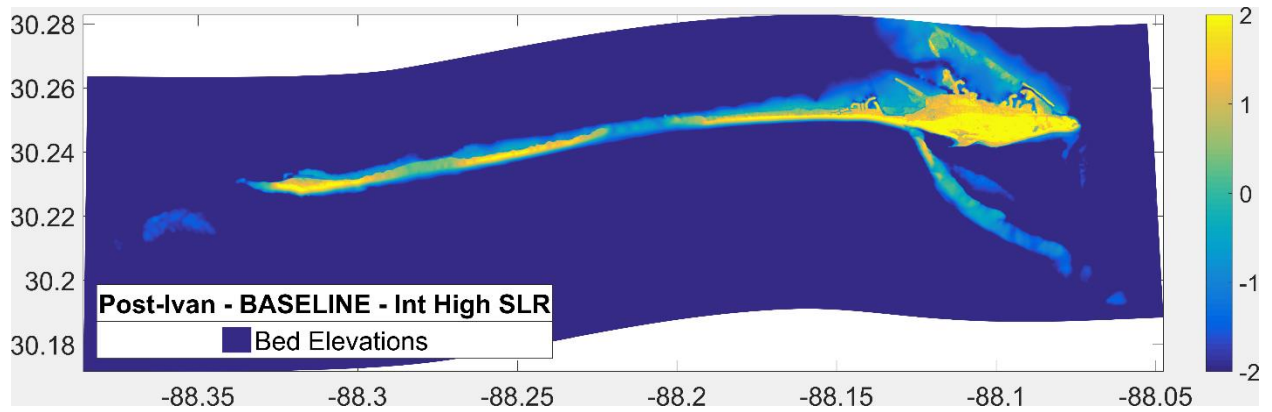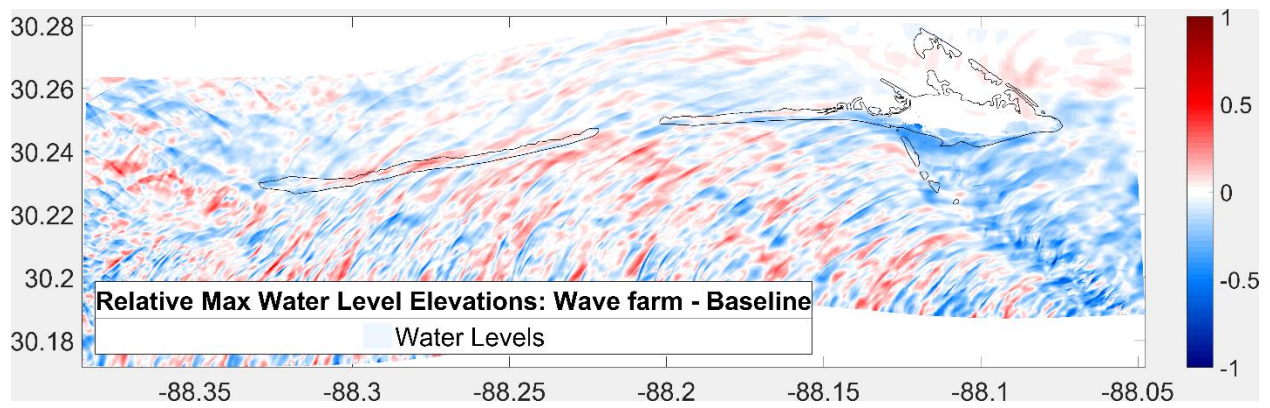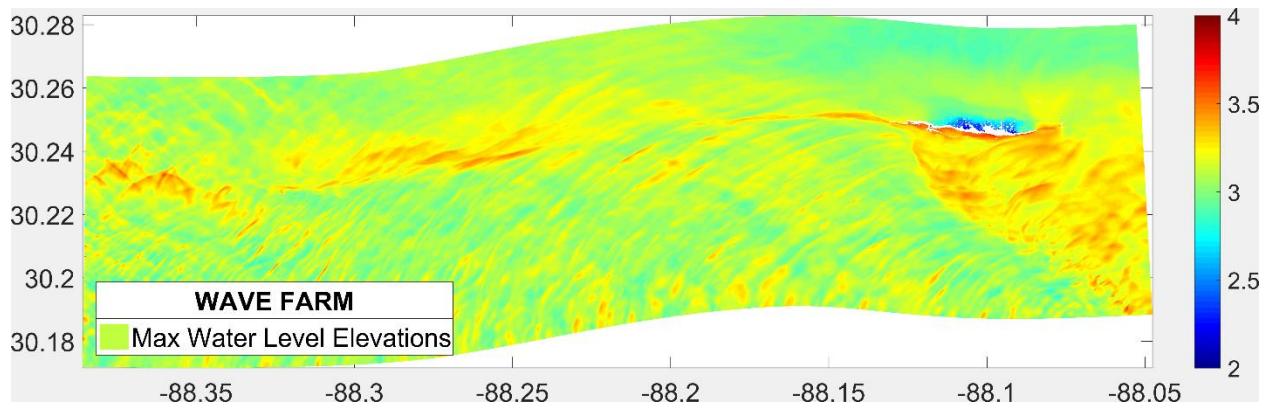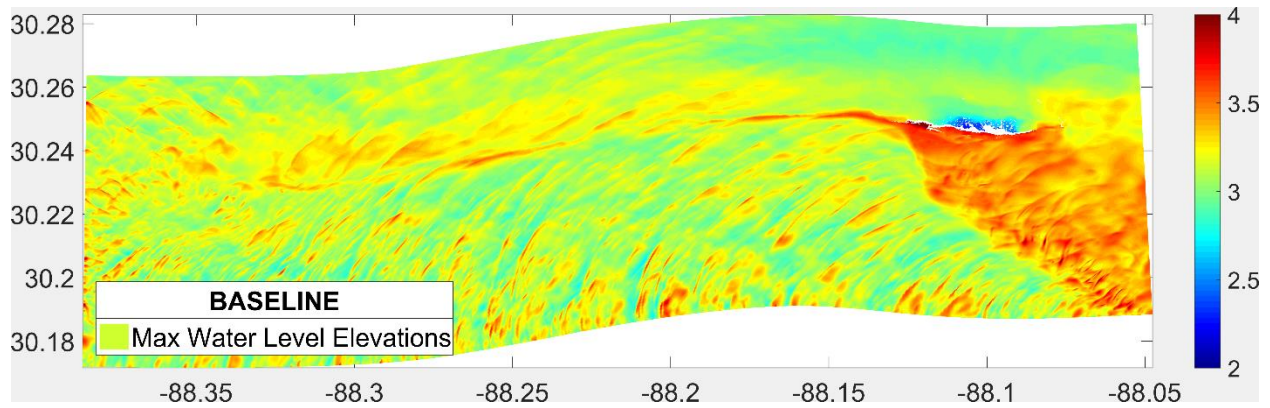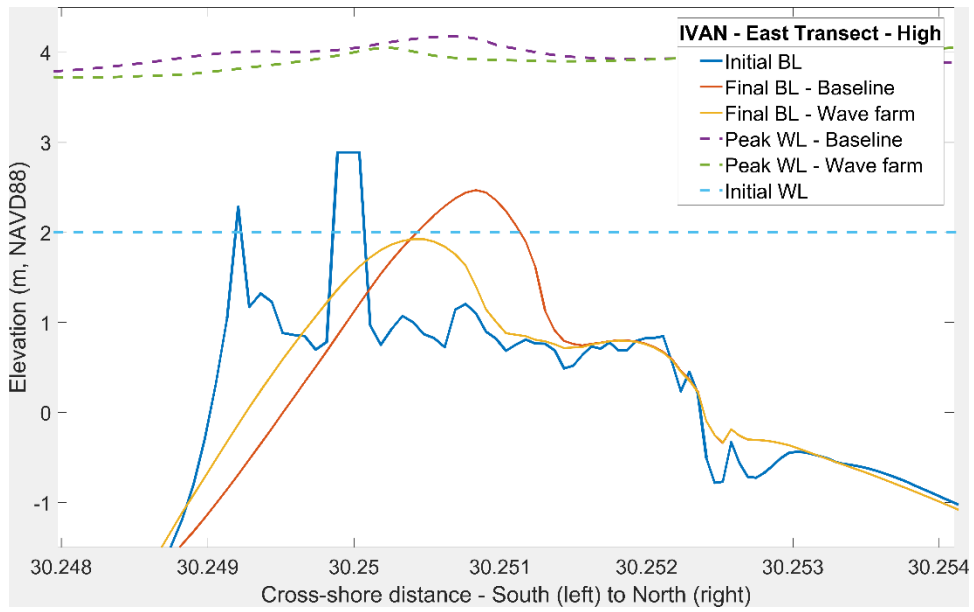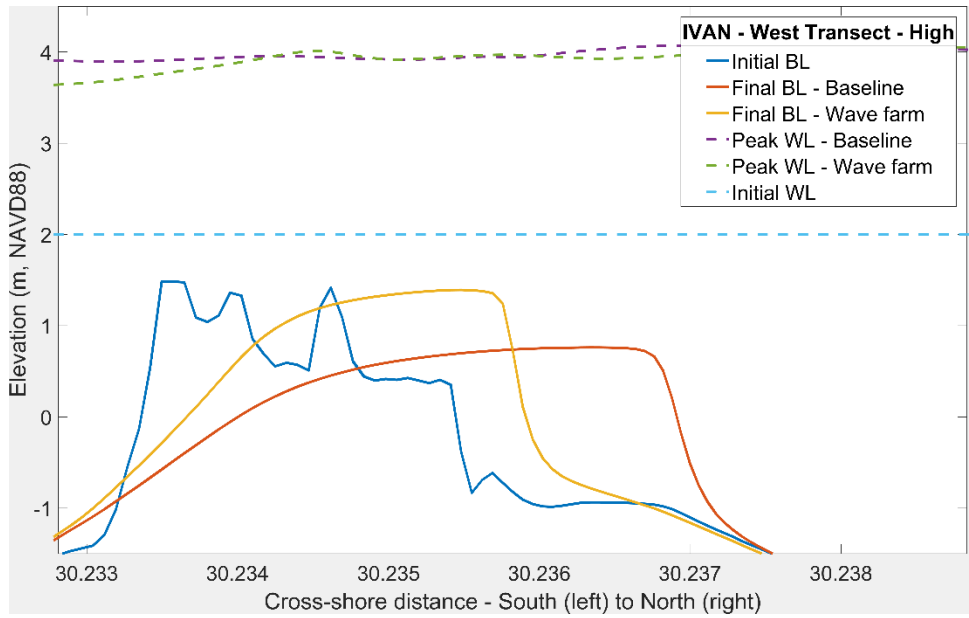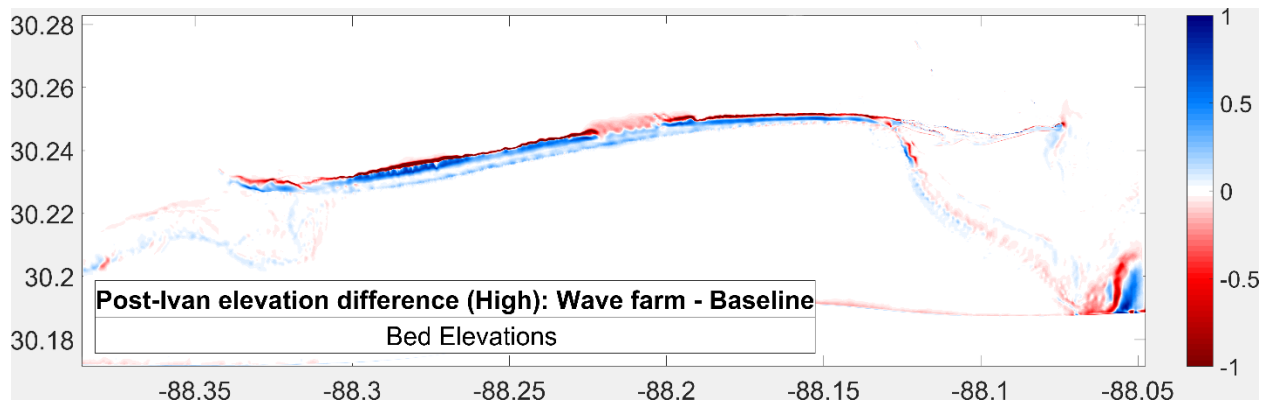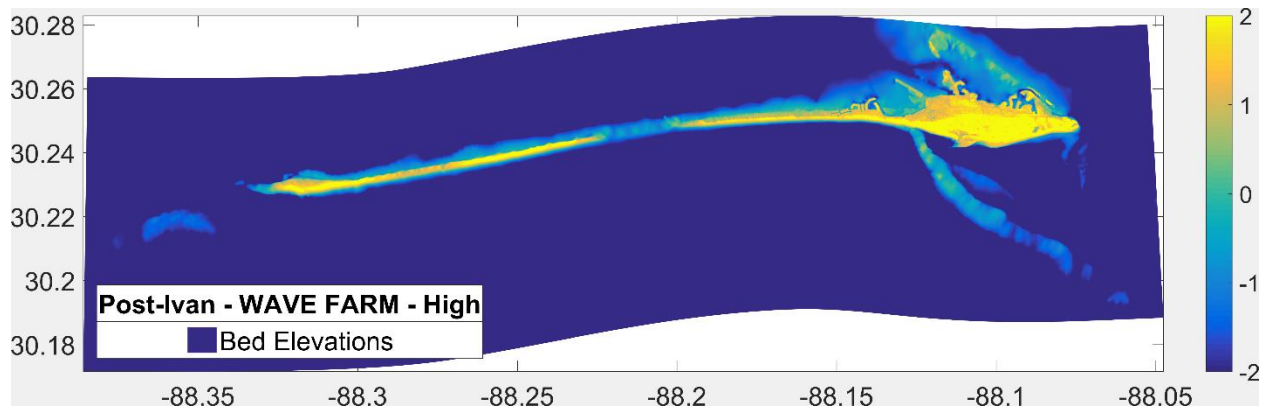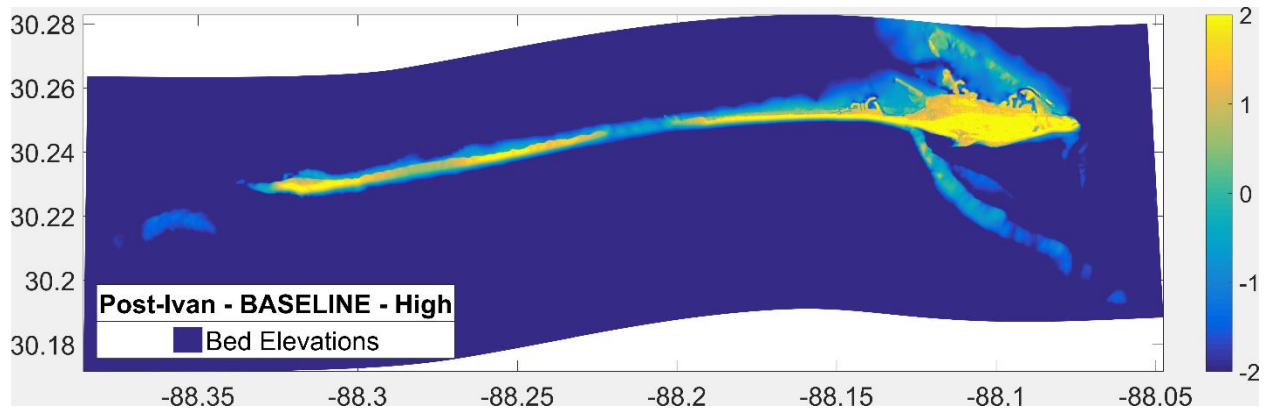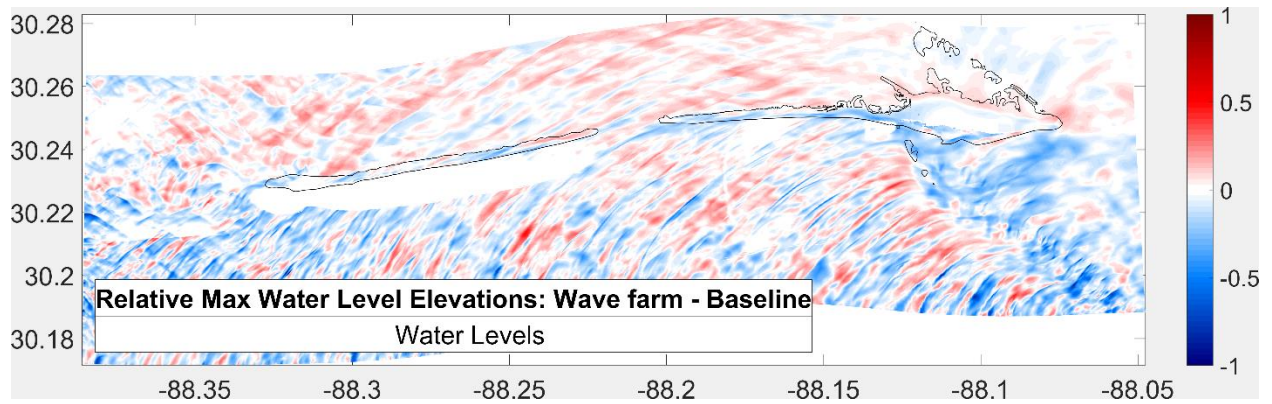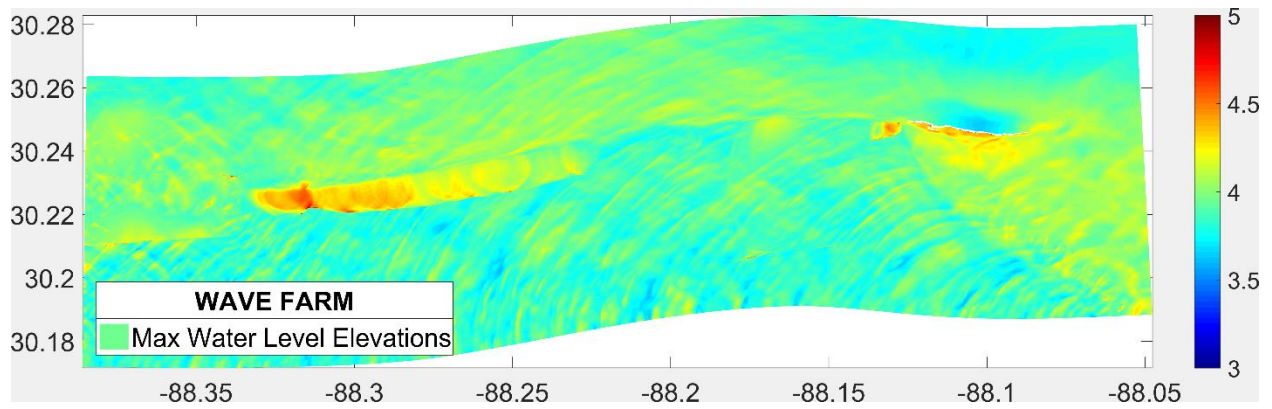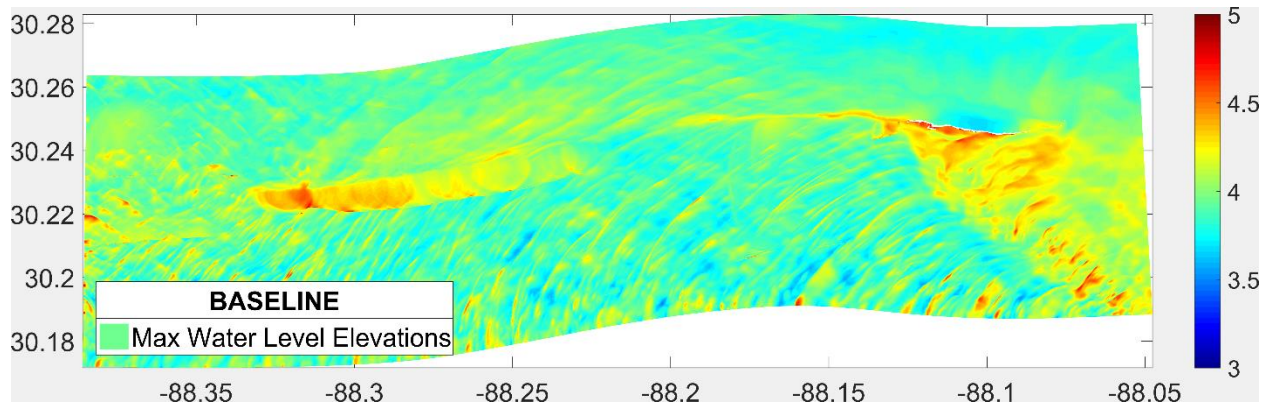
High SLR
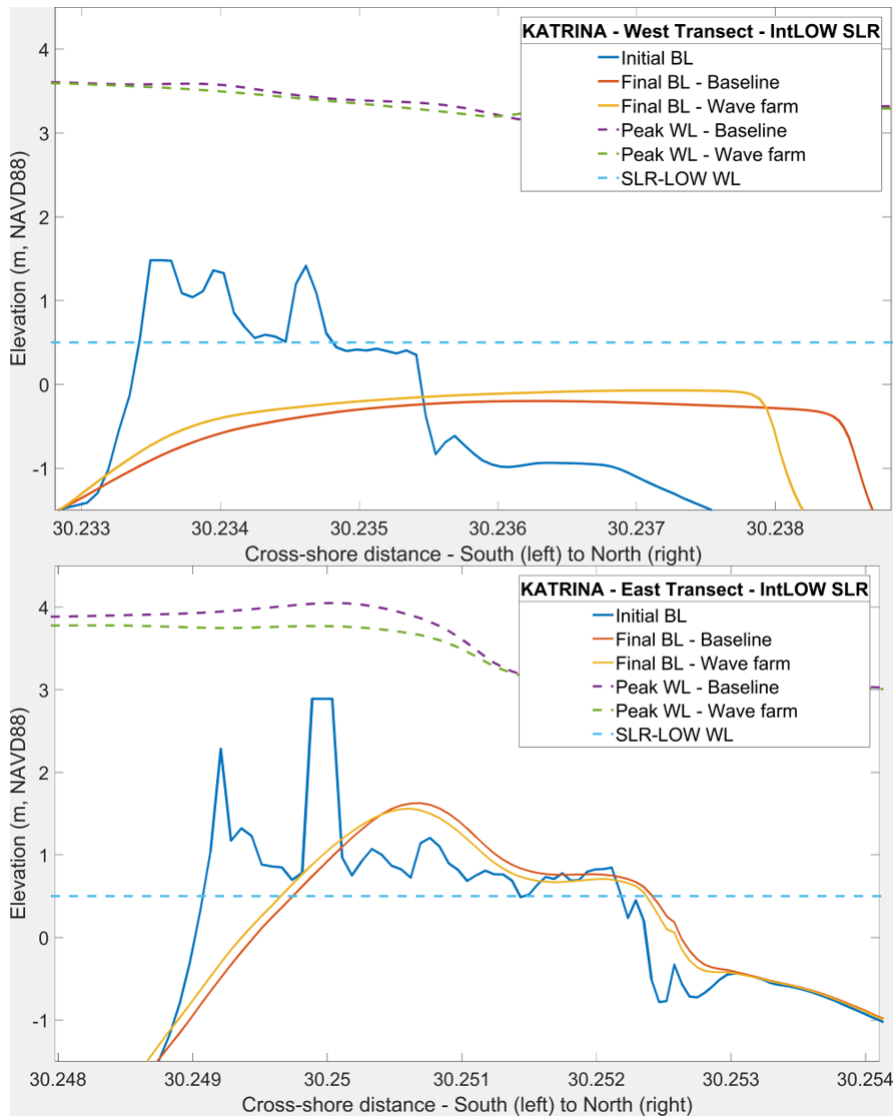
Figure A- 5: Bed levels (BL) and water levels (WL) before and during Hurricane Katrina, at the west transect (a), and the east transect (b) under Int-Low SLR scenario. Blue dashed line indicates the mean sea level (0.5 m)
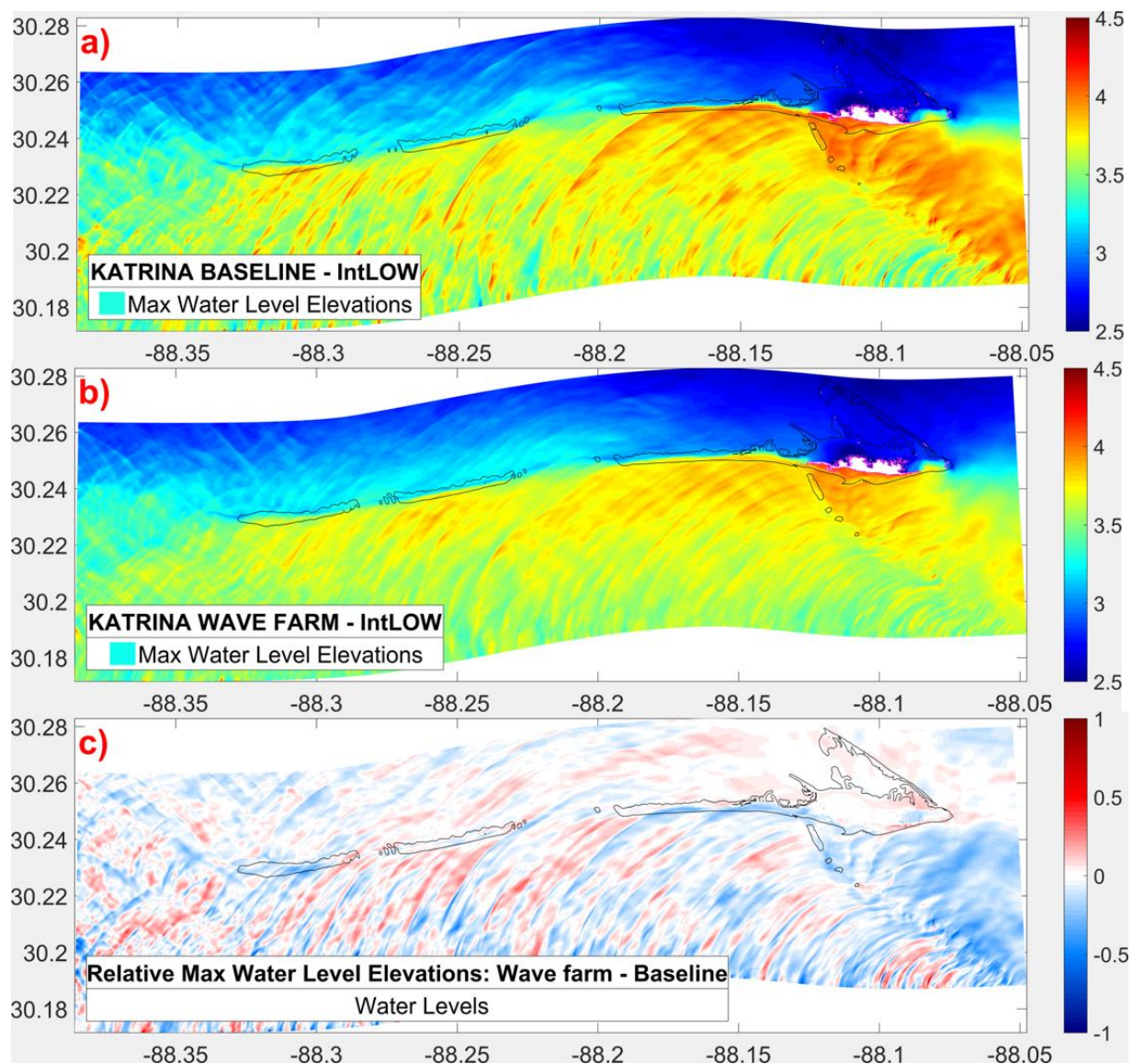
Figure A- 6: Hurricane Katrina - Int-Low SLR scenario: Max Water Levels for baseline (a) and wave farm (b) cases (c) Difference between the two cases: b subtracted from a. (Blue color represents the areas where maximum TWLs are lower in the wave farm scenario compared to the baseline scenario, and the red color represents the areas where the TWLs are higher with the presence of a wave farm) The black line is the post-storm zero-meter contour of the island.
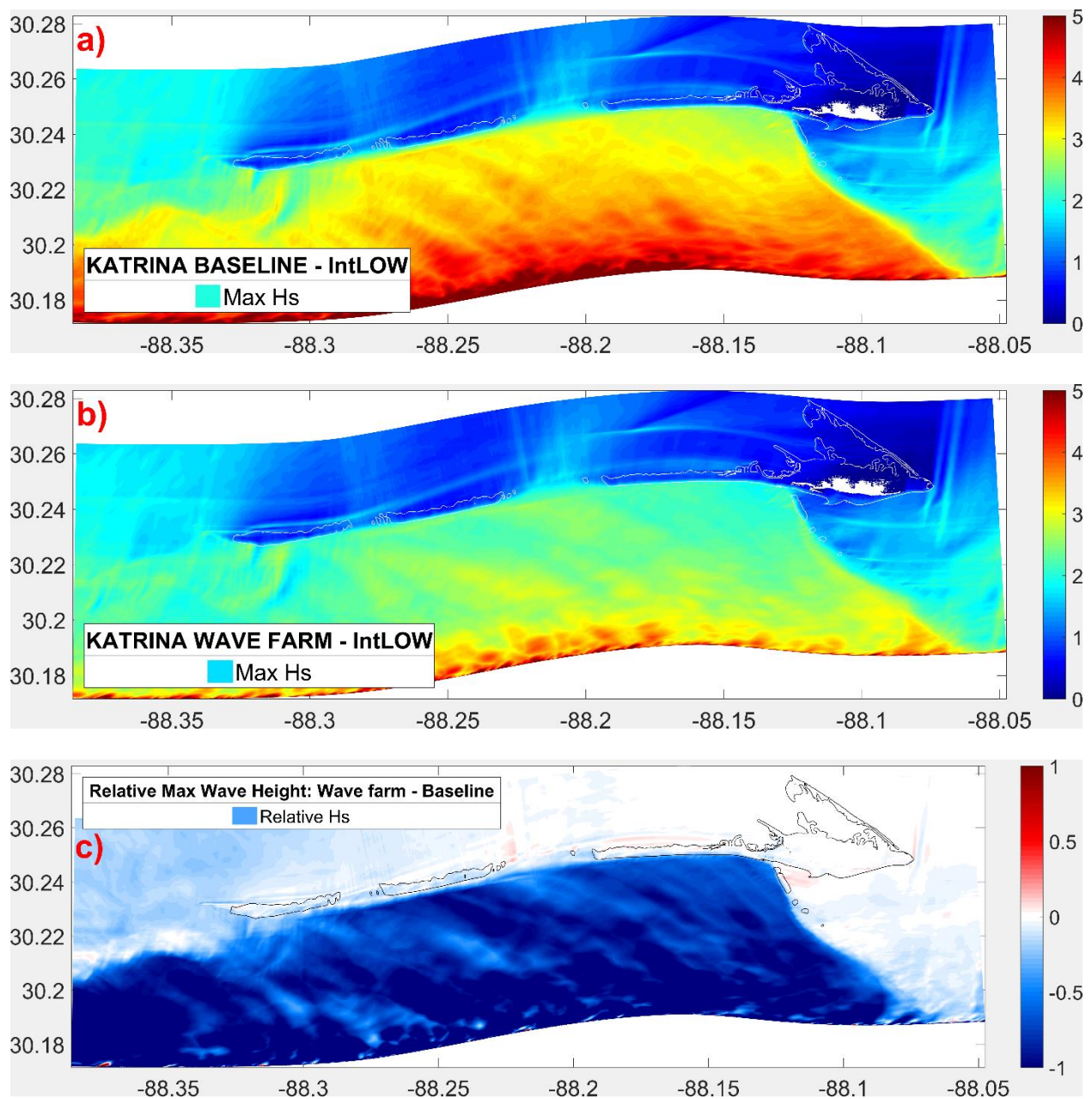
Figure A- 7: Hurricane Katrina- Int-Low SLR: Maximum wave heights (Hs) across the domain: (a) baseline scenario, (b) wave farm scenario (c) Hs difference between the two scenarios in [m] Baseline values are subtracted from wave farm values. The blue color represents the reduction in Hs due to WECs, and the red color represents the increase in Hs due to WECs. Black lines are the post-storm zero-meter contours of the island
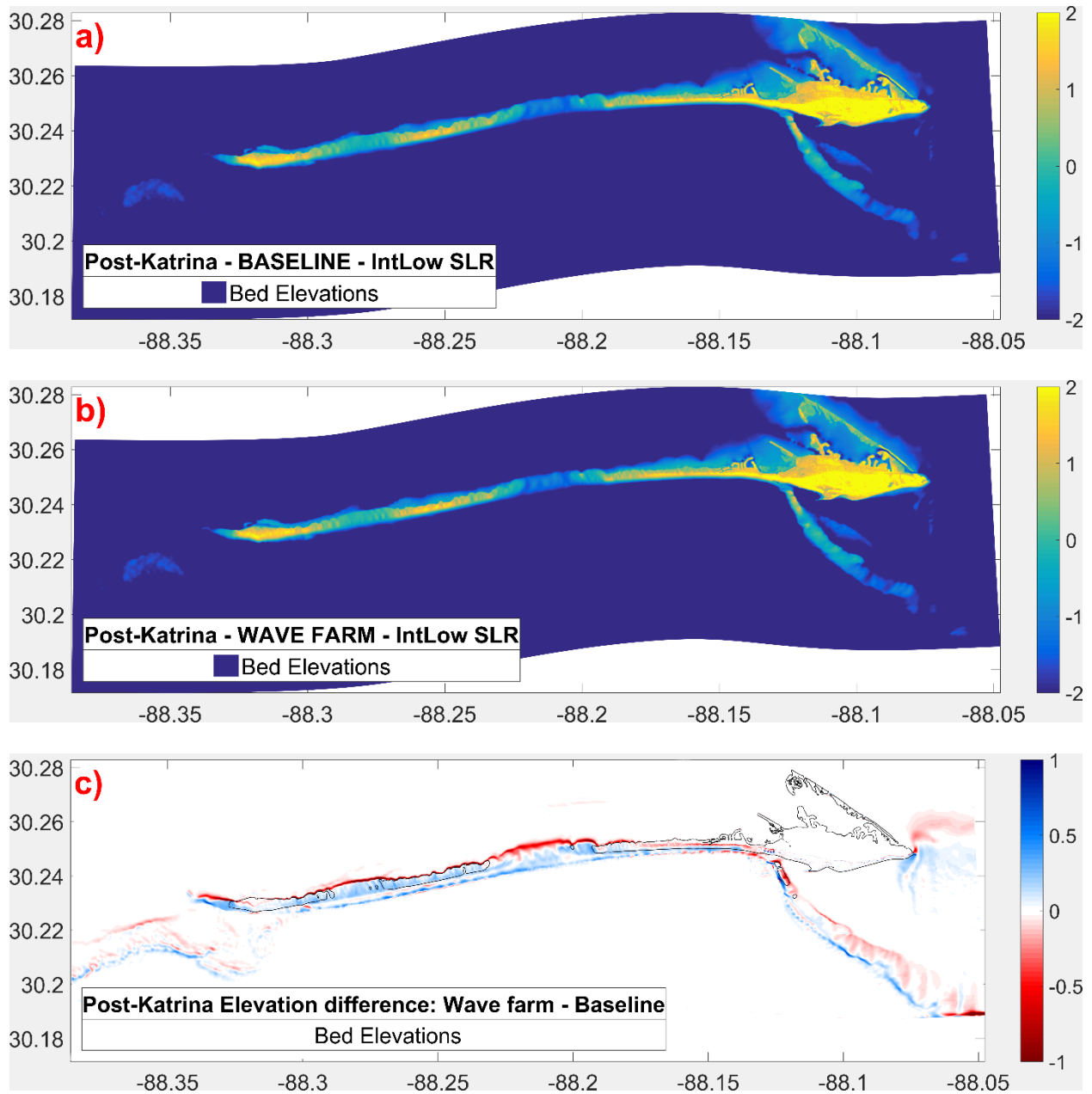
Figure A- 8: Hurricane Ivan - Final bed elevations [m] for baseline (a) and wave farm (b) cases under Int-Low SLR scenario (c) Difference between the two scenarios – Positive (blue) values show the locations where the final elevations are higher in the wave farm scenario. The black line is the post-storm zero-meter contour of the island.

Table A- 2: Inundated and dry areas, initial and final sand volume, net loss in sand volume, and max bed shear stress values in x- and y- directions [N/m2] averaged over time in the mid-domain nearshore area for Hurricane Katrina for baseline and wave farm cases under Int-Low SLR scenario.

Katrina Int-Low SLR	Baseline	Wave farm	Difference (m^2/m^3/%)	Impacts of WECs
Initial island area (millions of m^2)	11.61	11.61	0	-
Total dry area (millions of m^2)	1.11	1.14	0.03	More dry area w/ WECs
Total inundated area (millions of m^2)	10.5	10.47	-0.03	Less inundation w/ WECs
Initial sand volume (millions of m3)	19.04	19.04	0	-
Final sand volume (millions of m^3)	17.04	17.16	0.12	More sand volume w/ WECs
Net loss in sand volume (millions of m^3)	2.00	1.88	-0.12 (6%)	Less sand loss w/ WECs
Max τ_{bx}	322.69	289.75	-10%	Less τ_{bx} w/ WECs, less sediment mobilization
Max τ_{by}	171.86	168.1	-2%	Less τ_{by} w/ WECs, less sediment mobilization
Max $\tau_b = \sqrt{\tau_{bx}^2 + \tau_{by}^2}$	365.6	334.98	-8%	Less τ_b w/ WECs, less sediment mobilization

APPENDIX B.1: ADDITIONAL RESULTS OF WAVE ENERGY ASSESSMENT AT BUOY LOCATION ST42003 - QQ PLOTS OF AVAILABLE WAVE POWER ESTIMATED USING STANDARD AND SPECTRAL WAVE DATA

Each of the Q-Q plots shown for the station 42003 for the years between 2010 and 2014 is approximately linear, and thus it can be assumed that the shapes of the distributions underlying the available wave power values are the same. The quantiles corresponding to the spectral wave power data and standard wave power data lie along the line $y=x$ up to the last decile; i.e., the data comes from distributions that are nearly identical. This behavior is consistent between the plots of 2010 to 2014, meaning that the results of this analysis do not change temporally.
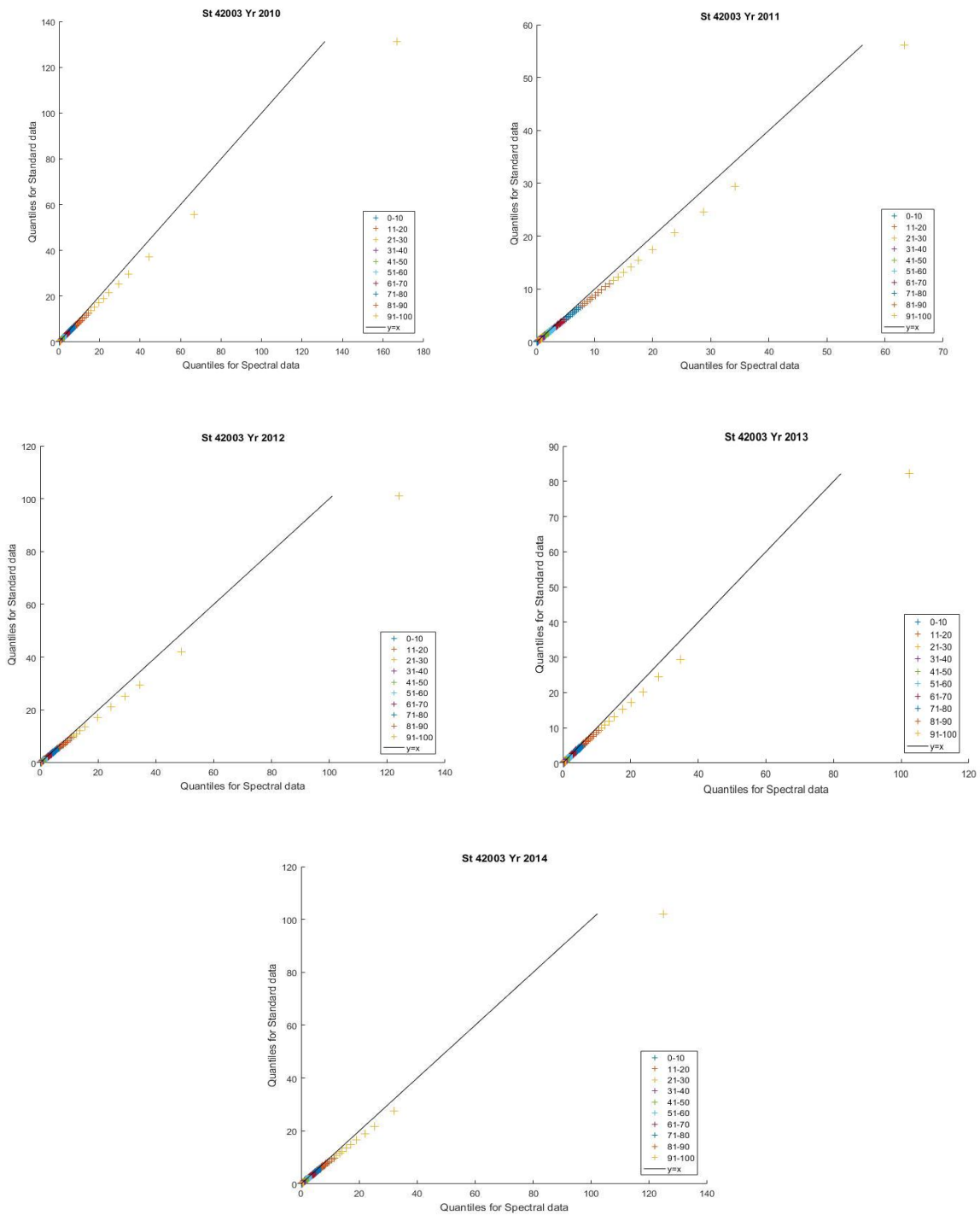
Figure B- 1: Quantile-Quantile plots for St42003 for five years 2010-2014

APPENDIX B.2: ADDITIONAL RESULTS OF WAVE ENERGY ASSESSMENT AT ALL BUOY LOCATIONS - REGRESSION ANALYSES OF AVAILABLE WAVE POWER COMPUTED USING STANDARD VS SPECTRAL DATA FOR YEAR 2010
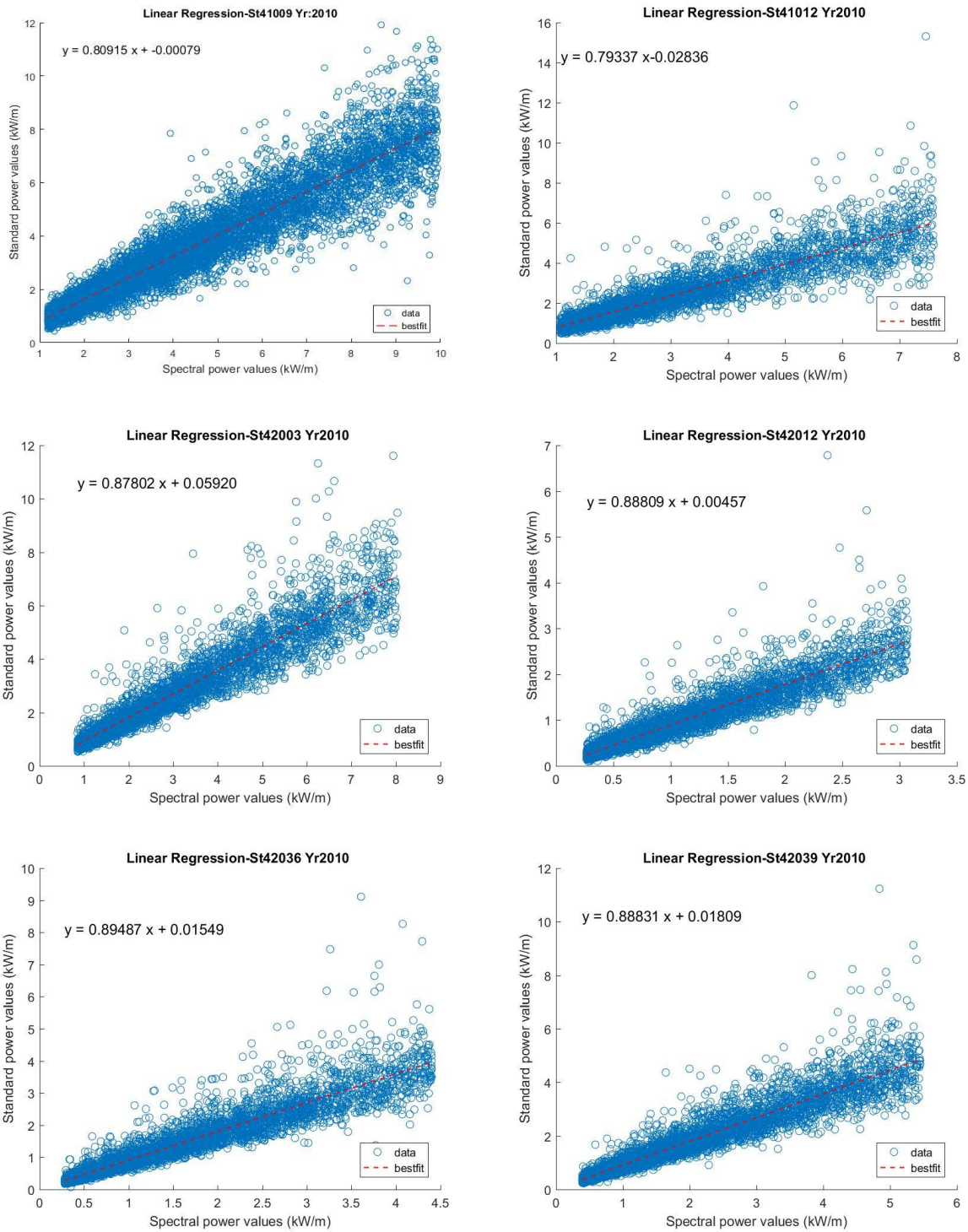
Figure B- 2:Regression analyses of available wave power computed using standard vs spectral data for 2010

REFERENCES

Abanades, J., Flor-Blanco, G., Flor, G., Iglesias, G., 2018. Dual wave farms for energy production and coastal protection. Ocean Coast. Manag. 160, 18–29. https://doi.org/10.1016/j.ocecoaman.2018.03.038

Abanades, J., Greaves, D., Iglesias, G., 2015a. Wave farm impact on beach modal state. Mar. Geol. 361, 126–135. https://doi.org/10.1016/j.margeo.2015.01.008

Abanades, J., Greaves, D., Iglesias, G., 2015b. Coastal defence using wave farms: The role of farm-to-coast distance. Renew. Energy 75, 572–582. https://doi.org/10.1016/j.renene.2014.10.048

Abanades, J., Greaves, D., Iglesias, G., 2014a. Coastal defence through wave farms. Coast. Eng. 91, 299–307. https://doi.org/10.1016/j.coastaleng.2014.06.009

Abanades, J., Greaves, D., Iglesias, G., 2014b. Wave farm impact on the beach profile: A case study. Coast. Eng. 86, 36–44. https://doi.org/10.1016/j.margeo.2015.01.008

Abanades, J, Greaves, D., Iglesias, G., 2014. Wave farm impact on the beach profile: A case study. Coast. Eng. 86, 36–44. https://doi.org/10.1016/j.coastaleng.2014.01.008

ABPmer, 2019. UK Atlas of Marine Renewable Energy Gateway [WWW Document]. URL https://www.renewables-atlas.info/ (accessed 3.13.19).

Alexandre, A., 2013. Wave energy converter strings for electricity generation and coastal protection.

Amoudry, L., Bell, P.S., Black, K.S., Gatliff, R.W., Helsby, R., Souza, A.J., Thorne, P.D., Wolf, J., 2009. A scoping study on : Research into changes in sediment dynamics linked to marine renewable energy installations, NERC Marine Renewable Energy Theme Action Plan Report. British Geological Survey, Edinburgh, UK.

Appendini, C.M., Urbano-Latorre, C.P., Figueroa, B., Dagua-Paz, C.J., Torres-Freyermuth, A., Salles, P., 2015. Wave energy potential assessment in the Caribbean Low Level Jet using wave hindcast information. Appl. Energy 137, 375–384. https://doi.org/10.1016/j.apenergy.2014.10.038

ASBPA, 2019. National Beach Nourishment Database [WWW Document]. URL https://gim2.aptim.com/ASBPANationwideRenourishment/ (accessed 4.8.20).

Atan, R., Finnegan, W., Nash, S., Goggins, J., 2019. The effect of arrays of wave energy converters on the nearshore wave climate. Ocean Eng. 172, 373–384. https://doi.org/10.1016/j.oceaneng.2018.11.043

Babarit, A., Hals, J., 2011. On the maximum and actual capture width ratio of wave energy converters. Proc. 9th Eur. Wave Tidal Energy Conf. 1–7.

Badulin, S.I., Korotkevich, A.O., Resio, D., Zakharov, V.E., 2008. Wave-wave interactions in wind-driven mixed seas, in: Proceedings of the Rogue Waves 2008 Workshop. Brest, France, pp. 77–86.

Bedard, R., Date, M.P., 2004. E2I EPRI Survey and Characterization of Potential Offshore Wave Energy Sites in Washington.

Bedard, R., Previsic, M., 2004. E2I EPRI Survey and Characterization of Potential Offshore Wave Energy Sites in Oregon.

Bergillos, R.J., López-Ruiz, A., Medina-López, E., Moñino, A., Ortega-Sánchez, M., 2018. The role of wave energy converter farms on coastal protection in eroding deltas, Guadalfeo, southern Spain. J. Clean. Prod. 171, 356–367. https://doi.org/10.1016/j.jclepro.2017.10.018

Bergillos, R.J., Rodriguez-Delgado, C., Allen, J., Iglesias, G., 2019a. Wave energy converter configuration in dual wave farms. Ocean Eng. 178, 204–214. https://doi.org/10.1016/j.oceaneng.2019.03.001

Bergillos, R.J., Rodriguez-Delgado, C., Allen, J., Iglesias, G., 2019b. Wave energy converter geometry for coastal flooding mitigation. Sci. Total Environ. 668, 1232–1241. https://doi.org/10.1016/j.scitotenv.2019.03.022

Bergillos, R.J., Rodriguez-Delgado, C., Iglesias, G., 2020. Ocean Energy and Coastal Protection - A Novel Strategy for Coastal Management Under Climate Change. SPRINGER BRIEFS IN ENERGY, Cham.

Bergillos, R.J., Rodriguez-Delgado, C., Iglesias, G., 2019c. Wave farm impacts on coastal flooding under sea-level rise: A case study in southern Spain. Sci. Total Environ. 653, 1522–1531. https://doi.org/10.1016/j.scitotenv.2018.10.422

Beyene, A., Wilson, J.H., 2007. Digital mapping of California wave energy resource. Int. J. ENERGY Res. 31, 1156–1168. https://doi.org/10.1002/er

Beyene, A., Wilson, J.H., 2006. Comparison of wave energy flux for northern, central, and

southern coast of California based on long-term statistical wave data. Energy 31, 1856–1869. https://doi.org/10.1016/j.energy.2005.08.008

Bilskie, M. V., Hagen, S.C., Medeiros, S.C., Cox, A.T., Salisbury, M., Coggin, D., 2016. Data and numerical analysis of astronomic tides, wind-waves, and hurricane storm surge along the northern Gulf of Mexico. J. Geophys. Res. Ocean. 121, 3625–3658. https://doi.org/10.1002/2015JC011400

Bird, E., Lewis, N., 2015. Causes of Beach Erosion, in: Beach Renourishment. Springer International Publishing, Cham, pp. 7–28. https://doi.org/10.1007/978-3-319-09728-2_2

Boden, T.A., Marland G., Andres R.J., 2010. Global, Regional, and National Fossil-Fuel CO2 Emissions, Carbon Dioxide Information Analysis Center. https://doi.org/10.3334/CDIAC/00001_V2010

BOEM, 2018. Renewable Energy on the Outer Continental Shelf [WWW Document]. Bur. Ocean Energy Manag. URL https://www.boem.gov/ocean-wave-energy// (accessed 3.24.19).

BOEM, 2009. Ocean Wave Energy | BOEM [WWW Document]. Bur. Ocean Energy Manag. URL https://www.boem.gov/Ocean-Wave-Energy/ (accessed 3.16.18).

Booij, N., Ris, R.C., Holthuijsen, L.H., 1999. A third-generation wave model for coastal regions 1. Model description and validation. J. Geophys. Res. Ocean. 104, 7649–7666. https://doi.org/10.1029/98JC02622

Buhring, B., 2017. Dauphin Island East End Beach and Barrier Island Restoration Project.

CDIP, 2019. Wave Measurement [WWW Document]. URL https://cdip.ucsd.edu/?nav=documents&sub=index&xitem=waves (accessed 10.19.17).

Cebrian, J., 2019. Living Shoreline: Using Natural and Artificial Breakwaters in Shoreline Restoration and Conservation | Dauphin Island Sea Lab [WWW Document]. URL https://www.disl.org/about/faculty/faculty-projects/living-shoreline-using-natural-and-artificial-breakwaters-in-shoreline-rest (accessed 5.8.20).

Chang, G., Ruehl, K., Jones, C.A., Roberts, J., Chartrand, C., 2016. Numerical modeling of the effects of wave energy converter characteristics on nearshore wave conditions. Renew. Energy 89, 636–648. https://doi.org/10.1016/j.renene.2015.12.048

Church, J.A., White, N.J., 2011. Sea-Level Rise from the Late 19th to the Early 21st Century. Surv. Geophys. 32, 585–602. https://doi.org/10.1007/s10712-011-9119-1

Conley, D., Magagna, D., Greaves, D., Aires, E., Leitao, J.C., Witt, M., Embling, C., Godley, B.J., Bicknell, A., Saulnier, J.-B., Simas, T., Marie O'hagan, A., O'callaghan, J., Holmes, B., Sundberg, J., Torre-Enciso, Y., Marina, D., 2013. Report on the Analysis of the Environmental Impact Assessment Experience for Wave Energy.

Contardo, S., Hoeke, R., Hemer, M., Symonds, G., McInnes, K., O'Grady, J., 2018. In situ observations and simulations of coastal wave field transformation by wave energy converters. Coast. Eng. 140, 175–188. https://doi.org/10.1016/j.coastaleng.2018.07.008

Coogan, J., Webb, B., Smallegan, S., Puleo, J., 2019. Geomorphic changes measured on Dauphin Island, AL, during Hurricane Nate. Shore & Beach 16–22. https://doi.org/10.34237/1008742

Dailymail, 2017. Miami beach saved by dumping 300,000 tons of sand | Daily Mail Online [WWW Document]. URL https://www.dailymail.co.uk/news/article-4359324/Miami-beach-saved-dumping-300-000-tons-sand.html (accessed 10.23.20).

Dalton, G., Madden, D., Daly, M.C., 2014. Life cycle assessment of the wavestar. 2014 9th Int. Conf. Ecol. Veh. Renew. Energies, EVER 2014 1–9. https://doi.org/10.1109/EVER.2014.6844034

Dalton, G.J., Alcorn, R., Lewis, T., 2009. Case study feasibility analysis of the Pelamis wave energy convertor in Ireland, Portugal and North America. Renew. Energy 35, 443–455. https://doi.org/10.1016/j.renene.2009.07.003

Danielson, J.J., Brock, J.C., Howard, D.M., Gesch, D.B., Bonisteel-Cormier, J.M., Travers, L.J., 2013. Topobathymetric Model of Mobile Bay, Alabama [WWW Document]. U.S. Geol. Surv. Data Ser. 769. URL https://pubs.usgs.gov/ds/769/ (accessed 5.27.20).

Davis, R.A., Hayes, M.O., 1984. What is a wave-dominated coast? Mar. Geol. 60, 313–329. https://doi.org/10.1016/0025-3227(84)90155-5

Defne, Z., Haas, K.A., Fritz, H.M., 2009a. Wave power potential along the Atlantic coast of the southeastern USA. Renew. Energy 34, 2197–2205. https://doi.org/10.1016/j.renene.2009.02.019

Defne, Z., Haas, K.A., Fritz, H.M., 2009b. Wave power potential along the Atlantic coast of the southeastern USA. Renew. Energy 34, 2197–2205. https://doi.org/10.1016/j.renene.2009.02.019

Department of Energy, 2019. Federal Agency Use of Renewable Electric Energy [WWW Document]. URL https://energy.gov/eere/femp/federal-agency-use-renewable-electric-energy (accessed 3.28.18).

Division of Water Resource Management, 2018. Strategic Beach Management Plan : Southeast Atlantic Coast Region.

EMEC, 2019. Pelamis Wave Power [WWW Document]. URL http://www.emec.org.uk/about-us/wave-clients/pelamis-wave-power/ (accessed 6.17.19).

Enríquez, A.R., Marcos, M., Falqués, A., Roelvink, D., 2019. Assessing beach and dune erosion and vulnerability under sea level rise: A Case study in the Mediterranean Sea. Front. Mar. Sci. 6, 1–12. https://doi.org/10.3389/fmars.2019.00004

EPRI, 2011. Mapping and Assessment of the United States Ocean Wave Energy Resource. Tech. Rep. 176. https://doi.org/1024637

Ergin, A., 2009. Coastal Engineering. Metu Press, Ankara.

Fairley, I., Smith, H.C.M., Robertson, B., Abusara, M., Masters, I., 2017. Spatio-temporal variation in wave power and implications for electricity supply. Renew. Energy 114, 154–165. https://doi.org/10.1016/j.renene.2017.03.075

FEMA, 2016. Hurricane Ivan Overview [WWW Document]. URL https://www.fema.gov/hurricane-ivan-overview (accessed 4.30.20).

Fernandez, H., Iglesias, G., Carballo, R., Castro, A., Fraguela, J.A., Taveira-Pinto, F., Sanchez,

M., 2012a. The new wave energy converter WaveCat: Concept and laboratory tests. Mar. Struct. 29, 58–70. https://doi.org/10.1016/J.MARSTRUC.2012.10.002

Fernandez, H., Iglesias, G., Carballo, R., Castro, A., Fraguela, J.A., Taveira-Pinto, F., Sanchez, M., 2012b. The new wave energy converter WaveCat: Concept and laboratory tests. Mar. Struct. 29, 58–70. https://doi.org/10.1016/j.marstruc.2012.10.002

Flocard, F., Finnigan, T.D., 2012. Increasing power capture of a wave energy device by inertia adjustment. Appl. Ocean Res. 34, 126–134. https://doi.org/10.1016/J.APOR.2011.09.003

Florida Department of Environmental Protection, 2019. Critically Eroded Beaches in Florida.

Florida Shore and Beach Preservation Association, 2017. Beach Nourishment on the Florida East Coast.

Gallagher, S., Tiron, R., Whelan, E., Gleeson, E., Ed Eric Dias, F., Mcgrath, R., 2016. The nearshore wind and wave energy potential of Ireland: A high resolution assessment of availability and accessibility. https://doi.org/10.1016/j.renene.2015.11.010

Garcia, C., Canals, M., 2015. Wave Energy Resource Assessment and Recoverable Wave Energy in Puerto Rico and the US Virgin Islands. IEEE 93.

Gaul, G.M., 2019. On the Alabama Coast, the Unluckiest Island in America [WWW Document]. Yale E360. URL https://e360.yale.edu/features/on-the-alabama-coast-the-unluckiest-island-in-america (accessed 5.19.20).

Givens, J., 2019. Dauphin Island's Shifting Sands [WWW Document]. Mob. Bay Mag. URL

https://mobilebaymag.com/dauphin-islands-shifting-sands (accessed 5.16.20).

Gonzalez-Santamaria, R., Zou, Q.P., Pan, S., 2013. Impacts of a Wave Farm on Waves, Currents and Coastal Morphology in South West England. Estuaries and Coasts 38, 159–172. https://doi.org/10.1007/s12237-013-9634-z

Gorsline, D.S., 1966. Dynamic characteristics of west Florida Gulf Coast beaches. Mar. Geol. 4, 187–206. https://doi.org/10.1016/0025-3227(66)90020-X

Greaves, D., Perez Collazo, C., Magagna, D., Conley, D., 2013. Enabling Wave Power: Streamlining processes for progress.

Gregory, J., Stocker, T., Lemke, P., Bindoff, N., 2007. Climate change 2007: The physical science basis.

Guarino, B., 2019. The oldest-known seawall could not stop sea-level rise 7,000 years ago - The Washington Post [WWW Document]. URL https://www.washingtonpost.com/science/2019/12/18/this-village-fought-sea-level-rise-years-ago-sea-won/ (accessed 12.4.20).

Gunn, K., Stock-Williams, C., 2012. Quantifying the global wave power resource. https://doi.org/10.1016/j.renene.2012.01.101

Hales, L.Z., 1981. Floating Breakwaters: State-of-the-Art Literature Review. Fort Belvoir.

Hansen, M., Sallenger, A.H., 2020. Barrier Island Vulnerability to Breaching: A Case Study on Dauphin Island, Alabama, in: Coastal Sediments '07, Proceedings. pp. 2002–2010.

https://doi.org/10.1061/40926(239)157

Hanson, H., 1989. GENESIS: Generalised Model for Simulating Shoreline Change: Report 1.

Hemer, M.A., Fan, Y., Mori, N., Semedo, A., Wang, X.L., 2013. Projected changes in wave climate from a multi-model ensemble. Nat. Clim. Chang. 3, 471–476. https://doi.org/10.1038/nclimate1791

Hemer, M.A., Zieger, S., Durrant, T., O'Grady, J., Hoeke, R.K., McInnes, K.L., Rosebrock, U., 2017. A revised assessment of Australia's national wave energy resource. Renew. Energy 114, 85–107. https://doi.org/10.1016/j.renene.2016.08.039

Hine, A.C., Belknap, D.F., Hutton, J.G., Osking, E.B., Evans, M.W., 1988. Recent Geological History and Modern Sedimentary Processes Along an Incipient, Low-Energy, Epicontinental-Sea Coastline: Northwest Florida. SEPM J. Sediment. Res. Vol. 58, 567–579. https://doi.org/10.1306/212F8DF5-2B24-11D7-8648000102C1865D

I. R. Young, S. Zieger, A.V.B., 2011. Global Trends in Wind Speed and Wave Height. Science (80-.). 159, 451–455.

Iglesias, G., Carballo, R., 2014. Wave farm impact: The role of farm-to-coast distance. Renew. Energy 69, 375–385. https://doi.org/10.1016/j.renene.2014.03.059

Iglesias, G., López, M., Carballo, R., Castro, A., Fraguela, J.A., Frigaard, P., 2009. Wave energy potential in Galicia (NW Spain). Renew. Energy 34, 2323–2333. https://doi.org/10.1016/j.renene.2009.03.030

Ingram, D.K., Isaacs, J.M., Gleason, J.S., Reynolds, M.O., Reetz, K.K., Yadamec, T.J., 2014. Loggerhead Nesting Ecology in Baldwin and Mobile Counties, Alabama, USA, 2003-2012. Spanish Fort.

IPCC, 2018. Global Warming of 1.5°C. An IPCC Special Report on the impacts of global warming of 1.5°C above pre-industrial levels and related global greenhouse gas emission pathways, in the context of strengthening the global response to the threat of cli.

Jadidoleslam, N., Özger, M., Ağıralioğlu, N., 2016. Wave power potential assessment of Aegean Sea with an integrated 15-year data. Renew. Energy 86, 1045–1059. https://doi.org/10.1016/j.renene.2015.09.022

Jones, C., Chang, G., Raghukumar, K., McWilliams, S., Dallman, A., Roberts, J., 2018. Spatial Environmental Assessment Tool (SEAT): A Modeling Tool to Evaluate Potential Environmental Risks Associated with Wave Energy Converter Deployments. Energies 11, 2036. https://doi.org/10.3390/en11082036

Kibler, K.M., Kitsikoudis, V., Donnelly, M., Spiering, D.W., Walters, L., 2019. Flow–Vegetation Interaction in a Living Shoreline Restoration and Potential Effect to Mangrove Recruitment. Sustainability 11, 3215. https://doi.org/10.3390/su11113215

Kim, J., Kweon, H.-M., Jeong, W.-M., Cho, I.-H., Cho, H.-Y., 2015. Design of the dual-buoy wave energy converter based on actual wave data of East Sea. Int. J. Nav. Archit. Ocean Eng. 7, 739–749. https://doi.org/10.1515/ijnaoe-2015-0052

Kim, Y.C., 1997. Assessment of California's Ocean Wave Energy Recovery. ASCE, pp. 175–182.

Knabb, R.D., Rhome, J.R., Brown, D.P., 2005. Tropical Cyclone Report Hurricane Katrina 23-30 August 2005.

Kopp, R.E., Horton, R.M., Little, C.M., Mitrovica, J.X., Oppenheimer, M., Rasmussen, D.J., Strauss, B.H., Tebaldi, C., 2014. Probabilistic 21st and 22nd century sea-level projections at a global network of tide-gauge sites. Earth's Futur. 2, 383–406. https://doi.org/10.1002/2014ef000239

Langhamer, O., 2012. Artificial reef effect in relation to offshore renewable energy conversion: State of the art. Sci. World J. https://doi.org/10.1100/2012/386713

Layne, R., 2019. Homes lose $15.8 billion in value as seas rise, Maine to Mississippi [WWW Document]. CBS News. URL https://www.cbsnews.com/news/homes-lose-15-8-billion-in-value-as-seas-rise-maine-to-mississippi/ (accessed 5.31.19).

Lee, J.L., Lee, J.Y., Kim, I.H., 2011. Managing Effect of Hot Spot Shoreline Behind a Power Buoy Energy Farm. J. Coast. Res. 309–316. https://doi.org/10.2112/SI61-001.31

Lehmann, J., 2007. A handful of carbon. Nature 447, 143–144.

Lenee-Bluhm, P., Paasch, R., Özkan-Haller, H.T., 2011. Characterizing the wave energy resource of the US Pacific Northwest. Renew. Energy 36, 2106–2119. https://doi.org/10.1016/j.renene.2011.01.016

López-Ruiz, A., Bergillos, R.J., Lira-Loarca, A., Ortega-Sánchez, M., 2018a. A methodology for the long-term simulation and uncertainty analysis of the operational lifetime performance of wave energy converter arrays. Energy. https://doi.org/10.1016/j.energy.2018.04.018

López-Ruiz, A., Bergillos, R.J., Ortega-Sánchez, M., 2016. The importance of wave climate forecasting on the decision-making process for nearshore wave energy exploitation. Appl. Energy. https://doi.org/10.1016/j.apenergy.2016.08.088

López-Ruiz, A., Bergillos, R.J., Raffo-Caballero, J.M., Ortega-Sánchez, M., 2018b. Towards an optimum design of wave energy converter arrays through an integrated approach of life cycle performance and operational capacity. Appl. Energy. https://doi.org/10.1016/j.apenergy.2017.10.062

Lorenzo-Trueba, J., Ashton, A.D., 2014. Rollover, drowning, and discontinuous retreat: Distinct modes of barrier response to sea-level rise arising from a simple morphodynamic model. J. Geophys. Res. Earth Surf. 119, 779–801. https://doi.org/10.1002/2013JF002941

Luettich, R.A., Westerink, J.J., Scheffner, N.W., 1992. ADCIRC: An Advanced Three-Dimensional Circulation Model for Shelves Coasts and Estuaries, Report 1: Theory and Methodology of ADCIRC-2DDI and ADCIRC-3DL., Dredging Research Program Technical Report DRP-92-6, U.S. Army Engineers Waterways Experiment Station, Vicksburg, MS,.

Luijendijk, A., Hagenaars, G., Ranasinghe, R., Baart, F., Donchyts, G., Aarninkhof, S., 2018. The State of the World's Beaches. Sci. Rep. 8. https://doi.org/10.1038/s41598-018-24630-6

Mackay, E.B.L., Bahaj, A.S., Challenor, P.G., 2009. Uncertainty in wave energy resource assessment. Part 1: Historic data. Renew. Energy 35, 1792–1808. https://doi.org/10.1016/j.renene.2009.10.026

Marta Gonçalves, P.M. and C.G.S., 2018. A 33-year hindcast on wave energy assessment in the

western French coast. ENERGY.

Masselink, Gerd; Hughes, Michael; Knight, J., 2014. Introduction to Coastal Processes and Geomorphology, 2nd ed. Routledge, London, U.K.

Masselink, G., Russell, P., 2013. Impacts of climate change on coastal erosion. https://doi.org/10.14465/2013.arc09.071-086

Masselink, G., Russell, P., Rennie, A., Brooks, S., Spencer, T., 2020. Impacts of climate change on coastal geomorphology and coastal erosion relevant to the coastal and marine environment around the UK. MCCIP Sci. Rev. 2020 158–189. https://doi.org/10.14465/2020.arc08.cgm

Masselink, G., Short, A.D., 1993. The Effect of Tide Range on Beach Morphodynamics and Morphology: A Conceptual Beach. J. Coast. Res. 9, 785–800.

McCormick, M.E., 2007. Ocean Wave Energy Conversion. Dover Publications, Mineola, New York.

Mendoza, E., Silva, R., Zanuttigh, B., Angelelli, E., Lykke Andersen, T., Martinelli, L., Nørgaard, J.Q.H., Ruol, P., 2014. Beach response to wave energy converter farms acting as coastal defence. Coast. Eng. 87, 97–111. https://doi.org/10.1016/j.coastaleng.2013.10.018

Millar, D.L., Smith, H.C.M., Reeve, D.E., 2007. Modelling analysis of the sensitivity of shoreline change to a wave farm. Ocean Eng. 34, 884–901. https://doi.org/10.1016/j.oceaneng.2005.12.014

Mirzaei, A., Tangang, F., Juneng, L., 2015. Wave energy potential assessment in the central and

southern regions of the south china sea. Renew. Energy 80, 454–470. https://doi.org/10.1016/j.renene.2015.02.005

Mora-Figueroa, V.O., Olivares, C.H., Holmes, B., O'Hagan, A.M., 2011. SOWFIA Streamlining of Ocean Wave Farms Impact Assessment - Catalogue of Wave Energy Test Centres.

Mori, N., Yasuda, T., Mase, H., Tom, T., Oku, Y., 2010. Projection of extreme wave climate change under global warming. Hydrol. Res. Lett. 4, 15–19. https://doi.org/10.3178/hrl.4.15

Morris, R.L., Boxshall, A., Swearer, S.E., 2020. Climate-resilient coasts require diverse defence solutions. Nat. Clim. Chang. 10, 485–487. https://doi.org/10.1038/s41558-020-0798-9

Morton, R.A., Miller, T.L., Moore, L.J., 2004. National Assessment Of Shoreline Change: Part 1 Historical Shoreline Changes And Associated Coastal Land Loss Along The U.S. Gulf Of Mexico. St. Petersburg.

Mota, P., Pinto, J.P., 2014. Wave energy potential along the western Portuguese coast. Renew. Energy 71, 8–17. https://doi.org/10.1016/j.renene.2014.02.039

Muste, M., 2002. Sources of bias errors in flume experiments on suspended-sediment transport. J. Hydraul. Res. 40, 695–708. https://doi.org/10.1080/00221680209499916

National Hurricane Center - NOAA, 2018. Costliest U.S. tropical cyclones tables updated. Miami.

National Ocean Service, 2020. Who Moved the Beach? [WWW Document]. NOAA. URL https://oceanservice.noaa.gov/education/lessons/who_moved_the_beach.html (accessed 5.25.20).

NDBC, 2018. How are spectral wave data derived from buoy motion measurements? [WWW Document]. URL http://www.ndbc.noaa.gov/wave.shtml (accessed 10.19.17).

Neumann, B., Vafeidis, A.T., Zimmermann, J., Nicholls, R.J., 2015. Future Coastal Population Growth and Exposure to Sea-Level Rise and Coastal Flooding - A Global Assessment. https://doi.org/10.1371/journal.pone.0118571

NOAA, 2016. Economics and Demographics [WWW Document]. URL https://coast.noaa.gov/states/fast-facts/economics-and-demographics.html (accessed 4.6.20).

NOAA, 2013. National Coastal Population Report [WWW Document]. URL http://stateofthecoast.noaa.gov (accessed 4.6.20).

NOAA, 2005. National Data Buoy Center (NDBC) [WWW Document]. URL http://www.ndbc.noaa.gov/ (accessed 3.9.18).

NREL, 2020. RE Atlas [WWW Document]. URL https://maps.nrel.gov/re-atlas/?aL=0&bL=groad&cE=0&lR=0&mC=40.21244%2C-91.625976&zL=4 (accessed 4.30.20).

Ocean Plug [WWW Document], 2019. URL http://www.oceanplug.pt/en-GB/quem_somos/ (accessed 6.26.19).

Ocean Power Technologies, 2018. PB3 [WWW Document]. URL https://www.oceanpowertechnologies.com/product (accessed 6.17.19).

Ozkan, C., Mayo, T., 2019. The Renewable Wave Energy Resource in Coastal Regions of the

Florida Peninsula. Renew. Energy 139, 530–537. https://doi.org/10.1016/J.RENENE.2019.02.090

Ozkan, C., Perez, K., Mayo, T., 2020. The impacts of wave energy conversion on coastal morphodynamics. Sci. Total Environ. 712, 136424. https://doi.org/10.1016/j.scitotenv.2019.136424

Parris, A., Bromirski, P., Burkett, V., Cayan, D.R., Culver, M., Hall, J., Horton, R., Knuuti, K., Moss, R., Obeysekera, J., Sallenger, A., Weiss, J., 2012. Global sea level rise scenarios for the United States National Climate Assessment, NOAA Tech Memo OAR CPO.

Passeri, D.L., Bilskie, M. V., Plant, N.G., Long, J.W., Hagen, S.C., 2018a. Dynamic modeling of barrier island response to hurricane storm surge under future sea level rise. Clim. Change 149, 413–425. https://doi.org/10.1007/s10584-018-2245-8

Passeri, D.L., Long, J.W., Plant, N.G., Bilskie, M. V., Hagen, S.C., 2018b. The influence of bed friction variability due to land cover on storm-driven barrier island morphodynamics. Coast. Eng. 132, 82–94. https://doi.org/10.1016/j.coastaleng.2017.11.005

Pelnard-Considère, R., 1956. Essai de theorie de l'evolution des formes de rivage en plages de sable et de galets, Les Energies de la Mer: Compte Rendu Des Quatriemes Journees de L'hydraulique, Paris 13, 14 and 15 Juin 1956; Question III, rapport 1, 74-1-10. Paris.

Poate, T.G., Russell, P., Masselink, G., Circus, D., 2012. Assessment of Potential Morphodynamic Response To Wave Hub, in: 4th International Conference on Ocean Energy. Dublin.

Policy Research Corporation, 2011. Country overview and assessment - Romania.

176

Pontee, N., 2013. Defining coastal squeeze: A discussion. Ocean Coast. Manag. https://doi.org/10.1016/j.ocecoaman.2013.07.010

Pontes, M.T., 1998. Assessing the European Wave Energy Resource. J. Offshore Mech. Arct. Eng. 120, 226. https://doi.org/10.1115/1.2829544

Previsic, M., Bedard, R., Hagerman, G., 2004. E2I EPRI Assessment Offshore Wave Energy Conversion Devices. E2I EPRI WP – 004 – US – Rev 1 1–52.

Prevosto, Marc, Kerbiriou, M.-A., Prevosto, M, Maisondieu, C., Clément, A., Babarit, A., 2007. Influence of Sea-States Description on Wave Energy Production Assessment Laying the foundations for wind energy harvesting in the high seas View project Resource characterisation for Offshore Renewable Energy Systems View project Influence of Sea-States D.

Reguero, B., Losada, I., Mendez, F., 2019. A recent increase in global wave power as a consequence of oceanic warming. Nature. https://doi.org/10.1038/s41467-018-08066-0

Reguero, B.G., Losada, I.J., Méndez, F.J., 2015. A global wave power resource and its seasonal, interannual and long-term variability. Appl. Energy 148, 366–380. https://doi.org/10.1016/j.apenergy.2015.03.114

Reguero, B.G., Méndez, F.J., Losada, I.J., 2013. Variability of multivariate wave climate in Latin America and the Caribbean. Glob. Planet. Change 100, 70–84. https://doi.org/10.1016/j.gloplacha.2012.09.005

Rijnsdorp, D.P., Hansen, J., Lowe, R., 2017. Improving predictions of the coastal impacts of wave

farms using a phase-resolving wave model, in: Proc. of the 12th European Wave and Tidal Energy Conference. pp. 1–5.

Rijnsdorp, D.P., Hansen, J.E., Lowe, R.J., 2020. Understanding coastal impacts by nearshore wave farms using a phase-resolving wave model. Renew. Energy 150, 637–648. https://doi.org/10.1016/j.renene.2019.12.138

Rodriguez-Delgado, C., Bergillos, R.J., Iglesias, G., 2019a. Dual wave farms for energy production and coastal protection under sea level rise. J. Clean. Prod. 222, 364–372. https://doi.org/10.1016/j.jclepro.2019.03.058

Rodriguez-Delgado, C., Bergillos, R.J., Iglesias, G., 2019b. Dual wave farms and coastline dynamics: The role of inter-device spacing. Sci. Total Environ. 646, 1241–1252. https://doi.org/10.1016/j.scitotenv.2018.07.110

Rodriguez-Delgado, C., Bergillos, R.J., Iglesias, G., 2019c. An artificial neural network model of coastal erosion mitigation through wave farms. Environ. Model. Softw. 119, 390–399. https://doi.org/10.1016/j.envsoft.2019.07.010

Rodriguez-Delgado, C., Bergillos, R.J., Ortega-Sánchez, M., Iglesias, G., 2018a. Protection of gravel-dominated coasts through wave farms: Layout and shoreline evolution. Sci. Total Environ. 636, 1541–1552. https://doi.org/10.1016/j.scitotenv.2018.04.333

Rodriguez-Delgado, C., Bergillos, R.J., Ortega-Sánchez, M., Iglesias, G., 2018b. Wave farm effects on the coast: The alongshore position. Sci. Total Environ. 640–641, 1176–1186. https://doi.org/10.1016/j.scitotenv.2018.05.281

Roelvink, D., Reniers, A., van Dongeren, A., van Thiel de Vries, J., McCall, R., Lescinski, J., 2009. Modelling storm impacts on beaches, dunes and barrier islands. Coast. Eng. 56, 1133–1152. https://doi.org/10.1016/j.coastaleng.2009.08.006

Roelvink, D., Van Dongeren, A., McCall, R., Hoonhout, B., Van Rooijen, A., Van Geer, P., De Vet, L., Nederhoff, K., 2018. XBeach Documentation: Release XBeach v1.23.5527 XBeachX FINAL.

Roelvink, D., Van Dongeren, A., McCall, R., Hoonhout, B., Van Rooijen, A., Van Geer, P., De Vet, L., Nederhoff, K., 2015. Xbeach Manual. https://doi.org/10.1590/S0100-54052009000400003

Roelvink, J., Van Banning, G., 1995. Design and development of DELFT3D and application to coastal morphodynamics. Oceanogr. Lit. Rev. 42, 925.

Ruol, P., Zanuttigh, B., Martinelli, L., Kofoed, J., Frigaard, P., 2010. Near-shore floating wave energy converters: applications for coastal protection. Coast. Eng. Proc. 1–12.

Rusu, E., Guedes Soares, C., 2013. Coastal impact induced by a Pelamis wave farm operating in the Portuguese nearshore. Renew. Energy 58, 34–49. https://doi.org/10.1016/j.renene.2013.03.001

Rusu, E., Onea, F., 2018. A review of the technologies for wave energy extraction. Clean Energy. https://doi.org/10.1093/ce/zky003

Saglam, M., Sulukan, E., Uyar, T.S., 2010. Wave Energy and Technical potential of Turkey. J. Nav. Sci. Eng. 6, 34–50.

Sallenger, A., 2000. Storm impact scale for barrier islands. J. Coast. Res.

Scott, D., Charles Simpson, M., Sim, R., 2012. The vulnerability of Caribbean coastal tourism to scenarios of climate change related sea level rise. J. Sustain. Tour. 20. https://doi.org/10.1080/09669582.2012.699063

SEAI, 2019. Atlantic Marine Energy Test Site [WWW Document]. URL http://www.oceanenergyireland.com/TestFacility/AMETS (accessed 6.26.19).

Seddon, N., Daniels, E., Davis, R., Chausson, A., Harris, R., Hou-Jones, X., Huq, S., Kapos, V., Mace, G.M., Rizvi, A.R., Reid, H., Roe, D., Turner, B., Wicander, S., 2020. Global recognition of the importance of nature-based solutions to climate change impacts. Glob. Sustain. 3, 1–12. https://doi.org/10.20944/preprints201810.0203.v2

SEM-REV [WWW Document], 2019. URL https://sem-rev.ec-nantes.fr/english-version/ (accessed 6.26.19).

Shafiee, S., Topal, E., 2009. When will fossil fuel reserves be diminished? Energy Policy 37, 181–189. https://doi.org/10.1016/j.enpol.2008.08.016

Siegenthaler, U., Sarmiento, J.L., 1993. Atmospheric carbon dioxide and the ocean. Nature 365, 119–125.

Sierra, J.P., Martín, C., Mösso, C., Mestres, M., Jebbad, R., 2016. Wave energy potential along the Atlantic coast of Morocco. Renew. Energy 96, 20–32. https://doi.org/10.1016/j.renene.2016.04.071

Smith, H.C.., Fairley, I., Robertson, B., Abusara, M., Masters, I., 2017. Wave resource variability: Impacts on wave power supply over regional to international scales. Energy Procedia 125, 240–249. https://doi.org/10.1016/j.egypro.2017.08.202

Smith, H.C.M., Haverson, D., Smith, G.H., 2013. A wave energy resource assessment case study: Review, analysis and lessons learnt. Renew. Energy 60, 510–521. https://doi.org/10.1016/j.renene.2013.05.017

Song, D., Kim, I., Choi, J., Lee, H., 2016. Evaluating of Coastal Erosion Status from CEMP results in Eastern Coast, South Korea. J. Coast. Res. 75, 1407–1411. https://doi.org/10.2112/SI75-282.1

Soulsby, R.L., Damgaard, J.S., 2005. Bedload sediment transport in coastal waters. Coast. Eng. 52, 673–689. https://doi.org/10.1016/j.coastaleng.2005.04.003

Stokes, C., 2015. Coastal impacts in the lee of a wave energy site: waves, beach morphology and water-users (Wave Hub, Cornwall, UK). University of Plymouth.

Stokes, C., Conley, D., 2018a. Modelling Offshore Wave farms for Coastal Process Impact Assessment: Waves, Beach Morphology, and Water Users. Energies 11, 2517. https://doi.org/10.3390/en11102517

Stokes, C., Conley, D., 2018b. Modelling Offshore Wave farms for Coastal Process Impact Assessment: Waves, Beach Morphology, and Water Users. Energies 11, 2517. https://doi.org/10.3390/en11102517

Stopa, J.E., Filipot, J.-F., Li, N., Cheung, K.F., Chen, Y.-L., Vega, L., 2013. Wave energy

resources along the Hawaiian Island chain. Renew. Energy 55, 305–321. https://doi.org/10.1016/j.renene.2012.12.030

Summers, A., Fletcher, C.H., Spirandelli, D., McDonald, K., Over, J.S., Anderson, T., Barbee, M., Romine, B.M., 2018. Failure to protect beaches under slowly rising sea level. Clim. Change 151, 427–443. https://doi.org/10.1007/s10584-018-2327-7

Taherkhani, M., Vitousek, S., Barnard, L., Frazer, N., Anderson, T.R., Fletcher, C.H., 2020. Sea-level rise exponentially increases coastal flood frequency. Sci. Rep. 10. https://doi.org/10.1038/s41598-020-62188-4

Taylor, J.R., 1997. An Introduction to Error Analysis: The Study of Uncertainties in Physical Measurements, 2nd Editio. ed. University Science Books, New York.

Temmerman, S., Meire, P., Bouma, T.J., Herman, P.M.J., Ysebaert, T., De Vriend, H.J., 2013. Ecosystem-based coastal defence in the face of global change. Nature 504, 79–83. https://doi.org/10.1038/nature12859

The White House, 2015. Executive Order 13693-Planning for Federal Sustainability in the Next Decade [WWW Document]. The White House. https://doi.org/EO 13693

THESEUS, 2009. THESEUS Project [WWW Document]. Eur. Comm. URL http://www.vliz.be/projects/theseusproject/index.php (accessed 4.30.19).

Thomson, R.C., Harrison, G.P., Chick, J.P., 2011. Full life cycle assessment of a wave energy converter, in: IET Conference Publications. pp. 1–6. https://doi.org/10.1049/cp.2011.0124

U.S. Climate Resilience Toolkit, 2016. Coastal Erosion [WWW Document]. URL https://toolkit.climate.gov/topics/coastal-flood-risk/coastal-erosion (accessed 5.31.19).

U.S. EIA, 2018a. Where Greenhouse Gases Come From - Energy Explained, Your Guide To Understanding Energy - Energy Information Administration [WWW Document]. Energy Explain. URL https://www.eia.gov/energyexplained/index.php?page=environment_where_ghg_come_fro m (accessed 3.24.19).

U.S. EIA, 2018b. Country Analysis Brief: South Korea [WWW Document]. URL https://www.eia.gov/beta/international/analysis_includes/countries_long/Korea_South/south _korea.pdf (accessed 6.20.19).

Uihlein, A., 2016. Life cycle assessment of ocean energy technologies. Int. J. Life Cycle Assess. 21, 1425–1437. https://doi.org/10.1007/s11367-016-1120-y

UNFCCC, 2015. Paris Climate Change Conference-November 2015, COP 21. Adopt. Paris Agreement. Propos. by Pres. 21932, 32. https://doi.org/FCCC/CP/2015/L.9/Rev.1

United States Energy Information Administration, 2009. Household Energy Use in Arizona [WWW Document]. eia.gov. URL http://www.eia.gov/consumption/residential/reports/2009/state_briefs/pdf/fl.pdf (accessed 3.28.18).

US Census Bureau, 2015. Coastal Areas [WWW Document]. URL https://www.census.gov/topics/preparedness/about/coastal-areas.html (accessed 6.1.19).

US Department of the Interior, 2016. Salazar, Menendez Announce $29 Million to Restore Ellis Island Seawall, Historic Structures under President's Recovery Plan [WWW Document]. URL https://www.doi.gov/news/pressreleases/Salazar-Menendez-Announce-29-Million-to-Restore-Ellis-Island-Seawall-Historic-Structures-under-Presidents-Recovery-Plan (accessed 4.8.20).

USGCRP, 2014. U.S National Climate Assessment: Overview of Climate Change Impacts in the United States 1–19.

USGS, 2017. The National Map - Advanced Viewer [WWW Document]. URL https://viewer.nationalmap.gov/advanced-viewer/ (accessed 5.7.20).

Van Nieuwkoop, J.C.C., Smith, H.C.M., Smith, G.H., Johanning, L., 2013. Wave resource assessment along the Cornish coast (UK) from a 23-year hindcast dataset validated against buoy measurements. Renew. Energy 58, 1–14. https://doi.org/10.1016/j.renene.2013.02.033

Venugopal, V., Nemalidinne, R., Vögler, A., 2017. Numerical modelling of wave energy resources and assessment of wave energy extraction by large scale wave farms. Ocean Coast. Manag. 147. https://doi.org/10.1016/j.ocecoaman.2017.03.012

Vethamony, P., Aboobacker, V.M., Menon, H.B., Kumar, K.A., Cavaleri, L., 2011. Superimposition of wind seas on pre-existing swells off Goa coast. J. Mar. Syst. 87, 47–54. https://doi.org/10.1016/j.jmarsys.2011.02.024

Vögler, A., Christie, D., Lidster, M., Morrison, J., 2011. Wave energy converters , sediment transport and coastal erosion, in: ICES Annual Science Conference. Gdańsk, Poland, pp. 1–

22.

Wang, Y., Yu, Q., Gao, S., 2011. Relationship between bed shear stress and suspended sediment concentration: Annular flume experiments. Int. J. Sediment Res. 26, 513–523. https://doi.org/10.1016/S1001-6279(12)60009-2

Wave Hub, 2019. Wave Hub Test Site [WWW Document]. URL https://www.wavehub.co.uk/ (accessed 3.9.19).

Waves4Power, 2017. Waves4Power [WWW Document]. URL https://www.waves4power.com/demo-runde/ (accessed 6.17.19).

Wavestar, 2013. Wavestar prototype at Roshage [WWW Document]. URL www.wavestarenergy.com (accessed 6.17.19).

Wilson, J.H., Beyene, A., 2007. California Wave Energy Resource Evaluation. J. Coast. Res. 233, 679–690. https://doi.org/10.2112/04-0240.1

Xu, C., Huang, Z., 2018. A dual-functional wave-power plant for wave-energy extraction and shore protection: A wave-flume study. Appl. Energy 229, 963–976. https://doi.org/10.1016/j.apenergy.2018.08.005

Young, I.R., Vinoth, J., Zieger, S., Babanin, A. V., 2012. Investigation of trends in extreme value wave height and wind speed. J. Geophys. Res. Ocean. 117, 1–13. https://doi.org/10.1029/2011JC007753

Zanopol, A.T., Onea, F., Rusu, E., 2014. Coastal impact assessment of a generic wave farm

operating in the Romanian nearshore. Energy 72, 652–670.

https://doi.org/10.1016/j.energy.2014.05.093

Zanuttigh, B., Angelelli, E., 2013. Experimental investigation of floating wave energy converters

for coastal protection purpose. Coast. Eng. 80, 148–159.

https://doi.org/10.1016/j.coastaleng.2012.11.007